A study of lanthanide energy transfer systems in aqueous micellar solutions and the photophysical properties of 1,4-bis(phenylethynyl)benzene and other polyarylethynylenes.

Karen Samantha Findlay

A STUDY OF LANTHANIDE ENERGY TRANSFER SYSTEMS IN AQUEOUS MICELLAR SOLUTIONS AND THE PHOTOPHYSICAL PROPERTIES OF 1,4-BIS(PHENYLETHYNYL)BENZENE AND OTHER POLYARYLETHYNYLENES.

Karen Samantha Findlay

Department of Chemistry, University of Durham

(Supervisor: Dr. A. Beeby)

MSc. Thesis

October 2002

DECLARATION

The work described in this thesis was carried out in the Chemistry Department in the University of Durham between October 2001 and September 2002. This thesis is the work of the author except where acknowledged by references, and has not been submitted for any other degree.

STATEMENT OF COPYRIGHT

Abstract

A literature review of the photophysical properties of luminescent lanthanide complexes and their behaviour in aqueous micellar systems is presented. The effects of the environment and the presence of sensitisers and quenching agents on the fluorescence properties, as well as the energy transfer mechanisms responsible for these properties, are discussed.

The study undertaken demonstrated the enhancement of europium phosphorescence due to an aqueous micellar environment. Here the micelles protect the lanthanide excited state from quenching mechanisms. There is some evidence that phenanthrene and 1,10-phenanthroline act as sensitisers and chelated ligands affect the luminescence of europium.

A review of recent studies of the physical and luminescence properties of ethynylated aromatic systems in solutions and as liquid crystals is presented. The details of a re-evaluation of the photophysical properties of 1,4-bis(phenylethynyl)benzene (**1**) are presented along with comparative data from other poly aryl systems studied. All the systems showed similar conventional photophysical properties at room temperature and inhomogeneous fluorescence behaviour in low temperature glasses and in viscous solvents. **1** showed wavelength – dependent excitation and emission spectra, indicative of a slow rate of relaxation of conformers of the excited states compared to the rate of fluorescence.

TABLE OF CONTENTS

CHAPTER 3

CHAPTER 4

Appendix

Acknowledgements

I would like to thank Dr. Andrew Beeby for his guidance, patience and support during this year.

Thanks also to Simon FitzGerald and Sylvia Bettington for all their help in showing me the ropes and making me feel welcome in the group.

LIST OF ABBREVIATIONS

acac	acetylacetone (anion of 2,4-Pentanedione)
cmc	critical micelle concentration
CTA	cetyltrimethylammonium
EPA	ether pentane alcohol
ff*	f-f orbital transitions
ΔH	enthalpy change
hfac	hexafluoroacetylacetonate
IC	internal conversion
ISC	intersystem crossing
IR	infrared
k_q	quenching rate constant
LCDs	liquid crystal displays
LEDs	light emitting diodes
Ln	lanthanide
Me_2SO	dimethyl sulfite
MRTD	molecular resonant □ unneling diode
Mos	molecular orbitals
P	oscillator strength
P_{MD}	magnetic dipole oscillator strength
PDC	dipicolinato
PL	photoluminescence
PPE	Poly(*p*-phenyleneethynylenes)
PPV	poly(phenylene)vinylene
PPyVPV	poly(*p*-pyridylvinylene phenylenevinylene)
SAM	self-assembled monolayer
VR	vibrational relaxation
HLG	HOMO-LUMO gap

CHAPTER 1

1.1 LUMINESCENCE

Luminescence or "cold light" is the emission of light occurring from the electronically excited states of any material that is not due to a raise in its temperature. Examples include photoluminescence from glow-in-the-dark paints and powders, the glow of phosphorus, in air the aurora borealis, triboluminescence from the grinding of sugar crystals and bioluminescence of many living organisms. Before a luminescent material can emit radiation it must absorb energy from a suitable source[1]. This excitation energy could be ultraviolet and visible radiation, direct electric excitation or a beam of electrons to name a few. In all of the work described here, ultraviolet and visible electromagnetic radiation was used to excite the systems and complexes studied to higher energy, in order to observe their photoluminescence.

The two categories of luminescence, fluorescence and phosphorescence, depend on the nature of the excited states involved in the transitions and the electron spin orientation [2]. Fluorescence is the term used to describe the process in which $\Delta S = 0$. Light is emitted from the excited singlet states in which the electron in the excited orbital is paired to a second electron in the lowest occupied molecular orbital. The return to the ground state is spin-allowed and occurs rapidly by emission of a photon. The rate constant for fluorescence is typically $10^8 s^{-1}$ [2].

Phosphorescence is the emission of light from triplet excited states in which the electron in the excited orbital has the same spin orientation as the electron in the lowest occupied molecular orbital i.e. $\Delta S \neq 0$. Emission rates are usually low ($10^{-3} - 10^0 s^{-1}$) because the transitions are spin forbidden. Non-radiative decay, quenching and other processes makes it unusual for phosphorescence to be seen in fluid solutions at room temperature[2].

Figure 1 is a simplified Jabłoński diagram illustrating the transitions that occur after the absorption of light by a typical organic molecule. S_0, S_1 and S_n represent the ground electronic state and the first two excited electronic states respectively. Each of these electronic energy levels has a number of vibrational energy levels (S_n^*) associated with them in which the fluorophores can exist. These vibronic levels are due to the motion of the nuclei. The instantaneous absorption of light of the appropriate wavelength populates the excited states at the expense of the ground state via the transitions ($S_0 \rightarrow S_n^*$). Prior to any emission, the molecule relaxes to the lowest vibrational excited state by non-radiative processes e.g. ($S_n^* \rightarrow S_n \rightarrow S_1^* \rightarrow S_1$). The first of these is vibrational relaxation (VR) in which the molecule loses its vibrational energy by collisions with solvent molecules. If the sample is in a solid matrix VR occurs by exchange with the vibrational motions or phonons of this matrix. This is followed by internal conversion (IC) whereby the molecule undergoes a transition to the lowest energy level in a highly excited vibrational level[1] e.g. ($S_1^* \rightarrow S_1$). The process involves little or no energy change and the lowest vibrational energy level of the ground state is reached by VR. Transitions can also occur between isoenergetic levels of different multiplicities e.g. ($S_1 \rightarrow T_2$) when it is termed intersystem crossing (ISC). VR and IC are usually very rapid processes and are complete within 10^{-8} s. IC is faster for the upper excited states but VR is always faster. Fluorescence lifetimes are typically 10^{-8} to 10^{-12}s so fluorescence emission generally results from the lowest-energy vibrational state of S_1[2]. The slower process of ISC ($k_{ISC} \approx 10^8 s^{-1}$) populates the first excited triplet state (T_1) from which phosphorescence occurs.

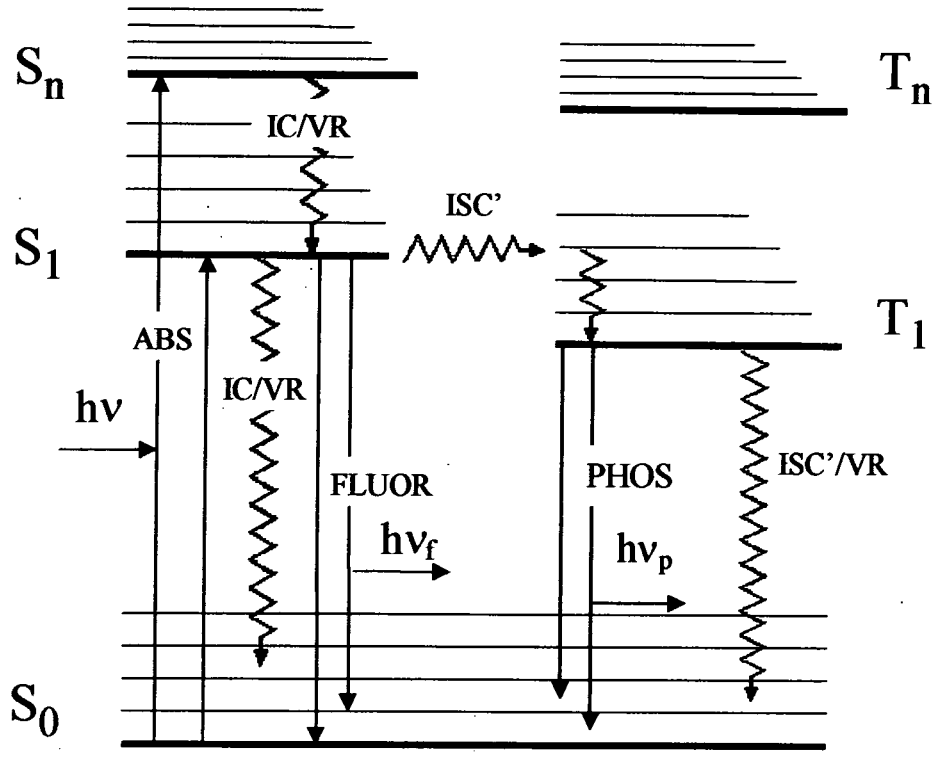

Figure 1. The Jabłoński diagram for a typical organic molecule. S_0 represents the ground state. S_1 - S_n and T_1-T_n represent the singlet and triplet excited states respectively. ABS hν - the light energy absorbed, IC/VR - internal conversion and vibrational relaxation, ISC' – intersystem crossing and FLUOR $h\nu_f$ and PHOS $h\nu_p$ – fluorescence and phosphorescence emissions.

1.2 LANTHANIDES

General Properties

The Lanthanides (Ln) consists of the 14 elements from cerium ($_{58}$Ce) to lutetium ($_{71}$Lu) and also include lanthanum ($_{57}$La)[3]. The free atoms are generally of the configuration $[Xe]4f^n5d^06s^2$ with the exceptions of Ce – $[Xe]4f^15d^16s^2$ and gadolinium ($_{64}$Gd) – $[Xe]4f^75d^16s^2$. Their aqueous solution chemistry is dominated by the 3+ oxidation state, the electronic configuration of which varies regularly from $4f^1(Ce^{III})$ to $4f^{14}(Lu^{III})$[3]. The directional characteristics of the $4f^n$ orbitals result in $4f^n$ electrons and other electrons being imperfectly shielded from

the nuclear charge. As the nuclear charge increases along the series there is a net increase in the attraction for the electron charge cloud and this causes a significant decrease in the ionic radii. This phenomenon is referred to as 'Lanthanide Contraction'[3]. Generally the properties of the Ln ions in the gas phase, including the atomic like spectra of the ions, are usually retained after formation of complexes with different ligands. This is due to the shielding of the 4f electrons from the ligand field by an outer core of 5s and 5p electrons[4].

Lanthanides are highly electropositive and reactive metals. Their reactivity tends to be dependent on size and thus europium (Eu), having the largest metal radius, is the most reactive. Lanthanides are classed as 'hard acids', with their bonding being predominantly ionic in character. They form their most stable complexes with ligands containing N, O or F donor atoms. They have a less extensive coordination chemistry than d – transition metals[3].

The luminescence of Eu^{3+} can be used as a probe of its environment. It gives information on ligand charges, binding constants, site symmetry of OH or NH bonds in the first coordination sphere and ligand rate exchange[5]. The paramagnetic Ln ions, especially Pr^{3+}, Eu^{3+} and Yb^{3+}, are used as nmr shift reagents[6]. Organic molecules with complex spectra can be coordinated to these ions and the large magnetic moments of the ions cause displacements and the spreading out of the spectrum, which assists in assigning and interpreting peaks. These properties are fully covered in a number of texts[3, 7].

Magnetic and spectroscopic properties

The transitions taking place between energy levels of the Ln ions determine their spectroscopic properties. Understanding of the electronic configurations of the ions enables one to understand their spectroscopic properties.

An electron in an atom can be described by four quantum numbers:

n- principal

l- orbital angular momentum

m- magnetic

m_s- spin angular momentum

The Russell – Saunders[8] coupling scheme is used to describe the electronic configurations of the lanthanide ions. The values of the quantum numbers S and L corresponding to the lowest energy are expressed for each ion in the as a term symbol of the form S, P, D, F, G, H, I... corresponding to L = 0, 1, 2, 3, 4.... respectively. The overall quantum number J is associated with the resultant angular momentum produced when the angular momentum vectors associated with S and L are coupled together in what is known as spin-orbit coupling[3]. The 4f electrons of the lanthanide ions are shielded from their chemical environment and as a result spin-orbit coupling (of the order of 2000 cm^{-1}) is much larger than the crystal field (100 cm^{-1}). The opposite is true in the case of the d-block elements where the crystal field is much greater than the spin-orbit coupling because the electrons are directly exposed to the influence of neighbouring groups.

J can take the values J = L+S, L+S-1, ..., L-S (or S-L if S>L), each of which correspond to a different energy, so a 'term', which is given by a pair of S and L values, splits into a number of component 'states' defined by the same pair of S and L values plus a value of J. The 'ground state' of the ion is that with J=L-S (or S-L) if the f shell is less than half full and that with J=L+S if the f shell is more than half full[3]. With the exception of Sm^{III} and Eu^{III}, as their first excited state lies close to the ground state, the strength of the spin-orbit coupling is enough to make the first excited state of the Ln^{III} ions thermally inaccessible. Thus the ground state of almost all the Ln ions have a single well defined J value which is used to determine their magnetic properties[4]. The magnetic behaviour of d-

block elements depend only on S values and is qualitatively different from the magnetic behaviour of the Ln[6]. External fields do not appreciably split the free ion terms (f^n configurations are split by about $100cm^{-1}$) or quench the orbital angular momentum in Ln. This is a result of the shielding of the f^n orbitals from the ion environment.

Absorption

Electronic absorption involves transitions in which the electrons are redistributed within the 4f orbitals (i.e. f-f transitions) and are thus formally forbidden by the Laporte selection rule. There is no great relaxation of the selection rule because of the small crystal field effects and hence the transitions of the Ln^{III} ions are not intense and their compounds are not highly coloured. The small crystal field effects of the ligands and thermal vibrations only slightly affecting the energies of the electronic states results in sharp absorption bands. Virtually all of the absorption bands in the visible and UV spectra of Ln^{3+} ions have this line like structure. Ln ions with partially filled 4f orbitals absorb electromagnetic radiation in the near-UV, visible and near-IR regions. The lower ionic charge of the Ln^{2+} ions results in their 4f orbitals not being stabilized relative to the 5d orbitals to the same extent as those of the Ln^{3+} ions. The Ln^{2+} spectra consist of broad orbitally allowed, 4f $\rightarrow$ 5d bands overlaid with weaker and sharper f $\rightarrow$ f bands.

For Ce^{3+}, Pr^{3+} and Tb^{3+} compounds $4f^n \rightarrow 4f^{n-1}5d$ occur in the near – UV region. The transitions are broad and the ligand field surrounding the ion splits the upper 5d level. Since transitions of the type $4f \rightarrow 4f^{n-1}5d^1$ are not orbitally forbidden ions, such as Ce^{III} and Tb^{III} have bands of higher intensities than usual in the ultraviolet region. In solution, the energy of these 4f $\rightarrow$ 5d transitions is lowered by ~15000 cm^{-1} compared to that of the gaseous ion[9]. The core electronic structures of Sc^{3+}, Y^{3+}, La^{3+}, Ce^{4+} (which is iso-electronic with La^{3+}) and Lu^{3+} are made up of completely filled shells. The process of promoting an

electron out of filled shells requires much higher energies and thus no electronic absorption spectrum is expected over 200 nm.

Charge transfer is the result of an easily oxidized ligand being bound to a Ln^{3+} ion which can be reduced to the divalent state, or when a ligand is bound to a tetravalent ion[10]. This is seen in Sm(IV), Eu(III), Yb(III) and Ce(IV). Pronounced absorption bands that extend well into the visible range are observed for complexes such as $CeCl_6^{2-}$ and $CeBr_6^{2-}$[11]. In these cases the absorption mechanism involved is an electron transfer process where the absorption of energy results in the transfer of an electron from the molecular orbitals on the ligands to the nl-shell of the central atom[12, 13]. Properties of the ligand and metal ions determine band positions in the spectra.

The intra-$4f^n$ transitions are the most interesting and useful in the spectra of Ln complexes[14]. For the f-f transitions that occur from one spectroscopic term of an f^n configuration to another term of the same configuration, the absorption is very sharp for previously mentioned reasons. These bands are quite unlike the broad bands observed for d-d transitions in transition metal complexes. Ce^{3+} and Yb^{3+} have only two electronic levels and thus the simplest absorption spectra. The numerous electronic levels of the other Ln ions result in their more complex spectra (Figure 2). The absorption spectra are characterized by small values of molar extinction coefficients in the visible range (<10 cm^2 mol^{-1})[4]. Spectroscopic studies of Ln complexes have been carried out in the past[9, 15, 16] to determine the influence of different ligands and solvents on absorption spectra in solution. The three main effects on the absorption bands were seen when the complexed Ln ions are compared to the aqueous ion. (1) There is a small displacement toward longer wavelengths. (2) The development of fine structure in specific bands. (3) Change in intensities in specific bands. Complexation does not profoundly alter the spectrum of a given Ln^{3+} ion[4], although it can change the relative intensities of certain metal ion bands referred to as hypersensitive bands.

In 1937Van Vleck initially concluded that the nature of the electronic transitions was a combination of electric dipole, magnetic dipole and electric quadrupole transitions[17]. This was contested by Broer *et al* who showed the intensities of the transitions were too great for magnetic dipole or electric quadrupole radiation to be important[18]. They also semi quantitatively demonstrated that electric dipole transitions could be responsible for the absorption intensities observed experimentally. The electric dipole transitions arise from the admixture into 4f configurations of opposite parity that made calculation of their intensities difficult.

Van Vleck and Broer indicated that an induced electric dipole mechanism (P_{ED}) must be invoked to account for the intensities of most Ln absorption bands while there is some magnetic dipole character in a few transitions [9]. There is no parity change involved in transitions within a configuration so the electric dipole transitions have to be forced or induced. Magnetic dipole transitions are parity allowed within a configuration. The intra f^n transitions were thus accounted for by assuming that a small amount of character of higher-lying opposite parity configurations is mixed into the f^n states via the odd terms in the potential due to the ligand field[19].

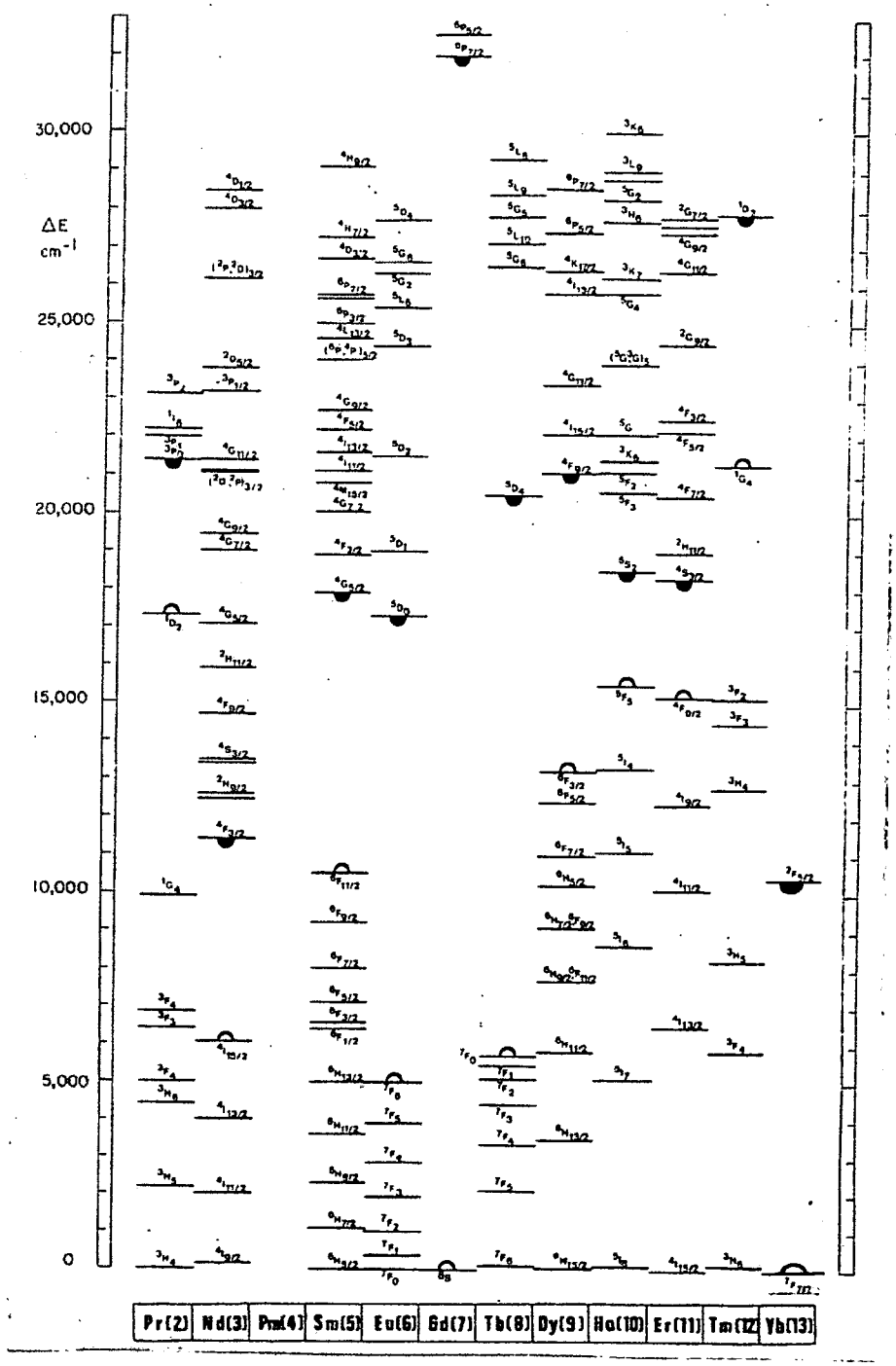

Figure 2. Comparison of electronic energy levels for triply charged lanthanide ions in solution[20]. Solid semicircles represent the lowest luminescent level. Open semicircles represent the highest non-luminescent level.

The expected probability of absorption of radiant energy P, termed the oscillator strength, is a summation of the magnetic dipole and induced electric dipole oscillator strengths. The Einstein coefficient plays a basic role in expressing the transition probability due to dipole radiation in both absorption and fluorescent processes in solution.

The transition probability is expressed as:

$$A(i,f) = \frac{64\pi^4\sigma^3}{3h}\left|\langle i|D|f\rangle\right|^2 \qquad \text{(eq 1)}$$

Here i and f signify the initial and final states, A is the transition probability per unit time, σ (cm^{-1}) is the energy difference between the states and D is the dipole operator[21].

Broer *et al*[18] tackled the problem of the absorption of energy by expressing equation 1 in terms of oscillator strength using the relationship

$$P = Amc/8\pi^2\sigma^2e^2 \qquad \text{(eq 2)}$$

Since the matrix elements of D are summed over all components of the initial state i the factor 2J+1 was added. After also adding a refractive index correction χ the expression became:

$$P = \frac{8\pi^2mc\sigma}{3he^2(2J+1)}[\chi\overline{F^2} + n\overline{M^2}] \qquad \text{(eq 3)}$$

Here $\overline{F^2}$ and $\overline{M^2}$ represent the matrix elements of the electric dipole and the magnetic dipole operators which join an initial state J to the final state J'. $\chi = (n^2+2)^2/9n$ and n is the refractive index of the medium.

In 1962 B. R. Judd[22] and G. S. Ofelt[23] independently derived expressions for the oscillator strength of the induced electric dipole transitions within the f^n configuration. The resulting Judd-Ofelt theory made possible the theoretical interpretation of the fluorescence process and the prediction of the properties of solid state Ln lasers[24]. The expression derived by Judd could be directly related to oscillator strengths derived from Ln solution spectra. He concluded that electric dipole transitions within 4f shells of Ln ions are permitted if the surroundings of the ion are such that its nucleus is not at a centre of inversion[22]. It was first assumed that the levels of each excited configuration of the type $4f^n n'd$ or $4f^n n'g$ extended over a small energy range compared to the energy of the configuration above the ground configuration. All the transitions between the components of the ground level ΨJ and those of an excited level $\Psi' J'$, both of $4f^n$, were summed so the oscillator strength P corresponded to the transition $\Psi J \rightarrow \Psi' J'$ of frequency ν. P was found to be given by:

$$P = \sum T_\lambda \nu \left(\Psi J \left\| U^{(\lambda)} \right\| \Psi' J \right)^2 \qquad \text{(eq 4)}$$

The symbol Ψ denotes the additional quantum numbers that may be necessary to define the level uniquely. $U^{(\lambda)}$ is a tensor operator of rank λ and the sum runs over the three values 2, 4, and 6 of λ. A similar contribution to P was given by transitions that involved changes in the vibrational modes of the complex encompassing the rare earth ions and its surroundings. It was also shown that sets of parameters T_λ can be chosen to give a good fit with experimental data on aqueous solutions of $NdCl_3$ and $ErCl_3$[22]. Equation 4 was modified by the substitution: $T_\lambda = T_\lambda / 2J+1$ to facilitate the intercomparison of parameters for different Ln ions. In the more recent expressions of the theory T_λ is expressed as Ω_λ.

The results of the work done by Condon and Shortly[21] lead to the magnetic dipole operator being expressed as:

$$M = (-e/2mc)\sum_i (L_i + 2S_i) \qquad \text{(eq 5)}$$

The matrix elements of the operator $\overline{M^2}$ in equation 3 can be written as:

$$\overline{M^2} = (e^2/4m^2c^2)(\Psi J \| L + 2S \| \Psi' J')^2 \qquad \text{(eq 6)}$$

The non-zero matrix elements will be those diagonal in the quantum numbers α, S and L. The selection rule on J, $\Delta J = 0, \pm 1$, restricts consideration to three cases, $J' = J, J' = J+1$ and $J' = J-1$ [9]. The matrix elements that are calculated for each of these cases must first be transformed into the intermediate coupling scheme i.e. J is taken as a good quantum number, but L and S are not, before computing the magnetic dipole contribution represented in equation 6. Calculated values of the quantity P' where $P_{MD} = P'n$ for all the Ln^{3+} ions were greater than 0.015×10^{-8}.

Emission

The emission spectra of the trivalent ions consist of a number of sharp bands corresponding to f – f transitions[4]. The characteristic line – like spectra are the result of the shielding of the 4f electrons from the environment by the 5s and 5p electrons. The importance of environmental and the consequent symmetry effects are highlighted when one realizes that not all possible transitions result in luminescence. Relaxation of excited states in solution occurs via both radiative and non-radiative processes. The Ln^{3+} towards the middle of the series (namely Sm, Eu, Tb and Dy) all form complexes which can emit visible radiation when excited in the near UV.

There are three typical types of Ln complexes which give different types of emission depending on the position and presence of the Ln lowest excited f orbital (ff*)[4]. When the radiative ff* level of the Ln is lower than the ligand's lowest T_1 state intramolecular energy transfer from the ligand to the Ln may

occur which results in Ln luminescence. Sm^{3+}, Eu^{3+}, Tb^{3+} and Dy^{3+} exhibit strong luminescence because they have an excited state lower than the T_1 state of the ligand and a large energy gap between the excited and ground state (Fig 2). Studies carried out on β-diketonates of Sm^{3+}, Eu^{3+}, Tb^{3+} and Dy^{3+} showed line-like emission spectra[25] characteristic of the f-f transitions. The emissions of Sm^{3+}, Tb^{3+} and Dy^{3+} originate from radiative transitions at unique resonance levels for each ion. It is possible to assign most of the lines to transitions between particular electronic states on the basis of the energy gaps only[4]. The spectral lines for Eu^{3+} may originate from both the $^5D_1$ and $^5D_0$ excited states, which are both populated by energy transfer and so assignment of transitions is made more difficult. It is possible to use time resolved spectroscopy to differentiate between the short lived (μ s) $^5D_1 \rightarrow {}^7F_n$ and the long lived (ms) $^5D_0 \rightarrow {}^7F_n$ transitions.

If the ff* level of the metal ion is energetically higher than the T_1 state of the ligand, ligand centred emission may be observed in the form of phosphorescence (eg Gd^{3+} complexes). Such phosphorescence, usually of very low efficiency, is also observed if the Ln ion has no ff* levels as is the case for La^{3+} and Lu^{3+}.

The Einstein coefficient is used directly to express the rate of relaxation of an excited state (ΨJ) to defined final state $(\Psi' J')$. The radiative relaxation rate $A(\Psi J, \Psi' J')$ is given by:

$$A(\Psi J, \Psi' J') = \frac{64\pi^4 \sigma^3}{3h(2J+1)}[\chi' \overline{F^2} + n^3 \overline{M^2}] \quad \text{.....(eq 7)}$$

Here, σ (cm^{-1}) signifies the energy gap between the excited and final states, $\chi = n(n^2+2)^2/9$ and n is the refractive index of the medium[9]. A total radiative relaxation rate, $A_T(\Psi J)$ is defined to account for excited state transitions to several lower states:

$$A_T(\Psi J) = \sum_{\Psi' J'} A(\Psi J, \Psi' J') \qquad \text{(eq 8)}$$

Here the sum runs over all states lower in energy than the emission state. The radiative lifetime of a state is expressed as,

$$\tau_R(\Psi J) = [A_T(\Psi J)]^{-1} \qquad \text{(eq 9)}$$

It is defined as the reciprocal of the radiative rate constant of the transitions generating fluorescence or phosphorescence[1]. The radiative lifetimes of Ln in the middle of the series (from Sm^{3+} to Dy^{3+}) are relatively long and range from 1.85 to 10.9 ms. These values are for the resonance level which is the excited state having the largest energy gap to the next lower state.

The total luminescence lifetime is expressed as the summation of the total radiative relaxation rate and the total non-radiative relaxation rate.

$$(\tau_R)^{-1} = A_T(\Psi J) + W_T(\Psi J) \qquad \text{(eq 10)}$$

Here $W_T(\Psi J)$ is the sum of the rates of the various non-radiative processes[9]. In crystalline hosts the dependence of the non-radiative rate on the energy gap (ΔE) between the excited level and the next lower-lying level is expressed as

$$W_T = Ce^{\alpha \Delta E} \qquad \text{(eq 11)}$$

Where C and α are constants characteristic of a particular crystal[26]. The relaxation mechanism is interpreted as a multiphonon process, which becomes less probable as the number of phonons that must be simultaneously excited to conserve energy increases.

The concept of multiphonon relaxation was extended to aqueous solutions on the basis of the observed enhancement of the luminescence yield of Ln ions in

D_2O compared to H_2O. The absorption spectra of Ln ions are not affected by D_2O being substituted by H_2O. It was shown by Kropp and Windsor[27-29] that the ratio of the intensity of luminescence of a given Ln^{3+} state in D_2O to that of the same state in H_2O bore an inverse relation to the energy gap.

They concluded that the quenching of fluorescence in aqueous solution occurred by –OH coupled modes and that the rate was proportional to the number of such modes associated with the Ln ions[9]. The experimentally observed decay curves of the Eu^{3+} (aq) $^5D_0 \rightarrow {}^7F_1$ emission as a function of increasing H_2O concentration in D_2O can be resolved into the sum of two exponentials[30]. These results indicated that the introduction of a single OH group into the inner coordination sphere of Eu^{3+} was enough to reduce the fluorescence lifetime of the $^5D_0$ state from 3.9 to 0.12 ms[9]. In 1966 Heller[31] used the relative intensity of fluorescence in D_2O to H_2O (I_D/I_H) as a function of $[H_2O]$ at low concentrations in D_2O to show that the rate determining step in the quenching of Ln fluorescence in H_2O was associated with the transfer of energy to a single vibrational mode (OH) which is subsequently excited to higher vibrational states[9]. The structure observed for Gd^{3+} (aq) was interpreted by Haas and Stein[32] as vibronic satellites due to coupling –OH or –OD to the 312 nm fluorescing state.

The ions with $\Delta E < 6500\ cm^{-1}$, namely Pr^{3+}, Nd^{3+}, Ho^{3+} and Er^{3+} and the ions Sm^{3+} and Dy^{3+}, which have very short lifetimes, barely luminesce in D_2O or H_2O[33]. These results were comparable to those pointed out by Barasch and Dieke in 1965[34] as characteristic of the $LaCl_3$ host. If the energy gap between the excited state and the next lowest level was less than $1000cm^{-1}$ no luminescence at room temperature was seen. This gap corresponded to an approximately 3 phonon process.

The gap in Gd^{3+}, however, is extremely large so multiphonon-like relaxation is a very high order, and thus low probability, process when the coordinating group is

OH[28]. Therefore there is no further detectable effect due to substitution of D_2O. The computed value of the lifetime of Gd^{3+} by Kropp and Windsor[28] based on integrated absorption measurements was 5.4 ms while that measured by Kondrat'eva and Lazeeva in 1960[35] was ~2 ms. It was concluded that non-radiative processes other than those associated with –OH modes must contribute to this relaxation process.

Hypersensitive bands

Although the crystal field is small, a number of band intensities have been found to be dependent on the ligands coordinated[36]. These are referred to as 'hypersensitive bands'[1, 3]. This phenomenon was observed from as early as 1930 by Selwood[37]. In his investigation of the effects of nitrate ion concentration on the spectra of various Ln, Selwood pointed out that one or two bands in the spectra of Nd^{3+}, Eu^{3+} and Ho^{3+} and Er^{3+} exhibited greatly increased intensities at high nitrate concentrations. Typical examples of hypersensitive bands are $^4G_{5/2} \leftarrow {}^4I_{9/2}$ for Nd^{3+}, $^5D_2 \leftarrow {}^7F_0$ and $^5D_0 \leftarrow {}^7F_0$ for Eu^{3+}, and $^3F_2 \leftarrow {}^3H_4$ for Pr^{3+}[1]. These hypersensitive bands were the result of transitions that followed the selection rules $\Delta J \leq 2, \Delta L \leq 2$ and sometimes $\Delta S = 0$ with possible exceptions[1]. In some environments the oscillator factor was observed to increased by an order of three[9].

Based on the Judd-Ofelt Theory Judd showed that the Ω_2 parameter most closely monitored changes in the environment and that hypersensitivity was strongly correlated with transitions having large matrix elements of $U^{(2)}$[10]. Mechanisms for hypersensitive transitions were examined by Jorgensen and Judd[38]. In 1966 Judd showed that the symmetry arguments could be brought in to classify site symmetries in which hypersensitivity might be induced. Hendrie *et al* looked at hypersensitivity in terms of a correlation which they found between oscillator strength and ligand basicity[39]. So far no consistent explanation has been found.

Energy Transfer

Energy transfer processes are studied in Ln ions such as Eu^{3+}, Tb^{3+}, Sm^{3+} and Dy^{3+} and their chelates as they make good model compounds because of their absorption and luminescence properties. This topic has been reviewed by Horrocks[40] *et al*[41, 42].

Intermolecular energy transfer is an important process in photochemistry and photophysics[4]. Its role, possible mechanisms and applications to mechanistic and practical problems in coordination chemistry have been previously outlined[43].

There are three main pathways via which intermolecular energy transfer may occur in a solution containing Ln ions or complexes[41]. (1) from singlet or triplet excited states of organic molecules to Ln ions or chelates. (2) from excited Ln^{3+} to organic molecules. (3) between Ln ions or chelates[44]. Intermolecular energy transfer between the excited triplet state of benzophenone and europium hexafluoroacetylacetonate was observed by El-Sayed and Bhaumik[45] in the early 1960s. Other reports of energy transfer from organic compounds to Ln ions were made by Almgren[46], Gelade[47] *et al*[48, 49]. Energy transfer from T_1 states of ketones and aldehydes to Ln ions was demonstrated by measuring the intensities of the acceptor emission[50]. After extensive investigations on the direct triplet energy transfer from various organic carbonyl compounds, Heller and Wassermann[48] concluded that a diffusion controlled collision process was the probable mechanism for excitation of Ln^{3+}. Work done by Filipescu and Mashrush[51] also confirmed this collisional transfer mechanism. In the mechanism shown in scheme 1 and the diagrammatical representation in figure 3, energy transfer from the lowest triplet state of the donor D (T_1) populates one of the luminescent levels (En) of the Ln ion via an intermediate level (Em). This results in emission from the (En) level[52].

Scheme 1[4]

$D(S_0) + h\nu \rightarrow D(S_1)$ (absorption) (eq 12)

$D(S_1) \rightarrow D(T_1)$ (intersystem crossing) (eq 13)

$D(T_1) + Ln \xrightarrow{k_q} D(S_0) + Ln(Em)$ (energy transfer) (eq 14)

$Ln(Em) \rightarrow Ln(En)$ (internal conversion) (eq 15)

$Ln(En) \rightarrow Ln + h\nu$ (luminescence) (eq 16)

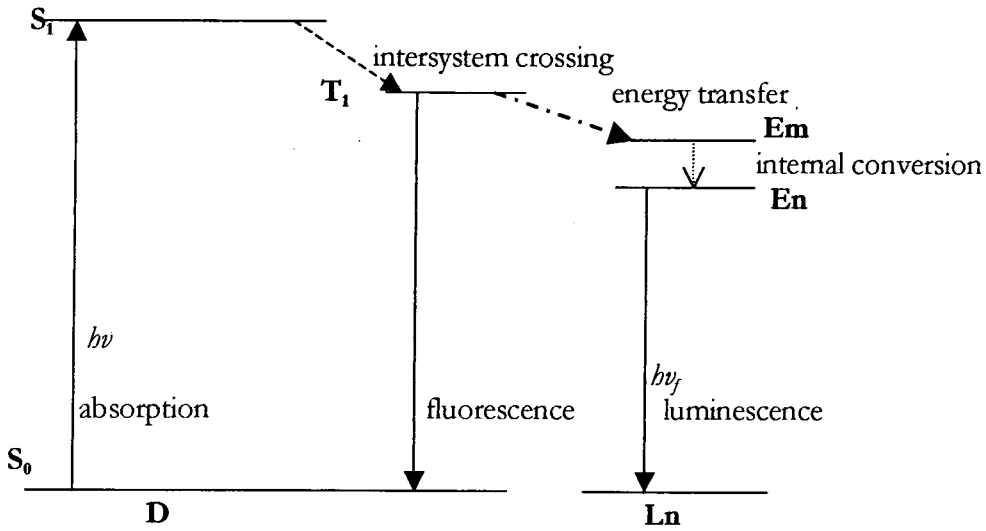

Figure 3. Energy level diagram illustrating the mechanism out lined in scheme 1.

Ln represents the trivalent Ln ion. The quenching rate constant (k_q) was determined from measurements of the time dependent decay of the triplet – triplet absorption of the ketones in the presence of Ln salts. Studies done by Filipescu and Muchrush[51] of the photoreduction of benzophenone derivatives in 2-propanol in the presence of Tb^{3+} confirmed this transfer mechanism. Values

of k_q were in the range $10^5 - 10^7$ M^{-1} s^{-1} and are much lower than the diffusion rate constant, which was about 10^{10} M^{-1} s^{-1}. This indicated that approximately one out of $10^3 - 10^5$ encounters of a triplet ketone with a Ln ion was effective for quenching[4]. These results and the lack of proportionality between k_q and the overlap integral of the spectra suggested a radiationless energy transfer by an exchange interaction mechanism[53]. Low temperature measurements made using steady state and phosphorescence decay techniques gave results which favoured the energy transfer mechanism over dipole – dipole, dipole – quadrupole and quadrupole – quadrupole interactions[54, 55].

The quenching of the excited singlet state of organic compounds by Ln ions has not been extensively studied. In 1969 Ermolaev and Shakhverdov[56] found some correlation between the overlap integral of the emission spectra of the organic donor and the absorption spectra of the acceptor and suggested that energy transfer was the cause of the fluorescence quenching. Eu^{3+} was observed to be the most efficient quencher of all the Ln ions, which indicated the involvement of an electron transfer process

$$D(S_1) + Eu^{3+} \rightarrow D^{\cdot+} + Eu^{2+} \qquad \text{(eq 17)}$$

This was later proved by Levin using flash photolysis experiments[57].

In the 1980s Sabbatini *et al*[58, 59] studied the quenching of both S_1 and T_1 states of a series of aromatic hydrocarbons by Eu^{3+} ions in acetonitrile using steady state and laser dynamic spectroscopy. The transient spectral changes in the visible region showed the presence of short-lived triplets and longer-lived radical cations of the aromatic hydrocarbons. These species were formed in about 20ns during the flash and the quenching of the triplet by Eu^{3+} is known to be a slow process ($\sim 10^6$ M^{-1} s^{-1}). It was assumed that the radical cations were derived from the singlet excited states.

The rate constant for quenching of the singlet states by Eu^{3+} is~ 10^{10} M^{-1} s^{-1}. Since the formation of radical cations and triplet species are the main quenching products, it indicates that the main processes involved are electron transfer and Eu^{3+} -induced intersystem crossing with the possible involvement of a charge transfer intermediate $[D....Eu^{3+}]^*$.

$$D(S_1) + Eu^{3+} \rightarrow D^{\cdot+} + Eu^{2+} \quad \text{(eq 18)}$$

$$\rightarrow D(T_1) + Eu^{3+} \quad \text{(eq 19)}$$

$$\rightarrow D(S_0) + Eu^{3+} \quad \text{(eq 20)} \quad [4]$$

Energy transfer from the S_1 state of aromatic hydrocarbons is energetically and spin allowed but does not make a significant contribution to the overall quenching constant. The dominant mechanism is electron transfer.

Eu^{3+} quenches aromatic hydrocarbons with very low rate constants. The energy transfer process for most hydrocarbons is endoergonic while the electron transfer process is strongly exoergonic for excited triplets and singlets.

$$D(T_1) + Eu^{3+} \rightarrow D^{\cdot+} + Eu^{2+} \quad \text{(eq 21)} \quad [4]$$

The energy transfer between excited states of aromatic molecules and Ln^{3+} chelates depends on the energy level of the Ln complex[4]. If the complex has ff* levels of the Ln ion above the T_1 of the ligand or no ff* levels (Lu^{3+} and La^{3+}) then sensitised ligand-localized phosphorescence is observed. If a donor has a higher triplet state energy than the T_1 state of the ligand the result is T-T energy transfer seen as ligand phosphorescence. An example of this process is seen when the benzophenone triplet state is used as the donor and $Gd(hfac)_3$ as the acceptor in ether pentane alcohol (EPA) glass at low temperature. A sensitised emission from the ligand of $Gd(hfac)_3$ appears while the benzophenone phosphorescence decreases. This points to an intermolecular energy transfer

process along with the fact that the presence of the heavy Gd ions does not enhance the T-T energy transfer[60].

In the case of complexes with low-lying ff* levels there is an efficient intramolecular energy transfer following the intermolecular energy transfer to the ligand localized triplet. This leads to emission from the ff* levels. This sensitised emission is seen for benzophenone and triphenylene as donor and $Eu(hfac)_3$ as the acceptor[45, 60] and is shown to be diffusion controlled. The evidence pointing to involvement of the ligand-localized T_1 state in the sensitisation process is the lack of red emission form Eu^{3+} when a mixture of benzophenone-$EuCl_3$ is used instead and for $Tb(acac)_3$, which has the ligand T_1 state close to that of benzophenone but has a high ff* level, emission is not observed however $Tb(hfac)_3$ has a triplet level lower than that of benzophenone and is sensitised by the latter.

The slow quenching of the excited triplet states by the Ln ions explains the first observation. $Ln(acac)_3$ where Ln=Sm, Eu, Gd, Tb and Dy, quenches the phosphorescence of benzophenone in benzene (and acetonitrile) with similar rate constants ($k_q \sim 6 \times 10^8\ M^{-1}\ s^{-1}$). Europium(III) and terbium(III) show sensitised emission and the results of Stern- Volmer analysis for quenching and sensitisation indicate energy transfer is the main quenching process. The diffusion controlled character of the of the energy transfer was indicated by comparing the rate constants of the quenching of benzophenone phosphorescence by $Tb(acac)_3$ and $Tb(hfac)_3$ with the donor acceptor energy differences. These data, along with similar values of Stern-Volmer quenching constants obtained for all $Ln(acac)_3$ used, were comparable with rate constants obtained from sensitised emission measurements which point to an energy transfer taking place from the triplet state of benzophenone to the ligand-localized triplet state of the lanthanide 1,3-diketonate chelates[61].

The luminescence of Eu^{3+}, Tb^{3+} and Dy^{3+} nitrate salts are quenched by organic compounds with triplet levels below or close to the emission levels of the Ln(III) ions[62]. The quenching occurs by a radiationless energy transfer via an exchange mechanism:

$$^{m}[Ln(III)]^{*} + {}^{1}Q \rightarrow {}^{n}[Ln(III)] + {}^{3}Q \qquad \text{(eq 22)} \qquad [4]$$

The quenching rate constants are lower than diffusion rate constants and depend on the possible coordinate bond formation between Ln ions and quencher molecules. They are strongly affected by temperature, solvent properties and possible penetration of quencher molecules into the first and second coordination sphere of the Ln(III) ions[4].

The non-radiative energy transfer from excited europium(III) and terbium(III) to dyes in solid and liquid solutions[63] and to organic radical ions[64] suggests that dipole-dipole energy transfer may also be a quenching mechanism

$$[Ln(III)]^{*} + {}^{1}Q \rightarrow Ln(III) + {}^{1}Q^{*} \qquad \text{(eq 23)} \qquad [4]$$

Solvent properties and interactions between dyes and Ln ions affect the rate constants. k_q is strongly influenced by electrostatic interaction forces between donor and acceptor in anionic and cationic dyes. The formation of neutral complexes with terbium(III) on the addition of acetate ion also affects k_q values[65].

Aromatic amines with T_1 states higher than the Ln emission levels are able to quench the luminescence of $Eu(NO_3)_3$. There is a proportionate decrease in the quenching rate constant with the increase in ionization potentials of the amines, suggesting an electron transfer mechanism for the quenching

$$^{m}[Ln(III)]^{*} + {}^{1}Q \rightarrow {}^{n}[Ln(II)] + {}^{2}Q^{+} \qquad \text{(eq 24)} \qquad [62]$$

Intramolecular energy transfer was first pointed out by Weissman who observed the atomic line emission of Eu^{3+} after the irradiation of the organic part of a europium complex[66]. He proposed that the internal energy transfer from the ligand to the 4f subshells of the Ln ion was responsible for the emission. Three mechanisms by which excitation energy can be transferred from ligands to Ln^{3+} have been put forward over the years[67-73]:

1) After intersystem crossing between the lowest singlet and triplet excited states of the ligand, energy transfer occurs from T_1 to a lower energy state (En) of the Ln (III) ion

$$S_1 \rightarrow T_1 \rightarrow En(ofLn) \rightarrow emission$$

2) There is a direct energy transfer from S_1 to a lower energy state (En) of the Ln(III) ion:

$$S_1 \rightarrow En(ofLn) \rightarrow emission$$

3) There is an energy transfer from S_1 to an upper intermediate level (Em) of the lanthanide (III) then back to T_1 to return finally to a lower energy level (En) of the Ln(III) ion before emitting:

$$S_1 \rightarrow Em(ofLn) \rightarrow T_1 \rightarrow En(ofLn) \rightarrow emission \qquad [4]$$

Mechanism 1 was demonstrated by Y.Matsuda[73] and other research groups. It was shown that europium dibenzoylmethide, $Eu(dbm)_3$ was excited by lanthanum dibenzoylmethide, $La(dbm)_3$, via intermolecular energy transfer between their T_1 excited states when a mixture of these two complexes was excited at 365 nm. Emission intensities for the direct excitation of Eu at 456 nm and the ligand at 365 nm were compared and gave clear evidence of an intramolecular energy transfer process from the chelate T_1 excited state to the Eu ion ^5D excited state.

Watson *et al*[74] reported the time resolved and spectrally resolved luminescence of several europium (III) and terbium (III) chelates in glass forming solvents using pulsed laser excitation to ligand localized singlet states. Watson concluded from his results and the literature data that the predominant energy transfer goes through a state as shown in mechanism 1. They also proposed a spin allowed enhanced intersystem crossing mechanism for the relaxation of the ligand localized S_1 state involving ^7F_j electronic levels of Eu(III) and Tb(III) complexes[4]. Studies on a series of Tb(III) and Eu(III) β–diketonates with ligands of different triplet energies were done by Sato and Wada[75] in 1970. They proposed that the energy transfer through the triplet state of the ligand takes place via an exchange interaction and an additional thermal deactivation process (via the triplet state) from emitting levels of Ln ions.

The emission from systems like terbium (III) complexes with a T_1 state below the $^5D_4$, from which emission is observed, can be explained as a direct $S_1 \rightarrow$ rare earth energy transfer (mechanism 2) as a dipole-quadrupole interaction. A study of the electronic relaxation processes of Ln chelates of benzoyltrifluroacetone and methylsolicylate was under taken by Tobita *et al* [76, 77]. They came to the conclusion that the paramagnetic properties of the metal ions significantly enhanced the radiative ($T_1 \rightarrow S_0$) and non radiative ($T_1 \rightarrow S_0$, $S_1 \rightarrow T_1$) rates from ligand-localized singlet and triplet excited states[4]. The luminescence properties of Ln β-diketonate chelates generally depend on the ligands, metal ions, solvents, temperature and weather they are tris or tetrakis form. These parameters must be considered when comparing the photophysical properties of these complexes. In the case of Eu(III) chelates the solvent and temperature effects are more complex because of the emission from both $^5D_1$ and $^5D_0$ levels. Fluorescence lifetimes from $^5D_1$ for most Eu(III) chelates is nearly the same regardless of the media and the nature of the ligands but fluorescence from $^5D_0$ depends on both the medium and the ligand type[78].

In 1990 Tran and Zhang [79] demonstrated for the first time energy transfer to the crown ether - lanthanide ions Eu^{3+}, Tb^{3+} and Dy^{3+} from benzoate counteranions. The lanthanide ion, crown ether and benzoate were compartmentalized into an ion pair complex to eliminate quenching and to induce energy transfer so the luminescence detection of the lanthanide ions could be selectively enhanced. The crown ether such as 18-crown-6 and 15-crown-5 were used as the synergistic extracting agent and the benzoate as the counter ion to selectively extract the Ln ions form water into an organic solvent where they were then determined by luminescence techniques.

The energy transfer occurred between the benzoate donor and the lanthanide acceptor when excitation was performed at 290 nm where only the donor absorbs significantly. Luminescence was observed as intense, narrow emission lines, which are characteristic of the Ln ions. The energy transfer in this case was the Förster type resonance energy transfer between the triplet state of the donor and the D states of the ion. According to Förster theory [80, 81] the efficiency of the energy transfer, E, between the donor and the acceptor is related to the actual distance of separation, r, and the critical distance for 50% energy transfer, R_0, by equation 25. R_0 is defined by equation 26 [82] where κ^2 is the orientation factor, ϕ_D is the quantum yield of the donor in the absence of acceptor, and n is the refractive index of the medium intervening between the donor and acceptor. J is the spectral overlap integral.

$$E = [1 + (r/R_0)^6]^{-1} \qquad \text{(eq. 25)}$$

$$R_0^{\,6} = 8.78 \times 10^{-25} \kappa^2 \phi_D n^{-4} J \qquad \text{(eq. 26)}$$

The distance between the donor and the acceptor could be as much as 100 A^0. Consequently the donor doesn't have to be directly chelated to the metal ion but just in close proximity as in the case of a counter anion. Benzoate was used as the counter anion because its absorption doesn't overlap with that of the Ln ions,

its triplet energy level of 27,000 cm^{-1} is much higher than the excited – state energy levels of the Ln ions and it is soluble in water as well as in organic solvents.

The luminescence of the Ln ions was substantially enhanced when they were extracted into the organic phase. In the case of the Tb^{3+} - crown ether – benzoate ion pair complexes in ethyl acetate, 325 nm excitation produced direct excitation of the Ln ion. The resulting low intensity emission spectrum was that characteristic of Tb^{3+} with narrow peaks centered at 494, 550, 597 and 625 nm. These peaks are attributed to the $^7F_6 \leftarrow {}^5D_4$, $^7F_5 \leftarrow {}^5D_4$, $^7F_4 \leftarrow {}^5D_4$ and $^7F_3 \leftarrow {}^5D_4$ transitions respectively. Excitation of this extracted ion pair at 290 nm produced a spectrum whose shape was the same as that obtained by 352 nm excitation but whose intensity was substantially higher than that of the 325 nm excitation. The benzoate anion's absorbance is 151 times more than the Ln ion at 290 nm so the enhancement in the observed emission is clearly due to energy transfer from the three benzoate counter anions to the Ln ion in the extracted ion pair complex. It was demonstrated that by using the donor aromatic compound as a counter anion, energy transfer from the donor to the rare earth ion acceptor could be achieved efficiently at much lower concentration.

The overlap integrals, J, were calculated for the Ln – crown ether – benzoate ion pair complexes. This value is a measure of the overlap between emission of the donor and the absorption of the acceptor. The luminescence enhancement was found to be in agreement with the overlap integral in that a higher enhancement value is obtained when the over lap between the donor emission and the acceptor absorption is large. The luminescence enhancement is highest for Eu^{3+} (67.6) and benzoate in agreement with the highest degree of overlap between their respective absorption and phosphorescence spectra ($J = 9.7 \times 10^{-16}$ cm^6 mol^{-1}). The Tb^{3+} ion and benzoate have the smallest overlap ($J = 1.1 \times 10^{-16}$ cm^6 mol^{-1}) and thus the lowest luminescent enhancement (23.4). This indicates that the energy transfer is governed by the Förster type resonance energy transfer from

the triplet state of the benzoate to the $^5D_4$ (Tb^{3+}), $^5D_0$ (Eu^{3+}) and $^4F_{9/2}$ (Dy^{3+}) states of the lanthanide ions. The magnitude of the luminescence enhancement by energy transfer was observed to be in reverse order with the lifetime of the lanthanide ions, which further confirmed that, the energy transfer is by the resonance mechanism rather than diffusion-controlled collisional transfer mechanism.

Beeby *et al* [83] have studied the time-resolved luminescence from the ytterbium ion in different solvents by direct excitation or energy transfer from co-dissolved chromophores and described examples of intramolecular energy transfer from energy matched aryl groups in stable complexes with aza-macrocycle based ligands. The time resolved studies of ytterbium offers opportunities for luminescent imaging in the near infrared and allows for the use of a wide range of aromatic antennae to sensitise the metal centre[83].

Ytterbium has one luminescent excited state ($^2F_{5/2}$) emitting at 980 nm ($^2F_{5/2} \rightarrow {}^2F_{7/2}$). Yb^{3+} is not readily reduced by simple aryl substrates so competitive photoinduced electron transfer to Yb from an excited singlet state of an antenna is not likely to occur. The possibility of intermolecular energy transfer from co-dissolved 4-carboxypropylpyrene (λ_{exc} = 355 nm, τ = 0.34 μs in 50:50 MeOH-H_2O) and 9-hydroxymethylanthracene (λ_{exc} = 266 nm, τ = 0.81 μs) was investigated. The lifetime of emission from the Yb centre was established by deconvolution and fitting of the decay curves. The lifetimes were much longer than neodymium in aqueous and methanolic solutions { τ_{H2O} [$Nd(NO_3)_3$]=30 ns, τ_{MeOH}[$Nd(NO_3)_3$]=70 ns} [84]. The differences are due to the Nd^{3+} being easily quenched by energy-matched O-H and C-H oscillators[84].

Demonstrating direct excitation of ytterbium in complexes and ytterbium salts is more difficult because its absorption and emission are very similar. Ytterbium was excited by using the output from a YAG driven optical parametric oscillator (OPO), which produced photons at 970 nm. Emission was observed in the low

energy tail of the emission band using a 1055 nm interference filter with a 40 nm band pass. The lifetimes were found to be solvent dependent. The lifetime was longer in strongly coordinated solvents, such as Me_2SO, in which the ligating group stretching harmonics do not correspond well to the energy of the Yb $^2F_{5/2}$ state. The luminescent lifetime of a (2-pyridazo)-2-naphthol and ytterbium complex with dibenzoylmethane (λ_{exc}=532 nm, H_2O) in a 3:1 ratio increased on solvent deuteriation. This is because the metal centre is not completely encapsulated by the complex formed in solution. Solvent molecules are thus able to quench the luminescence due to coupling between the O-H oscillators and the metal centre. Relaxation via O-D oscillators is much less efficient as only higher harmonics overlap with the metal excited state and the Frank-Condon overlap factor is less favourable.

Efficient intramolecular sensitisation of Tb^{3+} and Eu^{3+} by benzophenone-containing ligands has also been demonstrated by Beeby *et al* [85]. In this case excitation of the ketone, which has a triplet quantum yield of unity, resulted in very efficient sensitisation of the emissive states or the bound metal ions.

It has been shown that the triplet state of the chromophore plays an important part in energy transfer to the metal ion[84, 86]. The longer intrinsic lifetime of the triplet state means that it is likely to make a major contribution to the metal ion sensitisation. Substituted benzophenone has an n,π^* triplet state and a small singlet-triplet energy gap.

They prepared and studied the photophysical properties of ligand **1** (figure 4) in which a benzophenone moiety is coupled to 1,4,7,10-tetraazacyclododecane-1,4,7,10-tetraacetic acid (DOTA) via an amide linkage.

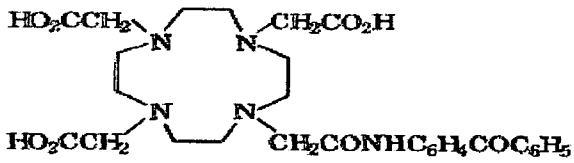

1

Figure4. Ligand 1[85]

Ligand 1 forms Ln(III) complexes of exceptional kinetic and thermodynamic stability[87]. The macrocyclic ligand effectively excludes water from the metal centre, which increases the efficiency of energy transfer. Kinetic measurements revealed interesting insights into the energy transfer mechanisms of the Eu and Tb complexes. The Tb emission was monitored at 545 nm and showed a rise time that was faster than the response time of the detection system, $\tau_{rise} < 50$ ns. The emissive $^5D_4$ state was probably formed in this time and hence the energy transfer step occurred with a rate constant of $>2x10^7$ s^{-1}. Eu emission showed a more complex kinetic profile. The intensity of the $^5D_0 \rightarrow {}^7F_1$ band was monitored at 595 nm to reveal two components to the raising edge of the signal. The first was rapid and contributed about 20% to the signal while the second had a lifetime of 1.45 ± 0.1 μs. The $^5D_1 \rightarrow {}^7F_1$ emission band was monitored at 583 nm and showed a short-lived emission and indicated that the lifetime of the $^5D_1$ state was 1.45 ± 0.1 μs. It was concluded that the europium complex energy transfer follows the scheme:

$$BP^* + Eu(^7F_0) \xrightarrow{i} BP + Eu(^5D_0)$$

$$BP^* + Eu(^7F_0) \xrightarrow{ii} BP + Eu(^5D_1)$$

$$Eu(^5D_1) \xrightarrow{iii} Eu(^5D_0) \qquad [85]$$

where BP* is the excited triplet state of the benzophenone moiety.

The triplet state of the benzophenone lies above the $^5D_1$ and $^5D_0$ levels of the Eu ion as shown in figure 5.

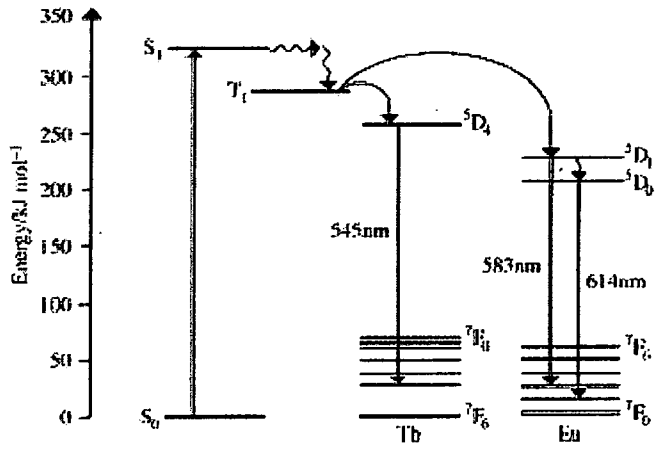

Figure 5. Energy level diagram showing the energy levels of the chromophore benzophenone and the two metal ions[85].

Hence energy transfer occurs rapidly via steps (i) and (ii) where k_i and k_{ii} $>10^7$ s^{-1} but the relaxation step (iii) occurs more slowly ,k_{iii} $=6.9x10^5$ s^{-1}. The decay and grow in times of the emission from the $^5D_1$ and $^5D_0$ states are illustrated in figure 6.

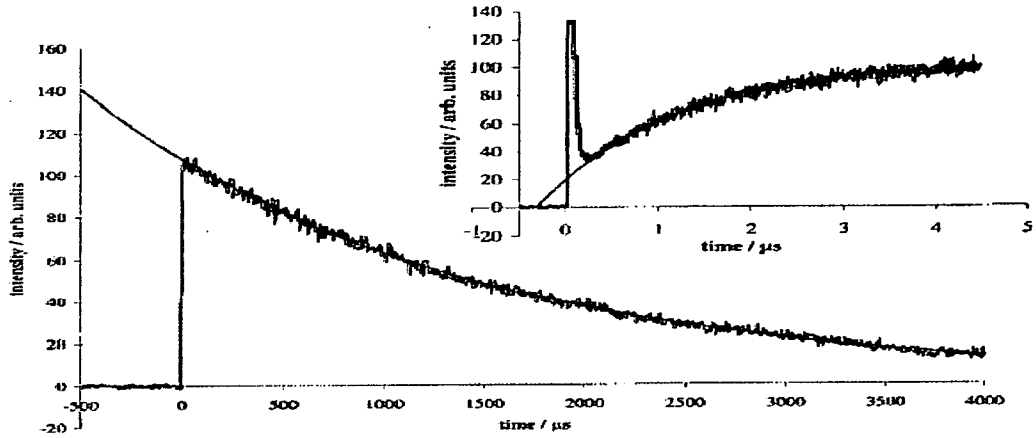

Figure 6. Time-resolved emission form Eu **1** in D_2O solution, monitoring the $^5D_0 \rightarrow {}^7F_1$ emission at 595 nm. The main curve shows the decay of the $^5D_0$ state, with a lifetime of 2.26 ms. The inset shows the rise-time of the signal, with saturation of the detector between t=0 and t=100 ns due to fluorescence. The characteristic lifetime of this rise is 1.45 ± 0.05 µs[85].

The Eu and Tb complexes showed two sets of emission bands in low temperature alcohol glasses. One set was characteristic of the emission bands of the metal center, the other of the benzophenone. The benzophenone was weak and short lived with an estimated luminescence quantum yield of < 0.01 and a lifetime of <200 μs. This indicated the Ln acceptor effectively quenched the triplet state of the benzophenone and that the energy transfer step is very efficient. It is expected that the triplet quantum yield would be unity and that the energy transfer should have a high efficiency. However the observed quantum yields are in the range 0.095-0.41 suggesting that the efficiency of the luminescence is limited to the efficiency of the Ln ion luminescence, which is determined by the relative radiative and non-radiative decay of the ions.

1.3 LANTHANIDES IN MICELLES AND SENSITISED EMISSION

Micelles

Micelles are colloidal – sized clusters of surfactant molecules in aqueous solution (Figure 7).

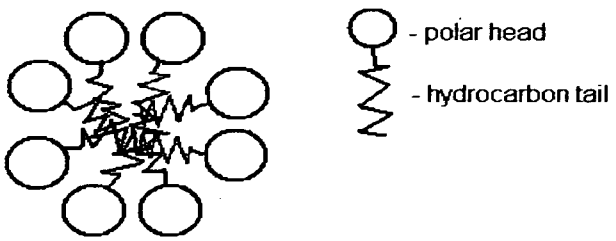

Figure 7. Simplified cross section of a micelle.

The clustering process can be described as $nS \leftrightarrow S_n$ where S represents the amphiphillic species and S_n is the micelle with a degree of aggregation n and occurs after the Critical Micelle Concentration. The reaction is reversible and is

shifted back to the monomeric surfactant by dilution. The surfactant molecules have the general formula RX in which R is a hydrocarbon chain and X is a polar head group. The hydrocarbon chain is generally C_8 or greater, saturated or unsaturated, linear or branched or may contain an aromatic ring[88]. The polar X group may be ionic or non-ionic. The non-ionic X groups are relatively short-chained polyoxyethylene moieties $-(C_2H_4O)_x-$, where x ranges from 3 to 20 or more. Examples of commercial surfactants of this kind include Triton X-45[88], Tween-21[88] Triton X-100[89]. The polyoxyethylene 'heads' of these molecules are essentially short chained polymers themselves and are thus generally polydisperse.

The most common anionic X groups are sulfate($-SO_4^-$), sulfonate($-SO_3^-$) and carboxylate($-CO_2^-$) while various quaternary ammonium groups ($-NR_3^+$) are common X substituents in cationic surfactants. The amphiphillic ion is accompanied by a counterion in ionic surfactants.

Micelles only form above the Critical Micelle Concentration (CMC) and the Kraft temperature. The CMC is detected by noting a pronounced discontinuity in the physical properties of the solution and can be observed by monitoring osmotic pressure, turbidity, surface-tension and the molar conductivity in the case of ionic surfactants[90].

Some generalisations can be made in regard to the state of aggregation and charge of micelles at the CMC. Firstly the aggregation number *n* increases as the length of the hydrocarbon chain increases. Studies suggest that the order of ion binding to negative micelles is $Cs^+ > Rb^+ > Na^+ > Li^+$ and for positive micelles $I^- > Br^- > Cl^-$. The larger ions that are more polarizable and that tend to be less hydrated bind more effectively[88]. For non-ionic surfactants with a polyoxyethylene chain, like Triton X, *n* decreases with increasing chain length for a constant R group. Factors that increase *n* lowers the CMC, and micelles tend to

be roughly spherical in shape with 50 – 100 amphiphillic units and relatively monodisperse.

Structure of micelles

It was Hartley (1936)[91] who gave the first definitive model for spherical micelles. The micelle core is predominantly hydrocarbon. A driving force behind micellization is the expulsion of the hydrophobic tails of the surfactant molecules from the polar medium. The molecules aggregate with their hydrocarbon tails pointing towards the sphere centre and their polar heads in the water at the surface. In ionic micelles a shell that is similar to a concentrated electrolyte solution surrounds the core. It is made up of ionic surfactants heads and bound counter ions in a region called the *Stern Layer*[88]. Water is present in this region as free molecules and as water of hydration. The counter ions in solution experience an electrostatic attraction drawing them to the micelle and thermal jostling which disperses them. The resulting equilibrium of these opposing forces is a diffuse ion atmosphere that makes up the second half of the double layer of charge at the surface. In non-ionic micelles the shell surrounding the hydrocarbon core is similar to a concentrated polyoxyethylene solution. The ether oxygens are heavily hydrated and the chains are jumbled into coils.

The micelles exist in a state of dynamic equilibrium. The spatial extension of the hydrocarbon chains varies with rotations around the carbon – carbon bonds resulting in the head being pulled deeper into the core or allowing it to protrude into the Stern layer. Also the water molecules and ions are free to come and go from the surface. The micellar surface is thus not sharply defined on a molecular scale. The hydration of bound ions and ionic surfactants are about the same in the micelle as would be observed for the independent ions. There is no evidence of a dehydration contribution to the ΔH of micelle formation. The bound counter ions in the Stern layer in ionic micelles help to overcome the electrostatic repulsion between the charged heads of the surfactant molecules.

Reverse micelles

Amphiphillic molecules in non-aqueous media cluster with their polar heads together in the micellar core and their tails in the organic phase. Water is solubilized in the core of these structures, which are known as reverse micelles or microemulsions. Aerosol –OT, Triton X-100 and various Spans[88] are widely used in the study of reverse micelles. The hydrophobic effect does not contribute to in the formation of reverse micelles. Specific interactions between head groups in the micellar core hold the surfactant molecules together, which are actively involved in reverse micelle formation. The differences in the solubility parameters of the hydrocarbon tail of the surfactant and the solvent also contribute to reverse micelle formation. Spontaneous reverse micellization is due to a large negative enthalpy change with an unfavourable entropy change opposing micellization. For reverse micelles n is 10 or smaller[88]. When water is solubilized in these micelles n increases. Consider the well studied surfactant Aerosol-OT. Close packing of the polar heads leaves an empty space in the centre of the micellar core that can only be filled with hydration water. Thus the presence of water is necessary for the formation of large surfactant aggregates[92].

Surfactant molecules packing

The surfactant can be represented geometrically by a cone when in a normal micelle system and as a truncated cone in a reverse micellar system. The respective ranges of hydrophobic and hydrophilic part interactions determine the dimensions. Ionic surfactants have small polar heads. The *surfactant parameter* gives a good indication of the shape of the aggregates, which form spontaneously. This parameter is expressed as

$$\frac{v}{\Sigma l} \qquad \text{(eq 25)} \qquad [92]$$

Where v is the surfactant molecular volume, Σ is the area per polar head group and l is the length of the hydrophobic chain. The value of the surfactant parameter determines weather spherical, rod like, lamellar or reverse micelles are formed.

If:

$\frac{v}{\Sigma l} < \frac{1}{3}$ -spherical micelles form in water

$\frac{1}{3} < \frac{v}{\Sigma l} < \frac{1}{2}$ -rod like micelles form in water

$3 < \frac{v}{\Sigma l}$ -spherical reverse micelles form in oil

Limitations on the composition of reverse micelles and inter micellar interactions are discussed in books by Pileni and others[88, 92, 93].

Role of micelles in energy transfer

Micellar assembles provide convenient micro heterogeneous systems in which ions and molecules can be held in close proximity so that the dynamics of the energy transfer may be studied and perhaps exploited[44]. Considerable understanding of membrane-mediated interactions has been obtained through the investigations of model systems[94]. In 1980 Love, Skrilec and Habarta[95] demonstrated the first analytical application of micelle stabilized room temperature phosphorescence in aqueous solution. They also showed that even for species with small Stokes shifts, interference from scattered light and fluorescence are diminished in micellar systems. This allows for the use of conventional fluorimeters to measure the phosphorescence of many compounds of interest. Structural information can be provided from the determination of

energy transfer from the photo excited donor to an acceptor, localized in different parts of given membrane models[96].

Intramoleular energy transfer from ligand molecules to Ln complexes is well known[74, 78, 97]. Theoretical arguments[98] and high pressure studies[99] suggest that the transfer is from the triplet state of the donor to an approximately isoenergetic state of the Ln ion. One reliable way of demonstrating the states involved in energy transfer is to show the identity of the decay time of the donor state and the rise time of the acceptor state under a range of experimental conditions[44]. For an organic triplet donor state and a Ln acceptor state it is difficult to achieve this demonstration in practice because the phosphorescence quantum yield of the donor triplet state is very small and it may occur in the same spectral region as the emission from the acceptor Ln ion state[44].

The interaction between the complex ions and the micelle are not significantly strong for the excited state energy levels to be greatly affected. However the radiative and non-radiative rates for excited state relaxation are markedly different for cations associated with the anions associated with micellar surfaces and the cations in free solution[100]. Three main factors contribute to this difference as outlined by Flint and Dong for $Ln(pdc)_3^{3-}$ (pdc-pyrine 2,6- dicarboxylate) ions in dilute aqueous cetyltrimethylammonium (CTA) micellar solution[100]. Firstly the rate of excited state non-radiative relaxation is reduced by the presence of the micellar 'head' which excludes water from the outer coordination sphere of the complex ion. Secondly the $Ln(pdc)_3^{3-}$ complex is distorted from its idealised geometry by the electrostatic effect of the head groups that results in an increase in the transition dipole and thus the radiative relaxation rate. Thirdly the electrostatic and steric effects of the neighbouring anions on the micellar surface cause further distortion.

In previous investigations of Ln acceptors and organic donors in micellar systems in the late 1970's energy transfer was not observed from micellar phenanthrene to

Eu aqua ion[46] and the triplet was not observed directly whilst energy transfer between micellar naphthalene and Tb aqua ion was shown by Fendler[94]. About ten years later Darwent, Flint and Sharpe[44] demonstrated that long lived emission from the $^5D_1$ state in tris(dipicolinato)europium(III) $[Eu(PDC)_3]^{3-}$ was due to energy transfer from the phenanthrene triplet state. It is likely that the initial energy transfer to the Eu centre occurs to the $^5D_2$ state of the $[Eu(PDC)_3]^{3-}$ as this energy level is close to the phenanthrene triplet state. However the $^5D_2$ excited state relaxes non-radiatively too quickly for significant emission to be detected.

Under the conditions stated by Sharpe[44], the cetyltrimethylammonium micelles would be occupied by a single phenanthrene molecule and the majority of the $[Eu(PDC)_3]^{3-}$ anion concentration would be on the positively charged micellar surface. The phenanthrene singlet state was generated by 347 nm radiation from a ruby laser and underwent intersystem crossing to give the triplet state (T_1). The decay of this triplet state was monitored by the transient $(T_1 \rightarrow T_2)$ absorption at 490 nm and gave a rate constant $k_T = 9.1 \pm 0.3 \times 10^4 s^{-1}$ [44]. Sensitised emission from the $^5D_1$ state of the Ln ion complex was monitored at 540 nm $(^5D_1 \rightarrow {}^7F_1)$. It was found to decay exponentially with a rate constant $k_1 = 8.5 \pm 0.3 \times 10^4$. The emission from $^5D_1$ is very weak in the absence of phenanthrene with a rate constant $k_1 = 9.6 \times 10^5 s^{-1}$ which is typical of Eu complexes in aqueous solution[44]. The phenanthrene triplet energy closely matches that of the $^5D_2$ state of $[Eu(PDC)_3]^{3-}$ and it was suggested that the initial transfer to the Eu centre occurs to this state which then relaxes non-radiatively before any emission can be detected. The emission from the $^5D_0$ state of $[Eu(PDC)_3]^{3-}$ was monitored at 616 nm $(^5D_0 \rightarrow {}^7F_2)$ and the rise time was found to be exponential with a rate constant of $k_{ET} = 1.16 \pm 0.08 \times 10^5 s^{-1}$. The emission was found to decay on a millisecond time scale, which is characteristic of a well shielded Eu^{3+} complex in solution. It was concluded from these results that the energy transfer process was

phenanthrene $T_1 \rightarrow Eu(^5D_1) \rightarrow Eu(^5D_0)$. The fact that admission of oxygen quenched the triplet added to the evidence that the before-mentioned process is occurring.

In 1993 Darwent, Flint and Sharpe[101] reported a new phenomenon while working with $Tb(pdc)_3^{3-}$ phenanthrene systems in a CTA micellar solution. The $^5D_4$ state of $Tb(pdc)_3^{3-}$ is 1200cm^{-1} below the phenanthrene triplet state and energy transfer from the phenanthrene T_1 state to Tb does not dominate. The $T_1 \rightarrow T_2$ transition of phenanthrene is isoenergetic with the $^5D_4 \rightarrow {}^7F_6$ Tb transition. 347 nm excitation populates both the phenanthrene S_1 state and the highly excited Tb states. Rapid radiationless relaxation results in the population of the T_1 state of phenanthrene and the terbium $^5D_4$ state. It was proposed that the initial rapid decay of the $^5D_4$ metal localized state was due to resonant energy transfer to the triplet phenanthrene molecules, which resulted in the excitation of the phenanthrene molecules to the T_2 state. This significant donor-acceptor resonance coupling was said to be a result of the organisation afforded by the micellar assembles.

It has been shown that micelles provide charged surfaces on which energy transfer can occur as well as hydrophobic interiors in which neutral molecules may be localized. It is possible to hold two or more molecules inside the micelle so that the mean distance between these molecules is small and the resulting energy transfer is significant. It has also been shown that the mean distance between a molecule in the interior and one on the surface is also small enough for energy transfer from the interior to the surface or visa versa is possible. Studies on Ln micellar systems and energy transfer in these systems have been done by various groups including E.Gelade' *et al*[102], A. G. Mwalupindi *et al*[103, 104] Beeby *et al*[105] and others[46].

1.4 POLYARYLETHYNYLENES

Conjugated Polymers.

Polymers containing loosely held electrons in their backbones are often referred to as conjugated or conducting polymers[106]. They initially attracted interest over 20 years ago when it was observed that the doping of polyacetylene, at a level equivalent to removing/adding an electron in one out of 5-15 repeat units, increased the conductivity of the matrix by many orders of magnitude[106]. The electrons in these delocalised systems are easily polarized by an external electric field such as that found in light. Polyarylethynylenes contain carbon-carbon triple bonds between aryl rings. Their conductivity and structural rigidity is highly dependent on the presence of the triple bond. The low barriers to rotation of adjacent aryl rings suggest that in solution any dihedral angle between two aryls rings can be assumed.

Electroluminescent conjugated polymers are fluorescent polymers which emit light when excited by an electric current[107]. Their discovery has led to major developments in the molecular electronics industry and they are set to challenge the domination by inorganic materials of the commercial market in light emitting diodes (LEDs). These polymers are particularly versatile because their physical properties can be fine-tuned by the manipulation of their chemical structures[107]. An increased understanding of the processes involved in device function and breakdown, and the systematic modification of the properties of the emissive polymers by synthetic design, has become a vital component in the optimisation of light emitting devices[107]. Fluorescent polymers are used to make LEDs such as backlights for crystal displays and emissive material in alphanumeric displays in the near future[107]. Conjugated polymers like dialkyl-substituted poly(*p*–phenyleneethynylene)s are organic semiconductors and therefore have applications in photonic and electronic devices. Examples include polymeric LEDs, plastic lasers and polymer based photovoltic cells[108]. In

principle, conjugated polymers should be able to carry out all the functions of an inorganic semiconductor and in the future may be used in molecular electronics.

The structure of all conjugated polymers, with the exception of polysilanes, have the same signature. Each atom along the backbone is involved in a π bond, which is much weaker than the σ bonds holding the atoms in the polymer chain together[106]. The linear π-conjugation which runs along the principal molecular axis is dependent on the relative orientation of the planar aromatic moites[109]. When conjugated, these π bonds can delocalise over all atoms. The single bonds, even when part of a conjugated system, can rotate once given the thermal energy available at room temperature. The rotational potential of a single bond in polyacetylene was calculated as about 25.2 kJ/mol and 12.6 kJ/mol in polythiophene (gas phase calculations)[110] (figure 8). The delocalisation of the electrons in the π system is reduced by these rotations. A case in point is the thermochromism of polythiophene derivatives.

PP PT

Figure 8. Structure of the repeat units of the conjugated polymers trans-Polyacetylene (PP) and Polythiophene (PT).

The lowest energy optical absorbance in a conjugated chain is typically due to a $\pi \rightarrow \pi^*$ transition. The more conjugated the double bonds are in the polymer the lower the energy of this absorption. Therefore, twisting about the chain will reduce the amount of conjugation and increase the energy (i.e. blue shift) the absorption[111].

Baeriswyl *et al* reviewed advances in theoretical modelling of π-conjugated polymers. It was found that neither the Hückel/Su-Schrieffer-Heeger (SSH) nor the Pariser-Par-Pople (PPP)/Hubbard models are sufficient for a complete description of the observed behaviour of these polymers[112]. They concluded that in the first approximation π-conjugated polymers could be interpreted as quasi-one-dimensional materials in which electron-phonon and electron-electron interactions both play crucial roles [112]. The non-linear excitations originally associated with purely electron-phonon interactions are expected to survive in the presence of electron-electron interactions. However detailed calculations of their properties requires the use of many-body techniques which are substantially more demanding than those used to solve independent-electron theories.

The effect of ring torsion in conjugated polymers on their photophysical properties

Brédas *et al* [113] and Ginder and Epstein[114] established the use of quantum chemical modelling to study the effects of ring torsion in conjugated polymers. In 1985 Brédas presented *ab initio* Hartree-Fock and Valence Effect Hamiltonian (VEH) calculations on polyparaphenylene, polypyrrole, and polythiophene dimers and polymer chains. The derivatives of these compounds have substituents that increase the torsion angle between adjacent rings. The evolution of electronic properties, such as the ionisation potential, the band gap and the width of the highest occupied bands and the carbon-carbon bond length between rings, were examined as a function of the torsion angle between consecutive rings. They determined that on moving from a coplanar to a perpendicular conformation, the ionisation potential and band gap values increase and the width of the highest occupied bands decreases. This makes it more difficult to ionise or reduce the polymer chains and can result in achieving lower maximum conductivities on doping[113]. The evolution of the electronic properties was found to follow a cosine law, which is related to the decrease of the overlap between the π orbitals on adjacent rings. Thus modifications up to a ~40^0 torsion angle are not very

large. For example, the ionisation potential value for a 40^0 torsion angle is about 0.04 eV larger than that of the coplanar conformation value. Thus substituents that lead to torsion angles between consecutive rings smaller than 40^0 are acceptable.

In 1998 Fahlman *et al* [115] carried out an experimental and theoretical study of ring substituent induced effects on the structural and optical properties of poly(*p*-pyridylvinylene phenylenevinelyne)s (PPyVPV). This new class of PPyVPV based polymers was synthesised for use as an active material in light emitting diodes[115, 116]. The effects of ring substitutions on the optical absorption and photoluminescence energies were qualitatively explained through the use of semiempirical quantum chemical modelling of the ring torsion angles.

Ring substituents were used to improve the solubility of the PPyVPV polymers. The addition of substituents to phenylene rings can affect the electronic structure, both directly by withdrawing or donating charge and thereby lowering or raising the energy bands and indirectly by sterically induced ring torsion[115]. Ring torsion strongly affects the optical band gap and bandwidths and thus the wavelengths of the absorption and luminescence. Inter-ring torsion has a lesser effect on the photoluminescence maximum. The excitons tend to migrate to the lowest energy segment of the polymer chain, i.e. the most planar one, before recombining and emitting light[113]. Thus photoluminescence is associated with the most planar segments of a polymer, where as optical absorption gives an average of the various band gaps/ring torsions of the polymer solution or film[115].

Fahlman theoretically proved that the ring substitutions affect the polymer backbone of the structures in (Figure9). The (C2-C3-C4) bond angle, for example, in (a), (b) and (d) is much larger than that for (c) and (e). This is due to steric interactions between the ring substituents and the hydrogen attached to C4.

The methoxy oxygen in (c) forms a weak hydrogen bond with the C4 hydrogen. This results in the (C3-C2-O) angle being reduced to 115.4^0.

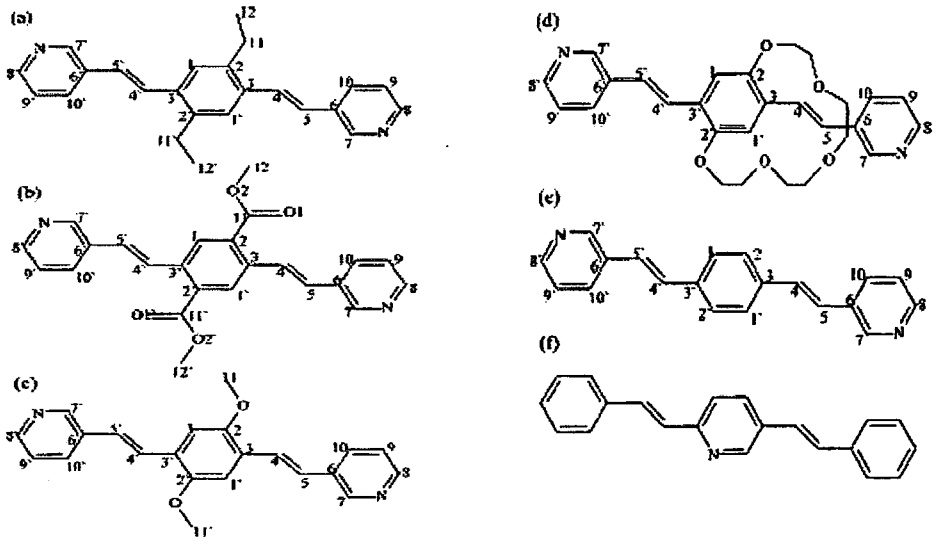

Figure 9. The molecular structures of three-ring oligomers of (a) diethylsubstituted Poly(*p*-pyridylvinylenephenylenevinylyne); (b) diformylsubstituted Poly(*p*-pyridylvinylenephenylenevinylyne); (c) dimethoxysubstituted Poly(*p*-pyridylvinylenephenylenevinylyne); (d) (alkoxy) strapsubstituted Poly(*p* pyridylvinylenephenylenevinylyne); (e) unsubstituted Poly(*p*-pyridylvinylenephenylene-vinylyne) with a center phenyl ring; (f) unsubstituted poly(*p*-pyridylvinylenephenylene-vinylyne) with a center pyridyl ring[115].

The torsion potential curves associated with the rotation of the middle ring while the outer rings were fixed in position for the structures (a) to (f) have been computed. Figure 10 shows the potential energy curves for (f) and (b). The lowest energy conformation of (f) had a torsion angle of 5^0. The barrier towards a coplanar conformation was less than 0.42 kJ/mol when compared to the lowest energy conformation of (f) and the torsion potential curve between +30^0 to –30^0 is relatively flat. The potential curve for (c) is somewhat similar and the barrier towards coplanar conformation was found to be 0.55 kJ/mol. The barrier

towards 0^0 torsion in (c) and (f) is so small that solid state packing is likely to drive the trimer/polymer into a coplanar conformation in films as is the case for poly(phenylene)vinylene (PPV)[117] and stilbene[118]. The barrier toward 90^0 rotation in (f) was found to be 15.96 kJ/mol. Substituents on the external phenylene rings do not affect the torsion potential curve for rotation of the pyridine ring. The low barrier in (c) is attributed to a weak hydrogen bond being formed between the methoxy oxygen and the C4 hydrogen, which locks the geometry into a coplanar conformation.

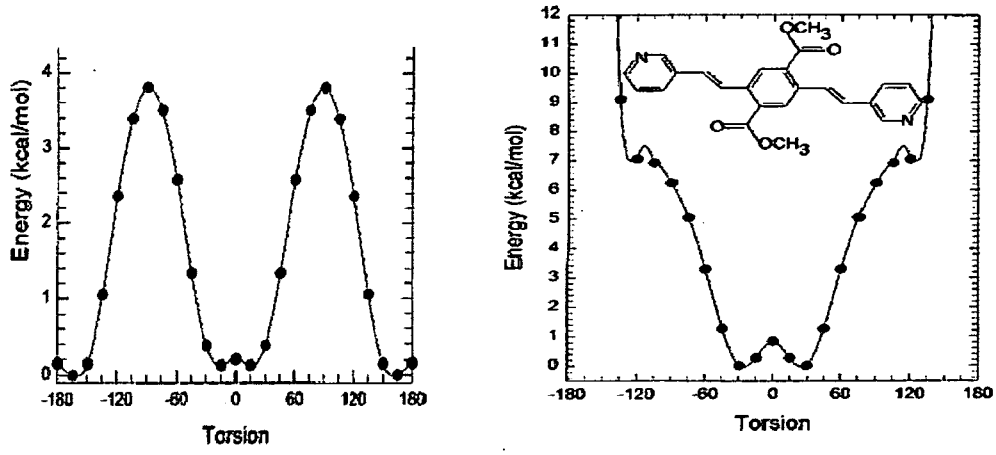

(A) (B)

Figure 10. (A) Potential energy curves associated with torsion of the middle pyridine ring in a phenylenevinylene–pyridine–vinylenephenylene trimer (f). All energies are given relative to that of the fully optimised conformation. (B) Potential energy curves associated with torsion of the diformyl substituted middle (phenylene) ring of trimer (b). All energies are given relative to that of the fully optimized conformation[115].

In the case of structure (b) where two formyl groups substitute the phenyl ring the barrier towards a coplanar conformation is 3.36 kJ/mol. This increase is due to the double bonded oxygen sterically interacting with the vinylene hydrogen[115]. The relatively low barrier suggests that angles between $|15^0|to|35^0|$ are present in films due to solid state packing. In solution the torsion angle would be approximately that of the energy minimum ~32^0.

The alkoxy chain, or strap, attached at the 2,5 ortho positions of the phenylene ring in (d) decreases aggregation in films. The luminescence and hence efficiency of LEDs is quenched by states formed due to aggregation. This alkoxy strap forms an ellipsoidal cross section, ~5x7A^0, which is nearly perpendicular to the direction of the polymer backbone. Although the oxygens in the alkoxy strap are chemically similar to the methoxy oxygen in (c) the expected hydrogen bonding does not result in a lower barrier of rotation than that determined for (c). The barrier toward coplanar conformation in (d) is 6.3 kJ/mol. The region between $|10^0|to|35^0|$ on the potential energy curve is relatively flat so torsion angles as low as $|10^0|$ are likely to be found in films due to solid state packing. The fully optimised geometry produces a torsional angle of 24.2^0, which is larger than case (c) but less than case (b).

Figure 11 shows the geometrical structures of the phenylene ring substituted PPyVPV polymers studied using absorption and photoluminescence spectroscopy. Figure 12 depicts the photoluminescence and absorption spectra of these polymers. Shifts in absorption and photoluminescence data can have several origins[115]. For polymers with large torsion angles and small barriers towards coplanarity, solid state packing in films can drive the system into a more coplanar configuration. This decreases the torsion angles and hence decreases the band gap thus affecting absorption and PL (photoluminescence) maxima. Aggregation in polymer chains in films may also cause a decrease in absorption and PL energies due to the formation of low energy aggregation states[115].

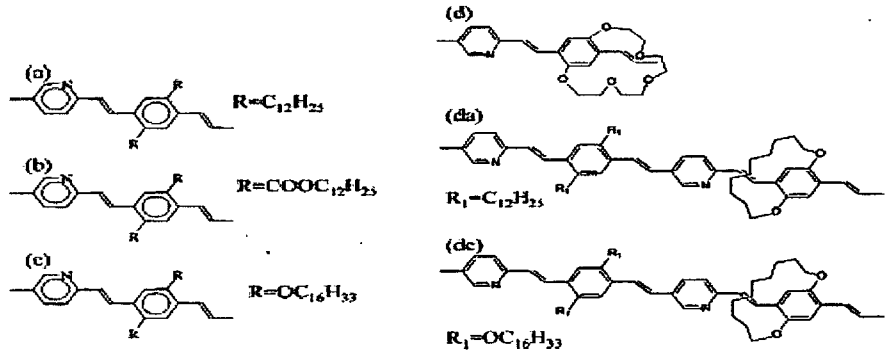

Figure 11. Geometrical structures of a group of phenylene ring substituted *p*-pyridylvinylenephenylene–vinelyne polymers[115].

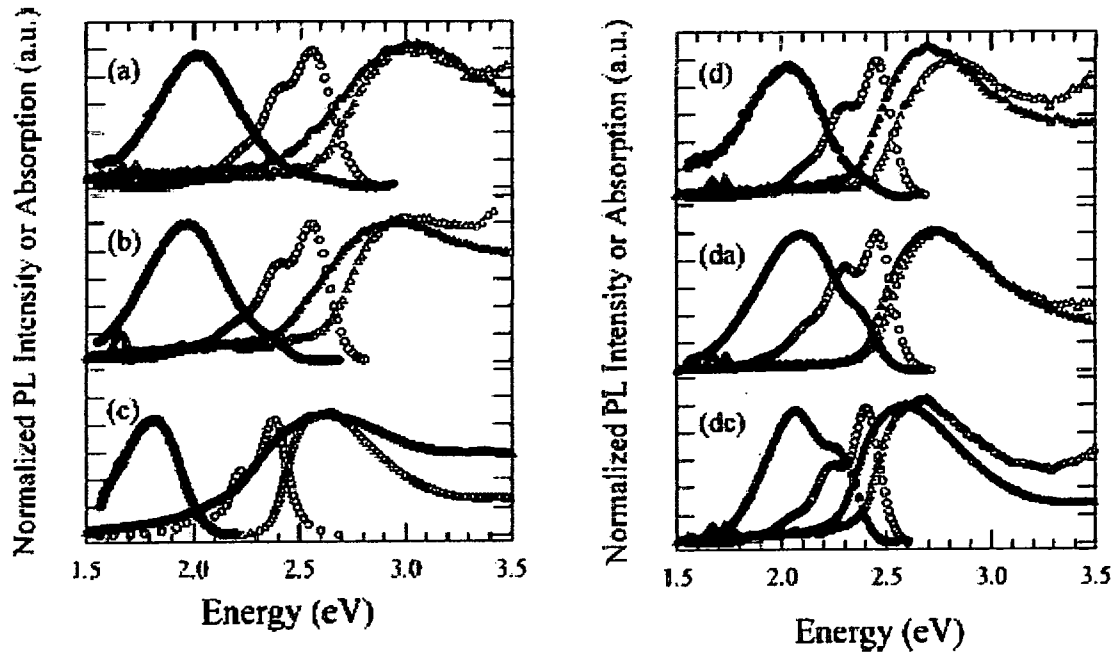

Figure 12. Photoluminescence (o●) and absorption (Δ▲) spectra for a group of phenylene ring substituted *p*-pyridylvinylenephenylenevinelyne polymers, geometries given in Fig11. Solution spectra (oΔ) and spectra from spun films (●▲) are shown for all polymers (a), (b), (c), (da), (d), and (dc)[115].

The absorption data agreed with the trends predicted by the calculations for both the films and the solutions. Polymers (b) and (a) have the highest energy absorption maximum in solution followed by (da), (d), (dc), and (c) in agreement

with predictions of (b) and (a) having the largest torsion angles[115]. The shift in absorption maximum when going from solution to film for polymer (b) (3.08 eV to 2.95 eV) agrees with the flat torsion potential region between $|35^0|to|15^0|$ and the relatively low barrier towards coplanarity (3.36 kJ/mol). A similar shift for polymer (d) (0.15 eV) is also attributed to the flatness of the of the torsion potential curve between $|35^0|to|10^0|$ [115]. Lesser shifts are expected for (da) and (dc) since the band gap is partly determined by the dialkoxy and dialkyl substituted phenylene rings, which are not expected to be significantly affected by solid state packing effects due to the shape of their torsional potential curves. The experimental data was found to be in agreement with their theoretical modeling. No significant shifts were expected for (a) as it has a sharp minimum at $\sim|30^0|$ with a high barrier to rotation of 8.4 kJ/mol which is unlikely to be overcome by solid state packing[115]. (c) has an optimal torsion angle of $|1^0|$ and is thus coplanar. The shifts (0.03 eV) were substantially smaller than those for (b) and (d) as was expected.

The PL maxima follow the same trend as the absorption maxima, the only change being a smaller energy difference which is the result of the excitons migrating to the lowest energy segments of the polymers. Based on the inter-ring torsion angles, with polymers (a) and (b) having the highest energy solution PL maxima, the experimental data were in qualitative agreement with the theoretical predictions. Both (b) and (c) had a PL energy difference of 0.17 eV which was less than the 0.44 eV difference in the absorption maxima as predicted.

The film data was expected to be of lower energy. By comparing of the energy of the position where the intensity is 20% of the absorption maximum (Abs edge), the shift between the solution and film data is found to be notably lager for the unstrapped cases. This suggests a greater fraction of aggregation states in these films[115]. For example, in comparing the absorption spectra of (a) and (da) the

shifts in the Abs edge in going form solution to film are 0.16 eV and 0.03 eV. This trend is also seen in the PL data. Going from solution to film the PL shifts are 0.54 eV for (a) and 0.38 eV for (da). The data showed that aggregation effects are greatly reduced by the strap substituents. This results in higher PL maxima in films with strapped polymers.

Poly(1,4-phenylene vinylene) (PPV) is a bright yellow fluorescent polymer with emission maxima at 551 nm and 520 nm. It is insoluble, intractable and infusible. It yields high-quality transparent thin films for the production of electroluminescent devices. Poly(*p*-phenylene ethynylenes) (PPE) has much more rigid polymer chain and shows yellow emission with a maxima at approximately 600 nm.

Fiesel *et al*[119] studied dialkyl-poly(*p*-phenylene ethynylenes)s (PPEs) in solution and showed that aggregate formation is accompanied by a dramatic shift in their UV/vis spectra. In the aggregated state a narrow red shifted band at 440 nm is reported. This solvatochromic effect is indicative of an order – disorder transition in dialkyl- substitued PPEs[111].

The monomeric and polymeric systems of PPEs are being studied as possible alternatives to PPV. They are the structurally closest relatives to PPV and have demonstrated properties which are applicable to explosives detection, molecular wires in bridging nanogaps, and polarisers in liquid crystal displays (LCDs)[108]. PPEs have been investigated as possible polymeric LEDs in electrolumenescent devices[108, 120]. Studies by Schmitz *et al*[120] of LEDs based on alkoxy-substituted poly(*p*-phenylene ethynylene) (EHO-OPPE) as an emitter material in combination with polytriphenyldiamine as hole transport material demonstrated the ability to improve devices and optimisation through careful design of device structure and composition. They reported increases in brightness from 4 cd/m^2 for a device of pure EHO-OPPE to 260 cd/m^2 in a device with 25% EHO-OPPE and 75% poly(N,N'-diphenylbenzidine diphenylether) as the hole-

transporting layer and an additional electron-transporter/hole-blocking spiro-qux layer[120].

It is known that the movement of exitons along a conjugated polymer back bone is strongly dependent on the interaction and orientation of an individual polymer relative to its neighbours[121]. Inter-chain distances greatly affect the performance of electrooptical devices based on conjugated polymers. McQuade *et al*[122] studied the relationship between cofacial interpolymer distances and solid-state photophysics. In both small molecules[123] and polymers[124] close association of π-systems causes a substantial decrease in the PL quantum yield relative to the isolated chromophores. However minimizing interpolymer distance is necessary for optimal energy transfer of excitons between polymer chains[124]. They synthesised polymers with varying degrees of side chain bulk as this influences the packing of the polymers at the air –water interface. Figure 13 (A) shows the PPEs containing a substitution where the hydrophilic and hydrophobic groups are para to each other producing an edge-on organisation at the interface.

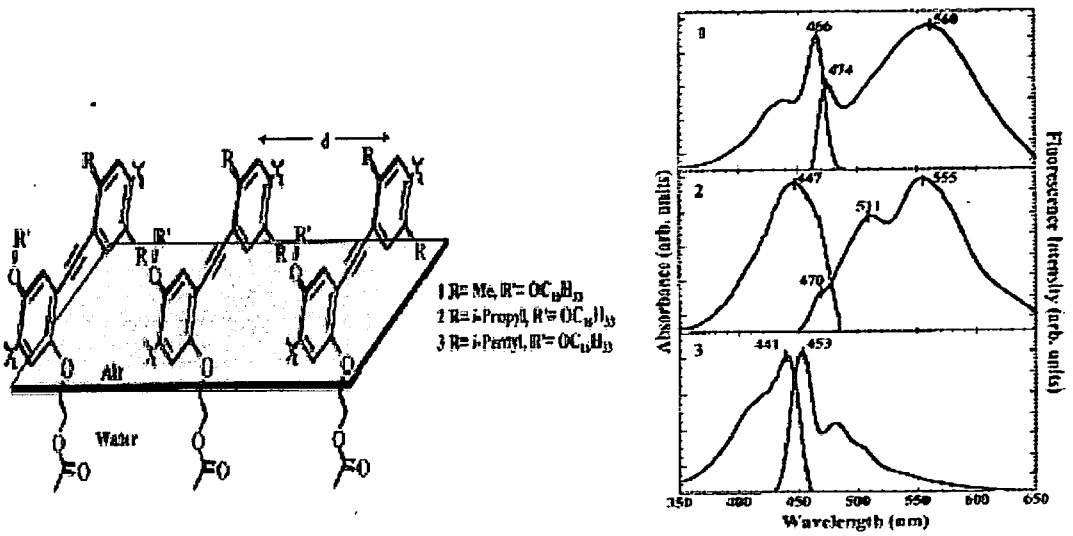

(A) (B)

Figure 13. (A) PPEs containing substitution where the hydrophobic and hydrophilic groups are para to each other producing an edge on organisation. (B) Normalized UV-vis and PL spectra of the monlayer LS films of polymers **1-3** cast onto hydrophobic glass slides[122].

Figure 13 (B) illustrates the normalized UV-vis and PL spectra of the monolayer Langmuir-Schaefer (LS) films of the three polymers studied. It is observed that PPE films composed of polymers that do not strongly π-stack display a broad absorbance spectrum with a λ_{max} between 440 nm and 450 nm and a narrowed emission spectrum with a λ_{max} between 450 nm and 470 nm. The absorption and emission spectra of polymer **3** (with an inter-chain distance of 4.9 A^0) are representative of this. In contrast, the UV-vis spectrum of polymer **1** (with an inter-chain distance of 4.0 A^0) had a sharp band at 466 nm in the LS film (figure 13 (B)) that is not seen in the solution spectra. This band is attributed to strong inter-chain π-stacking[122] and planarization of the aryl rings[125]. The LS film of polymer **2** (with an inter-chain distance of 4.4 A^0) did not contain a new band but had a red shifted λ_{max} of 12 nm relative to the solution data. The lack of a new band is indicative of the isopropyl groups diminishing π-stacking. The solid state PL spectrum of polymer **3** shows much sharper peaks than the PL spectra of polymers **1** and **2** which indicated the inter-chain spacing of **3** is lager than the distance required for the chains to form emissive aggregates and thus **3** had the

highest PL quantum yield of 16%. The PL quantum yield values of **1** and **2** were 7% and 12% respectively.

Conductivity in conjugated systems

The concept of a molecular wire became a reality nearly 25 years ago with the discovery of metallic conductivity in an organic polymer[126]. There have been many contributions made towards the understanding and advances in the synthesis of conducting polymers. Swager *et al*[127, 128] have reported on conducting polymer-based sensors which transduce reversible, non-covalent and non redox-dependent molecular recognition events into measurable changes in conductivity. They have also demonstrated how molecular wires can be used to interconnect receptors to produce fluorescent chemosensory systems. J. M. Tour *et al*[129] have described the development of molecular wire-like architectures based on the conjugated π–system as a cost effective and more easily manufactured alternative to solid-state wires. C. Zhou *et al*[130] have made electronic transport measurements in nanoscale metal/self-assembled monolayer/metal heterostructures which showed prominent rectifying behaviour arising from the asymmetry of the molecular heterostructure. Bredas *et al* have reported that conformational changes in a 1,4-bis(phenylethynyl)benzene derivative resulted in modifications of its conductive properties in the form of a negative differential resistance (NDR) behaviour[131]. This NDR signal was the result of resonant tunnelling processes through the central ring that acted as a tunnel barrier. These properties can be applied to the development of these systems as molecular switches and by extension logic gates and memory circuits[131]. The emissive properties, and hence the electro- and photo-luminescence characteristics, of these materials are dependent on the HOMO-LUMO gap, which varies with the effective conjugation length.

The rates of interfacial electron transfer through π -conjugated spacers have been measured by Sachs *et al*[132, 133]. It is expected that the rate of electron transfer

through insulating molecular spacers will strongly depend on the nature of the chemical bonding within the spacer. They determined the standard rate constants, k_0, for interfacial electron transfer between a gold electrode and a ferrocene group covalently connected to gold by π-conjugated mercaptooligo(phenyleneethynylene) (OPE) spacers[134]. The values of k_0 were found to be orders of magnitude larger for an OPE spacer than for a trans alkane spacer of similar length. The slope of $-\ln[k_0]$ vs the spacer length, l, i.e. β[135, 136] was 0.57 ± 0.02 A^{0-1} for OPE spacers compared with ~ 1.0 A^{0-1} for saturated spacers[136]. These values were consistent with calculations using the generalized Mulliken Hush theory[137]. The experimental value (0.57 A^{0-1}) of β for the OPE was found to be intermediate between the calculated values for the perpendicular (0.97 A^{0-1}) and the coplanar (0.39 A^{0-1}) ring geometries and was in closest agreement with the calculated value (0.51 A^{0-1}) for a uniform distribution of dihedral angles. Due to the small barrier to rotation, two possible explanations for these observations were put forward. Firstly, in order for homogeneous kinetics to be obtained in the case of the uniform distribution, interconversion among the dihedral angles would have to be rapid compared to the rate of electron transfer[138]. Alternatively, the dihedral angles may be narrowly distributed about an intermediate value that gives a T^2_{DA} (square of the donor/acceptor (D/A) electronic coupling elements) value similar to the average value of T^2_{DA} for the uniform distribution[133].

Seminario *et al*[139] used density function theory calculations to explain the electrical behaviour of a π-conjugated oligo(phenylene ethynylene) resembling a resonant tunnelling diode. The theoretical results are found to be compatible with the assumptions that electrical transport occurs through the lowest unoccupied molecular orbital, the conduction barrier is determined by the chemical potential of the molecule and that the molecule becomes charged as the external potential increases.

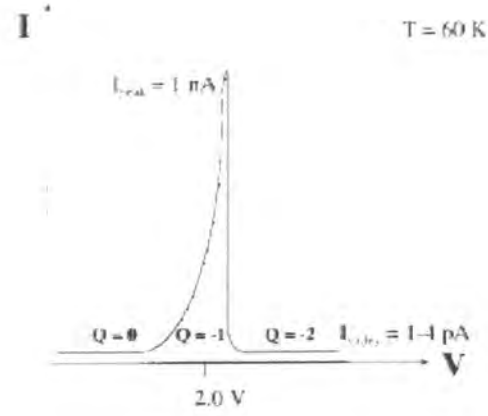

Figure 14

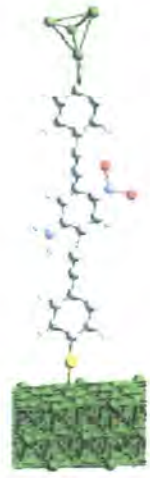

Figure 15

Figure 14. Experimental current-voltage characteristics of the molecular resonant tunnelling diode (MRTD) shown in Figure 15. The charge Q (in electrons) determines distinct conduction channels (shown in Figure 17) triggered by the bias voltage (in V)[139].

The curve in Figure 14 was obtained when electrons are injected from the vapour deposited gold terminal side to the self -assembled monolayer (SAM) side (Figure 15). The application of a negative potential to the SAM results in practically no current[139]. The system is referred to as a molecular resonant tunnelling diode (MRTD). The HOMO-LUMO gap (HLG) is a critical parameter for the molecular admittance because it is a measure of the hardness[140] of the electron density[139]. The molecules stability is increased when the HLG is large and hence the harder it is to rearrange its electron density under the presence of an external electron.

Changes in the molecular orbitals are excellent indicators of the molecular electron transport[139]. Seminario *et al* analysed small molecular units to determine what groups were responsible for the observed behaviours. This helped to determine the effects that are intrinsic to the molecules of the nanopore. They also analysed the temperature effects on the electron transport,

as these effects are connected to the temperature dependence of the torsional properties of the molecule[141].

Conduction in molecules cannot be treated using mesoscopic or macroscopic models as they fail even for mesoscopic systems[142]. It is necessary to perform a molecular level study using the well-established tools of quantum chemistry[143]. It is important to understand the electronic molecular transport of a charged molecule, i.e., when electrons are occupying *unoccupied* orbitals of the neutral system due to the action of an external voltage. In this context, the HLG energy and the spatial extent of the LUMO are respectively the logical candidates for a quantitative and qualitative prediction of the transport characteristics. The analysis was based on the assumption that, in a first approximation, transport occurs through the LUMO and other unoccupied orbitals, and as the molecule becomes charged, its chemical potential adapts to the local levels of the macroscopic electrodes addressing the molecule[139]. Initially two effects regarding the transport of electrons in molecules to investigate their electrical properties had to be quantified. First, the LUMO effect needs to be quantified because the molecular admittance (or the inverse of the molecular impedance) between two ends of a molecule increases when the LUMO is extended (delocalised) over the two ends. This yields a spatial contribution to the molecular admittance. The second effect is due to a directly quantifiable property, the HLG. When this gap decreases, the molecular admittance increases. In molecules, barriers are very flexible. Therefore, real Hamiltonians and many-electron techniques have to be used to obtain meaningful results[139].

It was noticed that the molecular energy levels decrease in value when electrons are transferred from one side of a molecule to the other by action of an external field. These energy drops were thought not to be relevant since the midpoint of the HLG is located between the Fermi local levels of the metal contacts[139]. For this reason they focused on the HLG, which decreases after one electron has been transferred and slightly increases when a second electron is transferred.

Although the shapes of the orbitals are not strongly changed, the relative values of the gaps were due to the non-rigid character of the molecular orbitals under external effects. Therefore, they can be used to explain the complex behaviour obtained in current-voltage characteristics of single molecules and single layers of few molecules[139].

The preliminary study suggested that one way to determine the transport characteristics of single molecules was to determine their HLG, then to study the spatial extent of the unoccupied orbitals to see if there was enough delocalisation to allow the transport of electrons between two end points. The following step would be to determine the effect of the incoming electrons on the shape of the unoccupied orbitals. The LUMO can become localised or delocalised due to the presence of an extra electron in the molecule[139].

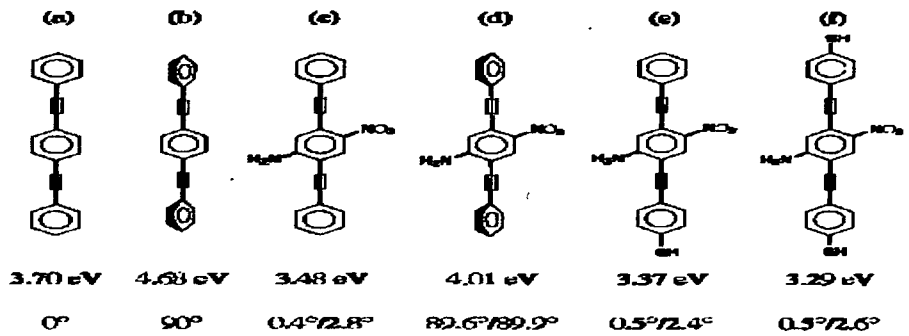

Figure 16. Several of the systems and conformations studied Seminario *et al* corresponding to the optimized geometries at the B3PW91/6- 31G* level of theory. The HOMO-LUMO gap (in eV) for each case is indicated, as well as the torsion angle (degrees) between the top and the central rings followed by the angle between the central and the bottom rings (only one angle is shown when both are identical)[139].

Figure 16 shows the systems and conformations studied and the HLGs for each case. The shapes of the HOMO and LUMO were practically identical. The torsion of the central ring in (c) did not dramatically affect the form of the LUMO orbital, but the HLG increased by 0.53 eV with the torsion of the central ring (from (c) to (d)). However, for the unsubstituted molecule, the torsion

increases the HLG by 1 eV (from (a) to b), and the shape of LUMO changes radically (from delocalised to localised). The torsional angles are precisely 0° and 90° for (a) and b, respectively. However, in the substituted molecules, the rings were not perfectly planar or perpendicular to each other. The torsion angle for (c) was 0.4° on the nitro side and 2.8° on the amine side. For the rotated case (d), the angles were 89.9° and 89.7° on the nitro and amine sides, respectively. The torsional angles are kept practically unmodified by the presence of the SH groups[139]. Charging systems (a) and (b) did not affect the torsional angles but it slightly reduces the torsion of (c) to 0.2^0 on the nitro side and 1.9^0 on the amide side. The charging of the rotated conformation of (d) to -1 or -2 forces the molecule back to the planar configuration (c).

An increase of the number of units in the oligomers also reduces the HLG. It is known experimentally that the band gap of the π-conjugated oligo(phenylene ethynylene)s with 13 units is approximately 3.0 eV[144], which coincides with the theoretical trend of values for the smallest oligomers of that family: 6.78 eV for benzene, 4.76 eV for p-diethynylbenzene, 4.44 eV for tolane (diphenylethyne), and 3.70 eV for 1,4-(ethynylphenyl)phenylene (figure 16 a).

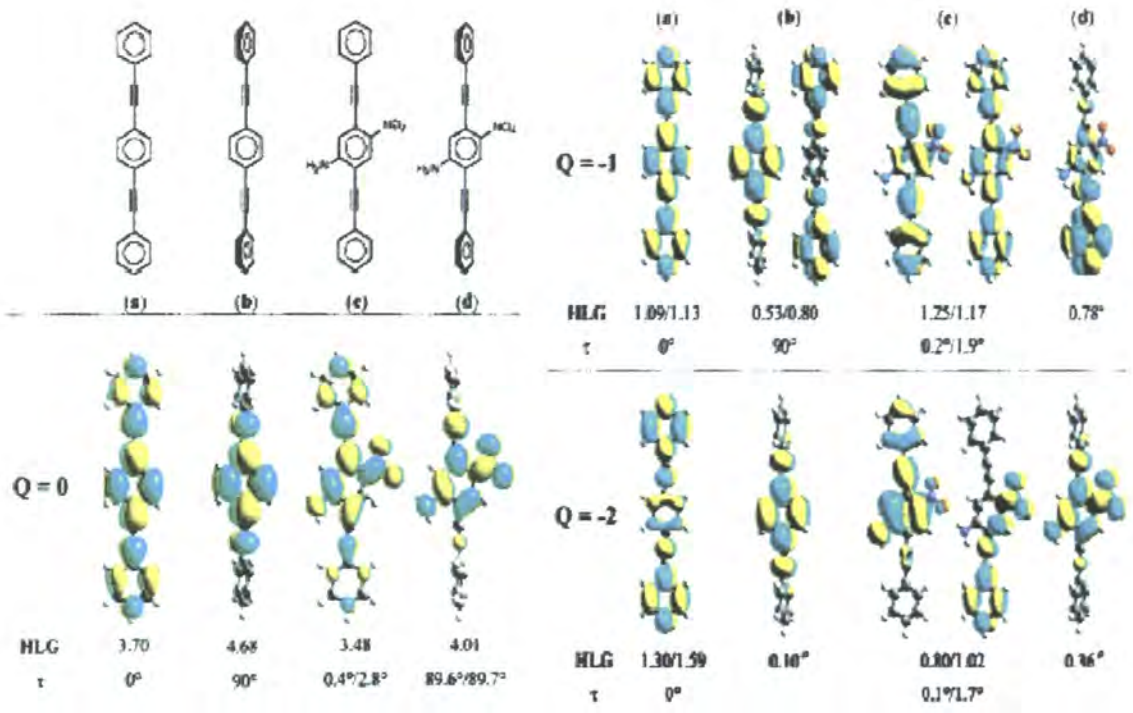

Figure 17. LUMO plots, HLG energies (in eV), and torsion angles for the optimised neutral and for the vertical and adiabatic structures of the anions. Only one LUMO is shown if the vertical and adiabatic shapes are similar. The torsion angle (τ) between the top and the central rings is indicated first followed by the angle between the central and the bottom rings (only one angle is shown when both are identical) for all optimised structures. For those structures designated with a super *a*, only vertical HLG is shown because the structure becomes planar during the optimisation[139].

The very small molecular admittance of the MRTD at low voltages can be explained by the frontier orbitals (Figure 17) where, for charge $Q = 0$, there is clearly no connection of the LUMO between the two terminals of the molecule (c). This is very different from the case of the planar unsubstituted (a) where the LUMO provides the connection to the two terminals. This was also the case of the tolane molecule [141] and this is the case for these types of unsubstituted oligomers. The presence of the NO_2 and NH_2 substituents in the central ring modifies the characteristic admittance of the molecule. Figure 17 show that the torsion of the central ring of the MRTD (c) does not affect the localized nature

of its LUMO. On the other hand, (c) bends in the direction of its dipole moment created by the opposite position and function (push-pull) of the nitro and amine substituents. It was noted that all molecules, were fully optimised without any geometrical constraints, using the built-in defaults in the program Gaussian-94[139]. In all cases, it was found that the planar structures were more stable than the rotated ones [139].

The most interesting feature, observed in the experiment, was the sudden decrease in current at a given voltage. The complex behaviour of this system (MRTD) was explained as follows. Figure 17 shows the four cases studied: the unsubstituted (a and b) and substituted (c and d) molecules, planar (a and c) and rotated (b and d), for charges 0, -1, and -2, their corresponding HLG energies, and their LUMO orbitals. For the negative ions, the corresponding vertical and adiabatic results are given. Where two LUMOs are shown, the first one corresponds to the vertical case, i.e., the LUMO obtained using the geometry of the optimised neutral, and the second one corresponds to the adiabatic case, i.e., the LUMO obtained using the optimised geometry of the negative ion. The cases where the perpendicular structures for the ions did not converge and the geometry ended up in the corresponding planar structures are indicated in figure 17. This is the case of the molecule (b) with charge -2, and molecule (d) with charges -1 and -2. The torsional angles τ for the fully optimised structures are also indicated. The first one corresponds to the angle between the top and central rings, and the second one corresponds to the angle between the central and bottom ring. If the two torsion angles were identical only one value is shown. In the unsubstituted molecule (a), the HLG changed as it became charged, having the lowest gap for charge -1. However in the rotated (b) case, the lowest gap occurs for charge -2. In both cases the gap was maximum for 0 charge. For the unsubstituted case, the charge of the molecule did not change the shape of the LUMO orbital. As seen, the LUMO is totally delocalised for the planar configuration (a) and connects the two ends of the molecule[139]. In the case of the rotated configuration (b), the LUMO is localized in the central ring

and therefore it is not connecting both ends of the molecule. Conformation (b) can be catalogued as an insulator and the planar (a) as a conductor[139]. The geometry optimisations indicated that as (b) gets charged to -2, it becomes planar. The presence of the NO_2 and NH_2 substituents totally changed some of these features[139]. The planar case (c) has some degree of localization; its LUMO does not cover the lower ring for 0 charge. In this case, a partially conducting system with high molecular impedance was expected. However, as the MRTD (c) became charged to -1, the LUMO orbital extended over the two ends of the molecule, yielding maximum transport. When (c) became charged to -2, again its LUMO did not connect both ends. In fact, one of the rings is totally disconnected, bringing the molecular admittance to zero. Although the LUMO shapes are different for the vertical and adiabatic cases of both charged species of (c), the nature from localised to delocalised or vice versa does not change.

The three regions for charge 0, -1, and -2 are indicated in figure 14. Figure 17 shows the rotated substituted molecule (d) where the LUMO never connects the two ends of the molecule[139]. When uncharged, the LUMO localizes in the central ring, as in the case of the unsubstituted molecule. With charge -1, the LUMO localizes in one of the external rings, and with charge -2 the LUMO again localizes in the central ring[139]. It was noted that the rotated structure (d) for charges -1 and -2 tended to become planar during the geometry optimisation. This was also the case for the unsubstituted (b) with charge -2, suggesting that charging the molecules will tend to planarise them.

These observations and explanation were entirely in agreement with their original proposal that the conduction was through the LUMO, thus conduction depends on the LUMO spatial extent and on the HLG[139]. In a first approximation, the barrier for transport of electrons would be half of the HLG. Thus, they could predict that at 0 K the molecule would not conduct for voltages smaller than 1.74 V, which was the barrier corresponding to charge 0 in the molecule[139]. Once the molecule becomes charged by one electron upon reaching 1.74 V, the LUMO

extends over the whole molecule and the conduction will occur, increasing the current until the molecule becomes charged with two electrons. The charge of -2 in the molecule will take place when the input voltage increases another 0.63 V, which corresponds to half the HLG of the molecule charged to -1. At this voltage, 2.37 V, the LUMO corresponding to charge -2 in the molecule gets localized, thereby becoming disconnected from the lower ring, as indicated in figure 17, with an associated current drop to practically zero.

As temperature increases a decrease of the HLG if the molecule is charged to -1 is expected. Consequently, a reduction of the peak voltage is expected[139]. This explained qualitatively the peak found around 2.1 V at a temperature of 60 K and it is also consistent with the experimentally observed reduction in peak voltage. This is deemed important as it provides a way to produce amplification using single molecules, i.e., the ability to control the peak voltage or barrier (on the order of eV) using small torsional energies (on the order of meV). Also in order to make devices that are able to work at higher temperatures, all that is needed are similar molecules with higher torsional barriers, which can be imposed intra- or intermolecularly[139].

More recently Seminario *et al* [145] theoretically interpreted the conductance switching observed in experiments with phenylene ethynylene oligomers isolated in matrices of dodecanethiolate monolayers[146]. The oligomers analysed in the experiment are shown in figure 18. The three oligomers showed conductance bistability, and it was reported that the substituents in molecules **2** and **3** were not a determining factor in their conductance switching[145]. The experiment suggested that restricting conformational changes through environmental arrangements reduces switching between the on and off states, since a well-ordered matrix reduces the rate at which switching occurs, while a poorly ordered matrix yields much more frequent switching. They suggested that rotations of the oligomers take place by a mechanism similar to earlier nanopore studies featuring devices with almost linear behaviour[139, 141]. The mechanism is

found to be different from charge transfer, which is the main mechanism for switching indicated in recent nanopore studies featuring devices with nonlinear characteristics[139, 147]. The experimental evidence demonstrated that the switching behaviour of these molecules persists on a much longer time scale (a few hours) than that expected from the predicted rotation barrier. According to earlier calculations[141] the rotational barrier of one ring with respect to another adjacent in the oligomer is ~ 4.2 kJ/mol. When this barrier is used in molecular dynamics simulations of these molecules assembled on Au surfaces at 300 K, we obtain rotational frequencies of 390.6 GHz, corresponding to a switching cycle of only 2.56 ps (picoseconds) for a molecule isolated from its neighbours. They argued that longer switching rates are expected because of steric effects when molecules are very close to each other forming a complex.

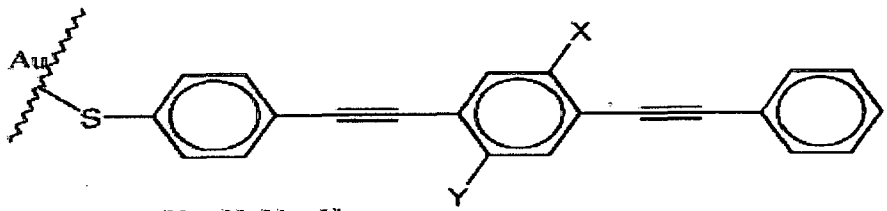

1 X = H, Y = H
2 X = H, Y = NO_2
3 X = NO_2, Y = NH_2

Figure 18. Oligomers analysed in the scanning tunnelling microscopy experiment[145]

They proved this quantitatively by calculating the rotational barrier of one ring with respect to the other in tolane, when it is forming a complex with an undecane. They found that the torsional barrier increases from 4.2 kJ/mol for the isolated tolane molecule to 159.6 kJ/mol for the tolane-undecane complex. From this evidence they concluded that the packing density of the SAM affects the switching rates by several orders of magnitude and effectively explained the much longer scales observed in the experiment. As the scanning tunnelling

microscope (STM) was operated at constant-current mode, the height of the tip was directly related to the molecule conductance[145]. The height occurrence distributions showed bimodal behaviour in the conductance, making it possible to estimate on/off ratios. Both experimental and theoretical studies concurred in that high conductance is only possible when all the rings in the molecule are aligned[145]. However, this condition alone does not warrant high conductance. On the other hand, a change in the charge state does not necessarily yield switching and cannot be observed unambiguously above the top benzene ring[145].

The electronic density and the molecular and electrostatic potential were calculated in order to explain the relationship between the theoretical and electrostatic results. It was determined that frontier MOs (HOMO, LUMO, and a few in their neighbourhood) fully delocalised along the whole molecule, making the molecule conductive[148]. Charge states rendering a nonconductive molecule show most of the frontier orbitals localized; however, some of them can show slight delocalisation, leading to a low but nonzero current. However, a perpendicular conformation of at least one ring with respect to another results in the impossibility of having fully delocalised MOs, yielding a very low conduction state[145].

Molecules **1** and **2** in figure 18 were found to conduct in their neutral charge state when theoretically analysed[139, 147]. Since the bias voltage range used in the experiment made both molecules remain uncharged during the whole experiment, only conformational changes intervene in the switching process. In this way, either molecule **1** or **2** switches to the low conductance state when the rings become perpendicular, and the conductance switches to high when the rings are parallel[145]. The experiment also revealed that **2** can be turned off when the applied voltage is increased to 3 or 4 V, and theory showed that it is nonconductive when its charge is -1; thus, when a high voltage is applied, **2** gets charged and stops conducting[145]. However, **1** did not show switching, and it

was always conducting as long as its rings were parallel; therefore, according to their theoretical analysis, a higher applied voltage would not have yielded switching in **1**.

Theoretical calculations[147] and other experimental results[149] showed that **3** is nonconductive when neutral, and conductive when charged. The observed switching for this molecule in the experiment was due to changes from the nonconductive (when compared to its anion) planar conformation to the perpendicular conformation, which is even less conductive than the nonconductive planar. MO analysis showed that the HOMO for the neutral is mostly localized in the central ring but with slight contribution from the external ring, rendering a low but nonzero conductance[139, 147]. Rotating the central ring fully localizes all the frontier orbitals[139, 147].

Liquid crystaline behaviour of polyarylethynylenes

Various ethynylated aromatic systems, namely 1,4-bis(phenylethynyl)benzenes, 9,10-bis(phenylethynyl)anthracenes, 2,5-bis(phenylethynyl)thiophenes and 2,5-bis(phenylethynyl)metallacylopentadienes display interesting structural, electronic, non-linear, optical and luminescent properties. The rigid, linear structure of these compounds usually results in liquid-crystalline (LC) behaviour[125, 150, 151] and in many models cylindrical symmetry along the ethynyl axis is assumed in order to rationalise the phase behaviour.

Miteva *et al*[152] studied the liquid crystal and thermocromatic behaviour of dialkyl-substituted poly(*p*-phenyleneethynylene)s (PPEs) in thin solid films. In the solid phase, rotation around the triple bond is restricted and a planar arrangement of the conjugated backbone with associated inter-chain $\pi - \pi$ stacking is observed. They wished to determine whether thermotropic LC behaviour and the observed aggregation band in PPEs were congruent. The effect of ordering and intermolecular interactions on the optical properties of

PPEs was studied. A film made of 2 (Figure 19) turned from yellow to almost colourless and its fluorescence changed from green to blue when heated.

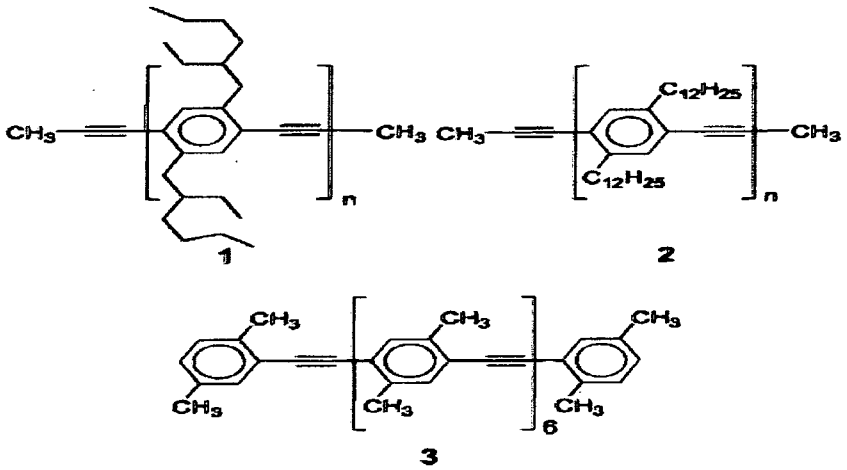

Figure 19. Poly (*p*-phenyleneethynylene)s studied by Miteva et al[125].

Variable temperature UV/vis spectroscopy showed that the aggregate band disappeared from films of **1** (at 436 nm) and **2** when their transition from LC state to the isotropic phase occurs. Their spectra also resembled that of the molecules in dilute solution. The occurrence of the aggregate bands and the observed optical properties were explained in terms of the planarisation of the conjugated backbone, which is induced by the ordering of the molecules entering the LC phase.

Chaoyang Dai *et al*[151] demonstrated that the solid state structure of 1:1 co-crystals of a series of 1,4-bis(phenylethynyl)benzenes containing 0, 4, 10 or 14 fluorine atoms was dominated by arene-perfluoroarene face to face stacking and C-H...F-C in-plane interactions with this supramolecular aggregation leading to the stabilisation of a nematic crystalline phase. Normally the mixing of two mesogenic species results in the reduction of the melting point and thus expands the temperature range of liquid crystallinity for both constituents. However they obtained two examples for which liquid crystallinity was promoted by mixing

compounds that showed only transient tendency to form a liquid crystal phase. It was also previously observed that the monotropically nematic 1,4-bis(phenylethynyl)benzene has an axial ratio of 4.45 which is barely sufficient to stabilize the liquid crystallinity at ambient pressure[153]. However molecules still can form liquid crystalline phases if there are adequately strong and anisotropic 'soft' interactions between them even if they lack the necessary shape anisotropy[154]. Liquid crystalline order is promoted in some systems by supramolecular aggregates which result from intermolecular attractions[155-157] Dai *et al* observed that the fully fluorinated compound studied did not exhibit liquid crystallinity. These observations lead them to suggest the possibility of intermolecular association in the LC phase, aggregation not due to hydrogen bonding may play a role in these cases and arene-perfluoroarene stacking interactions causes the proposed aggregation in the LC phases[158].

1,4-Bis(phenylethynyl)benzene

Compounds featuring phenylethynyl motifs have been studied for some time by several groups[108, 130, 131, 151, 159]. The barrier of rotation about the alklynyl aryl single bond is estimated to be less than 4.2 kJ/mol[160, 161]. The challenge has been to engineer control over the molecular conformation in materials based on the elementary framework **1** (Figure 20). Progress has been made in this regard by constraining molecular and polymeric materials in Langmuir films[162] self assembled mono-layers[163] as well as through the use of intra molecular tethers[164, 165]. McFarland *et al*[164, 165] showed that the conformational restriction of biaryacetylene fluorescent chemosensors induced by metal binding enhanced fluorescence. They went on to demonstrate that control of excited state dynamics could modulate intersystem crossing and internal conversion in simple fluorophores.

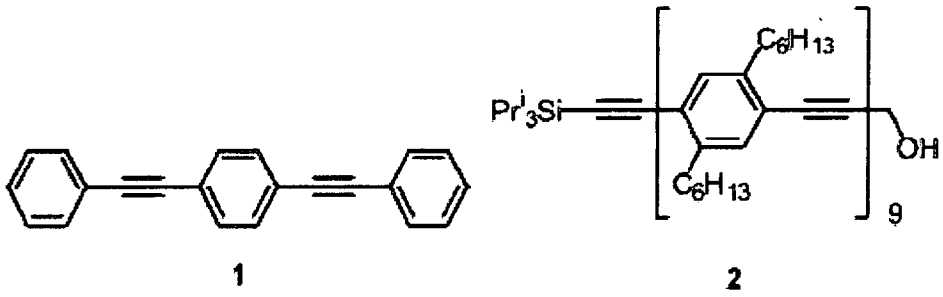

1 2

Figure 20. [109].

Sluch *et al*[166] have done measurements to establish the dynamic processes of materials based on the framework of **1** (Figure 20). They measured the absorption, steady-state and ps-time resolved emission of **2** (oligo(p-phenylene ethynylene) at ambient and low temperature. In $CHCl_3$ the absorption and emission spectrum were not mirror images of each other. The underlying Frank Condon envelope of the absorption spectrum was broadened much more than the emission spectrum. In a rigid matrix of oligostyrene at 77 K the absorption spectrum narrows while the emission spectrum broadens and overall they become roughly mirror symmetric. It was suggested that the spectral features and excited state dynamics of PPEs are dominated by the collective twisting of the phenyl rings relative to the fully planar configuration[166]. As a result of the shallow ground state potential there is a broad thermal distribution of planarity in the ground state.

In viscous solution the time required for planarisation in the excited state is similar to the fluorescence lifetime (350 ps)[166] and thus the steady state spectra is a mixture of relaxed and unrelaxed emission. Time-correlated single photon counting measurements with an instrument response time of 45 ps and at 397 nm pulse excitation of the PPE in $CHCl_3$ showed no shift of the peak in the emission spectrum and a dramatic collapse of the blue edge. The time constant for the collapse was 60 ps[166] thus the steady state spectrum is relaxed in this solvent. Measurements done in viscous solution showed the collapse time to be 0.5 ns,

which is closer to the fluorescence lifetime, and thus the steady state spectrum was only partially relaxed. The steady state and the time-resolved spectra show the rate of relaxation to be dependent on solvent viscosity. Torsional motion is expected to cause large solvent displacement and have strong quadratic coupling.

Thus the unusual features of the absorption and emission spectra of **2** were attributed to quadratic coupling between the ground and excited states. This coupling resulted from twisting about the polymer axis, which is relatively free in the ground state but becomes constrained in the excited state to a planer configuration. Sluch *et al* assumed that the first excited state of PPE is strongly influenced by quinoidal/cumuleric configurations. This results in the excited state potential favouring the planar configuration much more strongly than the ground state potential. Quantum calculations of PPE dimers and trimers made by Seminario *et al*[147] supported this assumption. The rotational barrier is small for the phenyl rings and was found to be 3.62 kJ/mol. Environmental and supramolecular forces are shown to strongly influence the planarity of the polymer and consequently its spectral properties[125]. The presence of the triple bond in PPEs enhances these effects.

Levitus *et al*[167] recently reported a series of photophysical measurements of the parent species **1**. They observed significant and systematic shifts in the fluorescence emission spectrum of the molecule with excitation wavelength. The two discrete spectral profiles observed by the group were attributed to planar and twisted configurational isomers of **1**. They also reported an unusually low energy shoulder at 360 nm on the UV/vis profile. These results were disputed by Beeby *et al*[109]. Such behaviour had not been observed in other systems closely related to **1** [159, 168-171] and the fluorescence of **1** has been reported to be independent of wavelength by Grummt *et al*[172]. The results of our re-examination of the spectroscopic properties of **1** are reported herein.

Other linearly conjugated aromatic chromophores of interest.

1,4-bis(9-ethynylanthracenyl)benzene[173] and 9,10-bis(phenylethynyl) anthracene[174], are reported to form conformational isomers in dilute viscous and non viscous solutions. They demonstrate interesting photo physical properties depending on aryl group orientation about the main axis, the rate of rotation, variation in temperature and the presence of substituents.

1.5 AIMS

This report describes two areas of research. The first section is an investigation into the photophysical properties of various Ln-ligand, Ln-ligand-sensitiser and Ln-sensitiser systems in aqueous micellar solutions. The intention was to determine which systems would enhance the phosphorescence of lanthanides in aqueous solutions via sensitisation and charge transfer mechanisms and to identify these mechanisms. The effect of the environment on Lanthanide absorption and emission was studied by observing the hypersensitive bands of the metal ions. The use of micellar solutions is intended to help bring the components of the systems together to aid energy transfer. Micellar solutions also provide a less hydrated environment for the complexes in question in order to reduce quenching mechanisms and optimise radiative energy transfer.

The second part describes a photophysics study of 1,4-bis(phenylethynyl)benzene and other aromatic chromophores. 1,4-bis(phenyleneethynylene)benzene (**1**) was studied to verify claims of novel photophysical properties observed by other research groups. Compound **1** and other aromatic chromophores linearly conjugated by alkyne linkages were also studied and compared in order to establish their photophysical properties under various conditions and in different environments. This included the study of their absorption and fluorescence spectra in viscous and non-viscous solutions at room and low temperature and their lifetimes and fluorescence quantum yields. For comparison the absorption and fluorescence spectra of the following molecules at room and low temperature

were also measured; 1,2,4,5-tetra(phenylethynyl)benzene, 1,4-bis(phenylethynyl)-2,5-bis (trimethylsilylethynyl) benzene, 1,4—bis (phenylethynyl) -2,5-dibromobenzne, 9,10-bis(phenylethynyl)anthracene, 1,4-bis(9-ethynylanthracenyl)benzene and 1,1,2,2-tetra(phenylethenyl)ethane.

REFERENCES

1. Bunzli J.-C., *Luminescence Probes*, in *Lanthanide Probes in Chemical and Earth Sciences*, J.-C.Bunzli and G. R. Chopin, Editors. 1989, Elsevier: Amsterdam. p. 219 - 293.
2. Lakowicz J. R., *Principles of Fluorescence Spectroscopy*. 2 ed. 1999, New York: Kluwer Academic/Plenum. 698.
3. Greenwood N. N. and A. Earnshaw, *Chemistry of the Elements*. 1994, Pergamon P.: Oxford.
4. Buono-Core G. E.. *Coordination Chemistry Reviews*, 1990. **99**: p. 55-87.
5. Horrocks W. D.. *Inorganic Chemistry*, 1985. **24**(895): p. 4591.
6. Cotton F. A., *Advanced Inorganic Chemistry*. 6 ed, ed. Cotton F. A. 1999, New York Chichester: Wiley.
7. Huheey J. E., E. A. Keiter, and R. L. Keiter, *Inorganic Chemistry: Principles of Structure and Reactivity*. 4 ed. 1993, New York: Harper Collins College Publishers.
8. Cotton S., *Lanthanides and Actinides*. 1991, New York: Oxford University Press. 192.
9. Carnall W. T., *The Absorption and Fluorescence Spectra of Rare Earth Ions in Solution*, in *Handbook on the Physics and Chemistry of Rare Earths*, GschneiderJr. K. A. and L. Eyring, Editors. 1979, North Holland Publishing Company: Amsterdam. p. 171-208.
10. Jorgensen C. K., *Progresses in Inorganic Chemistry*, ed. Lippard S. L. Vol. 12. 1970, New York: Wiley.
11. Ryan J. L. and C. K. Jorgensen. *J. Phys. Chem.*, 1966. **70**: p. 2845.
12. Jorgensen C. K.. *Struct. Bonding*, 1973. **13**: p. 199.
13. Jorgensen C. K. and J. S. Brinen. *Mol. Phys.*, 1963. **6**: p. 629.
14. Moller T., *Comprehensive Inorganic Chemistry*. Vol. 4. 1973, Oxford: Pergamon.
15. Legendziewicz J., G. Oczko, B. Keller, W. Strek, and B. Jezowska-Trzebiatowska. *Bull. Pol. Acc. Chem.*, 1984. **32**: p. 301.
16. Beltiukowa S.·W., N. S. Poluektow, and N. A. Nazarenko. *Dokl. Akad. Nauk SSSR*, 1982. **264**: p. 1146.
17. Vleck J. H. V.. *J. Phys. Chem.*, 1937. **41**: p. 67.
18. Broer L. J. F., C. J. Gorter, and J. Hoogschagen. *Physica*, 1945. **11**: p. 231.
19. Wybourne B. G., *Spectroscopic Properties of Rare Earths*. 1965, New York: Wiley.
20. Stein G. and E. Wurzberg. *J. Chem. Phys.*, 1975. **62**(1): p. 208-213.
21. Condon E. U. and G. H. Shortley, *The Theory of Atomic Spectra*. 1957, London: Cambridge Univ. Press. 91-109.
22. Judd B. R.. *Physical Review*, 1962. **127**(3): p. 750.
23. Ofelt G. S.. *J. Chem. Phys.*, 1962. **37**: p. 511.
24. Weber M. J., *Rare Earth Lasers*, in *Handbok on the Physics and Chemistry of Rare Earths*, GscheidnerJr. K. A. and L. R. Eyring, Editors. 1979, North-Holland Publishing Company: Amsterdam, New York, Oxford. p. 275.
25. Freeman J. J. and G. A. Crosby. *J. Phys. Chem.*, 1963. **67**: p. 2717.

26. Riseberg L. A. and H. W. Moos. *Phys. Rev.*, 1968. **174**: p. 429.
27. Kropp J. L. and M. W. Windsor. *J. Chem. Phys.*, 1963. **39**: p. 2769.
28. Kropp J. L. and M. W. Windsor. *J. Chem. Phys.*, 1965. **42**: p. 2419.
29. Kropp J. L. and M. W. Windsor. *J. Chem. Phys.*, 1966. **45**: p. 761.
30. Gallegher P. K.. *J. Chem. Phys.*, 1965. **43**: p. 1742.
31. Heller A.. *J. Am. Chem. Soc*, 1966. **88**: p. 2058.
32. Haas Y. and G. Stein. *Chem. Phys. Letrs.*, 1971. **11**: p. 143.
33. Ermolaev V. L. and E. B. Sveshnikova. *Opt. Spectry*, 1970. **28**: p. 98.
34. Barasch G. E. and G. H. Dieke. *J. Chem. Phys.*, 1965. **43**: p. 933.
35. Kondrat'eva E. V. and G. S. Lazeeva. *Opt. Spectry.*, 1960. **8**: p. 67.
36. Richardson F. S.. *Inorganic Chemistry*, 1984. **23**: p. 4607-4611.
37. Selwood P. W.. *J. Am. Chem. Soc*, 1930. **52**: p. 4308.
38. Jorgensen C. K. and B. R. Judd. *Mol. Phys.*, 1964. **8**: p. 281.
39. Hendrie D. E., R. L. Fellows, and G. R. Choppin. *Coord. Chem. Rev.*, 1976. **18**: p. 199.
40. Horrocks W. D. and N. Albin. *Prog. Inorg. Chem.*, 1984(31): p. 1.
41. Ermolaev V. L. and V. S. Tachin, *Luminescence of Crystals, Molecules and Solutions*, ed. Williams F. 1973, New York: Plenum.
42. Balzani V., L. Moggi, M. D. Manfrin, F. Bolletta, and G. S. Laurence. *Coordination Chemistry Reviews*, 1976(15): p. 321.
43. Scandola F. and V. Balzani. *J. Chem. Educ.*, 1983(60): p. 814.
44. Darwent J. R., C. D. Flint, and N. W. Sharpe. *J. Chem. Soc., Chem. Commun*, 1988: p. 747-748.
45. El-Sayed M. A. and M. L. Bhaumik. *J. Chem. Phys.*, 1963. **39**: p. 2391.
46. Almgren M., F. Greiser, and J. K. Thomas. *J. Am. Chem. Soc.*, 1979. **101**(8): p. 2021-2026.
47. Gelade E., N. Beons, and F. DeSchryver. *J. Am. Chem. Soc.*, 1982. **104**(23): p. 6288-6292.
48. Wasserman E. and A. Heller. *J. Chem. Phys.*, 1965. **42**: p. 949-955.
49. Wagner P. J. and H. N. Schott. *J. Phys. Chem*, 1968. **72**: p. 3702-3704.
50. Matovich E. and C. K. Suzuki. *J. Chem. Phys.*, 1963. **39**: p. 1442.
51. Filipescu N. and G. Mushrush. *J. Phys. Chem*, 1968. **72**: p. 3516.
52. McCarthy W. J. and L.Winefordner. *Aanl. Chem.*, 1966. **38**: p. 848.
53. Ermolaev V. L. and V. S. Tachin. *Opt. Spectrosc. (USSR)*, 1969. **27**: p. 546.
54. Brown A. and F. Wilkinson. *J. Chem. Soc., Faraday Trans. 2*, 1979. **75**: p. 880.
55. Mushrush G., F. L. Min, and N. Filipescu. *J. Chem. Soc. A*, 1971: p. 63.
56. Ermolaev V. and T. A. Shakhverdov. *Opt. Spectrosc. (USSR)*, 1969. **26**: p. 549.
57. Levin G.. *J. Phys. Chem*, 1978. **82**: p. 1584.
58. Sabbatini N., A. Golinelli, M. T. Gandolfi, and M. T. Indelli. *Inorg. Chim. Acta*, 1981. **53**: p. L213.
59. Sabbatini N., M. T. Indelli, M. T. Gandolfi, and V. Balzani. *J. Phys. Chem.*, 1982. **86**: p. 3585.
60. Bhaumik M. L. and M. A. El-Sayed. *J. Phys. Chem*, 1969. **69**: p. 275.

61. Marciniak B., M. Elbanowski, and S. Lis. *Monatsh. Chem.*, 1988. **119**: p. 669.
62. Ermolaev V. L. and V. S. Tachin. *Opt. Spectrosc. (USSR)*, 1970. **29**: p. 49.
63. Shakhverdov T. A. and V. L. Ermolaev. *Opt. Spectrosc. (USSR)*, 1972. **33**: p. 515.
64. Shakhverdov T. A.. *Opt. Spectrosc. (USSR)*, 1973. **35**: p. 96.
65. Shakhverdov T. A. and E. N. Bodunov. *Opt. Spectrosc. (USSR)*, 1973. **34**: p. 646.
66. Weissman S. I.. *J. Chem. Phys.*, 1942. **10**: p. 214.
67. Crosby G. A. and M. Kasha. *Spectrochim. Acta.*, 1958. **10**: p. 377.
68. Whan R. E. and G. A. Crosby. *J. Mol. Spectrosc.*, 1962. **8**: p. 315.
69. Kleinerman M.. *Bull. Am. Phys. Soc.*, 1964. **9**: p. 265.
70. Kleinerman M.. *J. Chem. Phys.*, 1969. **51**: p. 2370.
71. Bhaumik M. L. and M. A. El-Sayed. *J. Chem. Phys.*, 1965. **42**: p. 787.
72. Crosby G. A., R. E. Whan, and R. M. Alire. *J. Chem. Phys.*, 1961. **34**: p. 743.
73. Matsuda Y., S. Makishima, and S. Shinoya. *Bull. Chem. Soc. Jpn*, 1968. **41**: p. 1513.
74. Watson W. M., R. P. Zerger, J. T. Yardley, and G. D. Stucky. *Inoganic Chemistry*, 1975. **14**: p. 2675.
75. Sato S. and M. Wada. *Bull. Chem. Soc. Jpn.*, 1970. **43**: p. 1955.
76. Tobita S., M. Arakawa, and I. Tanaka. *J. Phys. Chem*, 1984. **88**: p. 2697.
77. Tobita S., M. Arakawa, and I. Tanaka. *J. Phys. Chem*, 1985. **89**: p. 5649.
78. Lustig H. R.-, A. Ron, and S. Speiser. *Chem. Phys. Lett*, 1982. **85**: p. 576.
79. Tran C. D. and W. Zhang. *Anal. Chem.*, 1990. **62**: p. 835-840.
80. Forster T., in *Modern Quantum Chemistry*, Sinanoglu O., Editor. 1965, Academic Press: New York. p. 93-137.
81. Forster T.. *Ann. Phys. (Leipzig)*, 1948. **2**: p. 55-75.
82. Horrocks W. D. and W. E. Collier. *J. Am. Chem. Soc.*, 1981. **103**: p. 2856-2862.
83. Beeby A., R. S. Dickins, S. Faulkner, D. Parker, and J. A. G. Williams. *Chem. Commun.*, 1997: p. 1401-1402.
84. Beeby A. and S. Faulkner. *Chem. Phys. Lett.*, 1997: p. 116.
85. Beeby A., L. M. Bushby, D. Maffeo, and J. A. G. Williams. *Perkin Transaction 2*, 2000: p. 1281-1283.
86. Darwent J. R., W. Dong, C. D. Flint, and N. W. Sharpe. *J. Chem. Soc. , Faraday Trans.*, 1993: p. 873.
87. Parker D. and J. A. G. Williams. *J. Chem. Soc. , Dalton Trans.*, 1996: p. 3613.
88. Hiemenz P. C. and R. Rajagopalan, *Principles of Colloid and Surface Chemistry*. 3 ed. Vol. Marcel Dekker, Inc. 1997, New York, Basel, Hong Kong.
89. *Biochem. Biophys. Acta.*, 1979. **40**: p. 553.
90. Atkins P. W., *Atkins' Physical Chemistry*. 7th ed. 2002, Oxford: Oxford University Press. 1149.
91. Hartley C. S., *Aqueous Solutions of Paraffin Chain Salts*. 1936, Paris: Hermann and Cie.

92. Pileni M. P., ed. *Structure and Reactivity in Reverse Micelles.* Studies in Physical and theoretical chemistry 65. Vol. 65. 1989, Elsevier Science Publishers B. V.: New York. 379.
93. Kalyanasundaram K., *Photochemistry in Microhetrogenous Systems.* 1987, London: Academic Press.
94. Escabi-Perez J. R., F. Nome, and J. H. Fendler. *J. Am. Chem,* 1977. **99**(24): p. 7749.
95. Love L. J., M. Skrilec, and J. G. Habarta. *Anal. Chem.*, 1980. **52**: p. 754-759.
96. Wehry E. L., *Modern Fluorescence Spectroscopy.* 1976, New York: Plenum Press.
97. Alpha B., J.-M. Lehn, and G. Mathis. *Angew. Chem. Int. Engl.*, 1987. **26**: p. 266.
98. Dexter D. L.. *J. Chem. Phys.*, 1953. **21**: p. 836.
99. Hayes A. V. and H. G. Drickamer. *J. Chem. Phys.*, 1982. **76**: p. 114.
100. Dong W. and C. D. Flint. *Acta Physica Polonica A*, 1993. **84**(5): p. 985-992.
101. Darwent J. R., W. Dong, C. D. Flint, and N. W. Sharpe. *J. Chem. Soc. Faraday Trans.*, 1993. **89**: p. 873-880.
102. Gelade E. and F. C. D. Schryver. *J. Am. Chem. Soc.*, 1984. **106**(20): p. 5871-5875.
103. Averrin G. Mwalupindi L. A. B., Thilivhali T. Ndou and Isiah M. Warner. *Anal. Chem.*, 1991. **63**: p. 1328-1332.
104. Mwalupindi A. G., T. T. Ndou, and I. M. Warner. *Anal. Chem.*, 1992. **64**: p. 1840-1844.
105. Beeby A., I. M. Clarkson, J. Eastoe, S. Faulkner, and B. Warne. *Langmuir,* 1997. **13**: p. 5816-5819.
106. Bredas J.-L. and R. J. Silbey, eds. *Conjugated polymers: the novel science and technology of highly conducting and nonlinear optically active materials.* 1991, Kluwer Academic Publishers: Dordrecht
London. 624.
107. Kraft A., A. C. Grimsdale, and A. B. Holmes. *Angew. Chem. Int. Ed.*, 1998. **37**: p. 402-428.
108. Bunz U. H. F.. *Chem. Rev.*, 2000. **100**: p. 1605-1644.
109. Beeby A., K. Findlay, P. Low, and T. Marder. *J. Am. Chem. Soc.*, 2002. **124**(28): p. 8280-8284.
110. Bredas J. L. and A. J. Heeger. *Macromolecules,* 1990. **23**: p. 1150-1156.
111. Rughooputh S. D. D. V., S. Hotta, A. J. Heeger, and F. Wudl. *J. Polym. Sci. B,* 1987. **25**: p. 1071-1078.
112. Kiess H., ed. *Conjugated conducting polymers.* Springer Series in Solid State Sciences, ed. Cardona M., P. Flude, K. v. Kiltzing, and H.-J. Queisser. Vol. 102. 1992, Springer-Verlag: Berlin
New York. 310.
113. Bredas J. L., G. B. Street, B. Themans, and J. M. Andre. *J. Chem. Phys.*, 1985. **83**: p. 1323.
114. Ginder J. M. and A. J. Epstein. *Phys. Rev. B,* 1990. **41**: p. 10674.

115. Fahlman M., D. D. Gebler, N. Piskun, T. M. Swager, and A. J. Epstein. *Journal of Chemical Physics*, 1998. **109**(5): p. 2031.
116. Wang Y. Z., D. D. Gebler, D. K. Fu, T. M. Swager, and A. J. Epstein. *Appl. Phys. Lett.*, 1997. **70**: p. 3215.
117. Fredricksson C. and J. L. Bredas. *J. Chem. Phys.*, 1993. **92**: p. 4253.
118. Lhost O. and J. L. Bredras. *J. Chem. Phys.*, 1992. **96**: p. 5279.
119. Fiesel R., C. E. Halkyard, M. E. Rampey, L. Kloppenburg, S. L. Studer-Martinez, U. Scherf, and U. H. F. Bunz. *Macromol. Rapid Commun*, 1999. **20**: p. 107-111.
120. Schmitz C., P. Posch, M. Thelakkat, H.-W. Schmidt, A. Montali, K. Feldman, P. Smith, and C. Weder. *Advanced Functional Materials*, 2001. **11**(1): p. 41-46.
121. Grell M. and D. D. Bradely. *Adv. Mater.*, 1999. **11**: p. 895.
122. McQuade D. T., K. Jinsang, and T. M. Swager. *J. Am. Chem. Soc.*, 2000. **122**: p. 5885-5886.
123. Turro N. J., *Modern Molecular Photochemistry*. 1991, Mill Valley California: University Science Books. 628.
124. Osaheni J. A. and S. A. Jenekhe. *Chem. Mater.*, 1995. **7**: p. 672.
125. Miteva T., L. Palmer, L. Kloppenburge, D. Neher, and U. H. F. Bunz. *Macromolecules*, 2000. **33**: p. 652.
126. Chiang C. K., C. R. Fincher, Y. W. Park, A. J. Heeger, H. Shirakawa, E. J. Louis, S. C. Gau, and A. G. MacDiarmid. *Phys. Rev. Lett.*, 1977. **39**: p. 1098.
127. Zhou Q. and T. M. Swager. *J. Am. Chem. Soc.*, 1995. **117**: p. 12593-12602.
128. Marsella M. J., P. J. Carroll, and T. M. Swager. *J. Am. Chem. Soc.*, 1995. **117**: p. 9832-9841.
129. Tour J. M.. *Acc. Chem. Res.*, 2000. **33**: p. 791-804.
130. Zhou C., M. R. Deshpande, M. A. Reed, L. J. II, and J. M. Tour. *Appl. Phys. Lett.*, 1997. **71**(5): p. 611-613.
131. Cornil J., Y. Karzazi, and J. L. Bredas. *J. Am. Chem. Soc*, 2002. **124**: p. 3516-3517.
132. Newton M. D.. *Chem. Rev.*, 1991. **91**: p. 767.
133. Sachs S. B., S. P. Dudek, R. P. Hsung, L. R. Sita, J. F. Smalley, M. D. Newton, S. W. Feldberg, and C. E. D. Chidsey. *J. Am. Chem. Soc.*, 1997. **119**: p. 10563.
134. Hsung R. P., C. E. D. Chidsey, and L. R. Sita. *Organometallics*, 1995. **14**: p. 4808.
135. Liang C. and M. D. Newton. *J. Phys. Chem.*, 1993. **97**: p. 3199.
136. Smalley J. F., S. W. Feldberg, C. E. D. Chidsey, M. R. Linford, M. D. Newton, and Y. P. Liu. *J. Phys. Chem.*, 1995. **99**: p. 13141.
137. Cave R. J. and M. D. Newton. *Chem. Phys. Lett.*, 1996. **249**: p. 15.
138. Tang J.. *J. Chem. Phys.*, 1993. **98**: p. 6263.
139. Seminario J. M., A. G. Zacarias, and J. M. Tour. *J. Am. Chem. Soc.*, 2000. **122**: p. 3015-3020.
140. Parr R. G. and R. G. Pearson. *J. Am. Chem. Soc.*, 1983. **105**: p. 7512-7516.

141. Seminario J. M., A. G. Zacarias, and J. M. Tour. *J. Am. Chem. Soc.*, 1998. **120**: p. 3970-3974.
142. Margaritondo G.. *Rep. Prog. Phys.*, 1999. **62**: p. 765-808.
143. Parr R. G. and W.Yang, *Density-functional theory of atoms and molecules.* 1989, New York: Oxford University Press.
144. JonesII L., J. S. Schumm, and J. M. Tour. *J. Org. Chem.*, 1997. **62**: p. 1388-1410.
145. Seminario J. M., P. A. Derosa, and J. L. Bastos. *J. Am. Chem. Soc. Communications*, 2002.
146. Donhauser Z. J.. *Science*, 2001. **292**: p. 2303.
147. Seminario J. M., A. G. Zacarias, and P. A. Derosa. *J. Phys. Chem. A*, 2001. **105**: p. 791.
148. Derosa P. A. and J. M. Seminario. *J. Phys. Chem. B*, 2001. **105**: p. 471.
149. Chen J.. *Appl. Phys. Lett.*, 2000. **77**: p. 1224.
150. Kloppenburge L., D. Jones, J. B. Claridge, H.-C. z. Loye, and U. H. F. Bunz. *Macromolecules*, 1999. **32**: p. 4460-4463.
151. Dai C., P. Nguyen, T. Marder, Andrew J. Scott, W. Clegg, and C. Viney. *Chem. Commun.*, 1999: p. 2493-2494.
152. Tzenka Miteva L. P., Lioba Kloppenburg, Dieter Neher and Uwe H. F. Bunz. *Macromolecules*, 2000. **33**: p. 652-654.
153. Twieg R. J., V. Chu, C. Nguyen, C. Dannels, and C. Viney. *Liq. Cryst.*, 1996. **20**: p. 287.
154. Maier W. and A. Saupe. *Z. Naturforsch. Teil A*, 1959. **14**: p. 882.
155. Imrie C. T.. *Trends Polym. Sci.*, 1997. **3**: p. 22.
156. Viney C.. *Suprmol. Sci.*, 1997. **4**: p. 75.
157. Huber A. E. and C. Viney. *Phys. Rev. Lett.*, 1998. **80**: p. 623.
158. Weck M., A. R. Dunn, K. Matsumoto, G. W. Coates, E. B. Lobkovsky, and R. H. Grubbs. *Angew. Chem. Int.*, 1999. **38**: p. 2741.
159. Biswas M., P. Nyugen, T. B. Marder, and L. R. Khundkar. *J. Phys. Chem.*, 1997. **101**: p. 1689-95.
160. Abramenkov A. V., A. Almenningen, B. N. Cyvin, S. J. Cyvin, T. Jonvik, L. S. Khaikin, C. Romming, and L. V. Vilkonv. *Acta Chim. Scanda*, 1988. **A42**: p. 674-84.
161. Inoue K., H. Takeuchi, and S. Konaka. *J. Chem. Phys. A.*, 1988. **105**: p. 6711-16.
162. Kim J. and T. M. Swager. *Nature*, 2001. **411**: p. 1030-34.
163. Reinerth W. A., L. J. II, T. P. Burgin, C. J. M. C. Zhou, M. R. Deshpande, M. A. Reed, and J. M. Tour. *Nanotechnology*, 1998. **9**: p. 246-250.
164. McFarland S. A. and N. S. Finney. *J. Am. Chem. Soc.*, 2002. **124**: p. 1178.
165. Crisp G. T. and T. P. Budner. *Tetrahedron*, 1997. **53**: p. 11881-11989.
166. Sluch M. I., G. Godt, U. H. F. Bunz, and M. A. Berg. *J. Am. Chem. Soc.*, 2001. **123**: p. 6447.
167. Levitus M., K. Schmieder, H. Ricks, K. D. Shimizu, U. H. F. Bunz, and M. A. Garcia-Gariby. *J. Am. Chem. Soc.*, 2001. **123**: p. 4259-4265.
168. Nguyen P., Z. Yuan, L. Agocs, G. Lesley, and T. B. Marder. *Inorg. Chim. Acta.*, 1994. **220**: p. 289-296.

169. Khan M. S., A. K. Kakkar, J. L. N. J. Long, P. Nguyen, P. Raithby, T. B. Marder, F. Whittmann, and R. H. Friend. *J. Mater. Chem.*, 1994. **4**: p. 1227-1234.
170. Nguyen P., S. Todd, D. V. D. Biggelaar, N. J. Taylor, T. B. Marder, F. Wiimann, and R. H. Friend. *Synlett*, 1994. **299**.
171. Nguyen P., G. Lesley, T. B. Marder, and J. Z. I. Ledoux. *J. Chem. Mater.*, 1997. **9**: p. 406-408.
172. Birckner E., U.-W. Grummt, A. H. Goller, T. Pautszch, D. A. M. Egbe, M. Al-Higari, and E. Klemm. *J. Phys. Chem. A*, 2001. **105**: p. 10307.
173. Schmieder K., M. Levitus, H. Dang, and M. A. Garcia-Gariby. *J. Phys. Chem. A*, 2002. **106**: p. 1551-1556.
174. Cherkasov A. S., T. V. Veselova, B. M. Krasovitskil, and V. M. Shershukov. *Opt. Spectrosc. (USSR)*, 1985. **59**: p. 59-63.

CHAPTER 2

2.1 GENERAL EXPERIMENTAL DETAILS

CHEMICALS

Lanthanide Systems

Europium (III) nitrate pentahydrate, europium tris(6,6,7,7,8,8,8 – heptafluoro - 2,2 – dimethyl - 3,5 - octanedionate) [Eu(fod)$_3$], t–octylphenoxypolyethoxyethanol (TritonX–100), cetyltrimethylammonium bromide (CTAB), 4,4 - bis(N,N – dimethylamino) benzophenone (Michler's ketone - MK), 2,2,6,6,-tetramethyl-1-piperidinyloxy free radical (TEMPO), pyridine dicarboxylic acid (pdc), diethylenetriaminepentaacetic acid tripotassium(I) dihydrogen salt (DTPA-K$_3$), phenanthrene and 1,10 – phenanthroline were all obtained from the Alderich Chemical Company. Dichloromethane (DCM) and toluene were obtained from the Fischer Chemicals Company. Water was purified by the 'Purite$_{stil}$ Plus' method.

Polyarylethynylene Study.

1,4-bis(phenylethynyl)benzene, 1,2,4,5-tetra(phenylethynyl)benzene, 1,4-bis (phenylethynyl)-2,5-bis(trimethylsilylethynyl)benzene, 1,4—bis(phenylethynyl)-2,5-dibromobenzene, 1-(3,3-dimethyl-but-1-ynyl)-4-phenylethynyl-benzene and 1,1,2,2-tetra(phenylethynyl)ethene were synthesised by the research group headed by Dr. P. Low. 9,10-bis(phenylethynyl)anthracene, 1,4-bis(9-ethynylanthracenyl) benzene and 1,4-diphenylbut-1,3-diyne were synthesised by the research group headed by Prof. T. B. Marder. Both groups are from the University of Durham.

Solvents used were cyclohexane, methylcyclohexane/2-methylbutane (MCH/IP), in the ratio 4:1 v/v, ether pentane alcohol (EPA) in the ratio 5:5:2 v/v, and glycerol. All were obtained from the Aldrich Chemical Company. The MCH/IP and EPA mixtures were selected for the low temperature studies since they form optically transparent glasses at low temperatures.

INSTRUMENTATION

Absorption, phosphorescence and fluorescence measurements.

An ATI Unicam UV / VIS UV2 spectrometer was used to record all absorption spectra. Corrected phosphorescence emission and excitation spectra were recorded on a Perkin Elmer LS-50B luminescence spectrometer using a bandpass of 5nm for all the lanthanide systems.

Fluorescence spectra of the polyarylethynylenes were recorded using a Jobin-Yvon Horiba Fluorolog 3-22 Tau-3 spectrofluorimeter[1] with a 0.5 – 2 nm bandpass (Figure 2[1]). The spectra of dilute solutions with absorbance of less than 0.1 in the 200 nm to 400 nm range were recorded using conventional 90 degree geometry while a front-face geometry was used to study highly absorbing solutions. Both the excitation and emission spectra were fully corrected using the manufacturers correction curves for the spectral response of the excitation and emission optical components. Excitation and emission matrices were acquired by recording the emission spectra over the range 300 to 500 nm and stepping the excitation wavelength from 230 to 400 nm in 2.5 nm increments.

Low temperature spectra were recorded with an Oxford Instruments DN1704 cryostat[2] (Figure 3) and a model ITC 6 temperature controller.

Lifetime measurements.

The lifetimes of the Eupdc micellar systems were measured using a home built ns-laser pumped fluorimeter. The samples were excited by a 10Hz train of 3rd harmonic 355 nm radiation from a Q-switched Nd:YAG laser (Spectra Physics GCR-150-10), with a typical pulse energy of 1-2mJ per pulse, and pulse duration of approximately 6ns. Stray light at 1064 nm (1st harmonic) and 532 nm (2nd harmonic) was removed by use of optical filters. The luminescence was collected at 90° and focussed onto the entrance slits of a monochromator (Jobin Yvon Horiba, Triax 320) using a bandpass range of 0.1-2.0 nm. The signal was monitored by a photomultiplier tube (Hamamatsu R928) at the appropriate wavelength, and captured and averaged by a digital oscilloscope (Tetronix TDS340) and transferred to a PC for analysis. The decays were analysed by non-linear

least squares analysis. The quality of the fit was judged by the randomness of the residuals and the minimisation of the sum of the squares of the residuals.

The lifetimes of the $Eu(fod)_3$-TEMPO micellar systems were measured on the LS-50B spectrometer. The samples were excited by a 317 nm radiation and the decay of the 614.5 nm wavelength emission was recorded. The decays were analysed by a non–linear least squares analysis with a single exponential.

The phase-modulation technique is used to determine the fluorescence lifetimes from cyclohexane solutions of 1,4-bis(phenylethynyl)benzene (**1**). In this method an intensity-modulated light source is used to excite the sample being studied. The time lag between absorption and emission results in the emission being delayed in time relative to the modulated excitation as illustrated in figure 1.

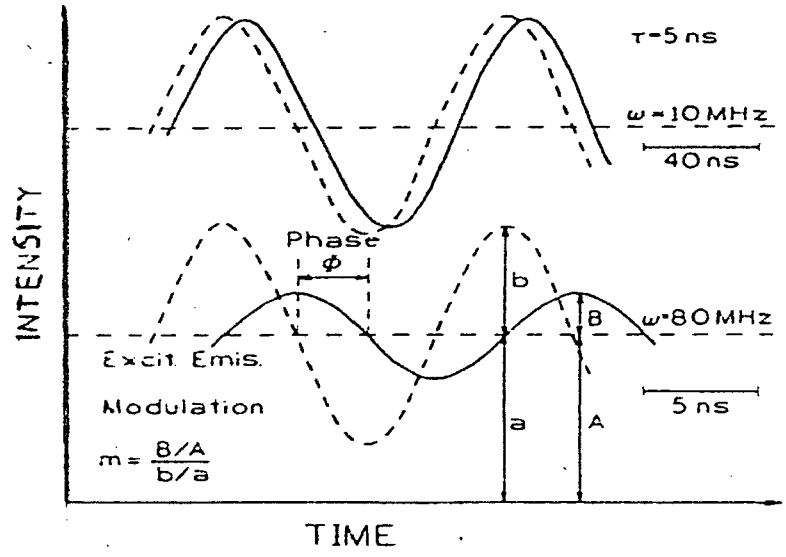

Figure 1. Schematic diagram of phase modulation. The solid line represents the phase and modulation fluorescence in response to intensity-modulated excitation represented by the dashed line. The lifetime is 5 ns and the modulation frequency is 10 MHz (top) and 80 MHz (bottom) [3].

At each modulation frequency this delay is described as the phase shift (ϕ_ω). This phase shift increases from 0^0 to 90^0 with increasing modulation frequency (ω). The phase angle displayed by any sample is usually a fraction of 90^0. The demodulation of the emission by a factor m_ω is also a result of the finite time response of the sample. m_ω decreases from 1.0 to 0 with increasing modulation frequency and increasing lifetime. The emission closely follows excitation at low frequency. However at higher modulation frequencies the finite lifetime of the excited state prevents the emission from

following the excitation intensity. The result is a phase delay in the emission, and a decrease in the peak-to-peak amplitude of the modulated emission measured relative to the modulated excitation. The phase modulation graph constitutes the frequency response of the emission from **1**. The decay of **1** is a single exponential. The lifetime can be calculated by using the phase angle or modulation at any frequency. The phase and modulation are related to the decay time (τ) by

$$\tan\phi_\omega = \omega\tau \quad \text{and}$$

$$m_\omega = (1+\omega^2\tau^2)^{-1/2} \quad [4].$$

Fluorescence lifetimes were recorded using the Jobin-Yvon Horiba Fluorolog 3-22 Tau-3 spectrofluorimeter operating in the phase-modulation mode. The phase shift and modulation were recorded over the frequency range 50-300 MHz and the data fitted using the Jobin-Yvon software package.

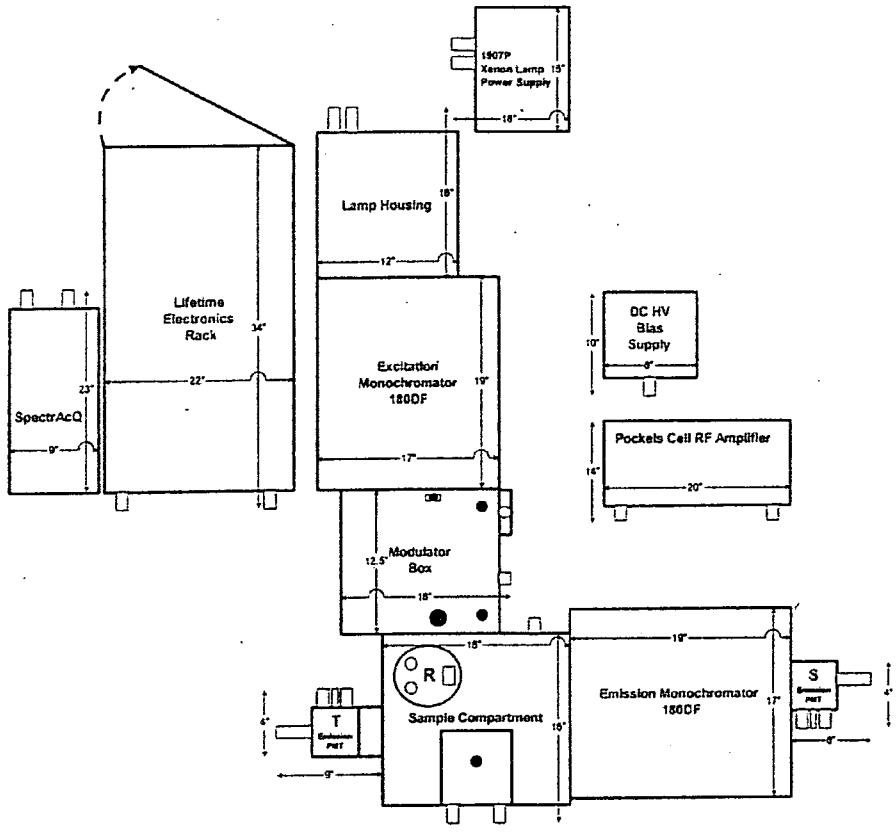

Fogure 2. Fluorolog-3 Model FL-3-22-T. Double excitation / double emission lifetime spectrofluorometer with T-side detector.

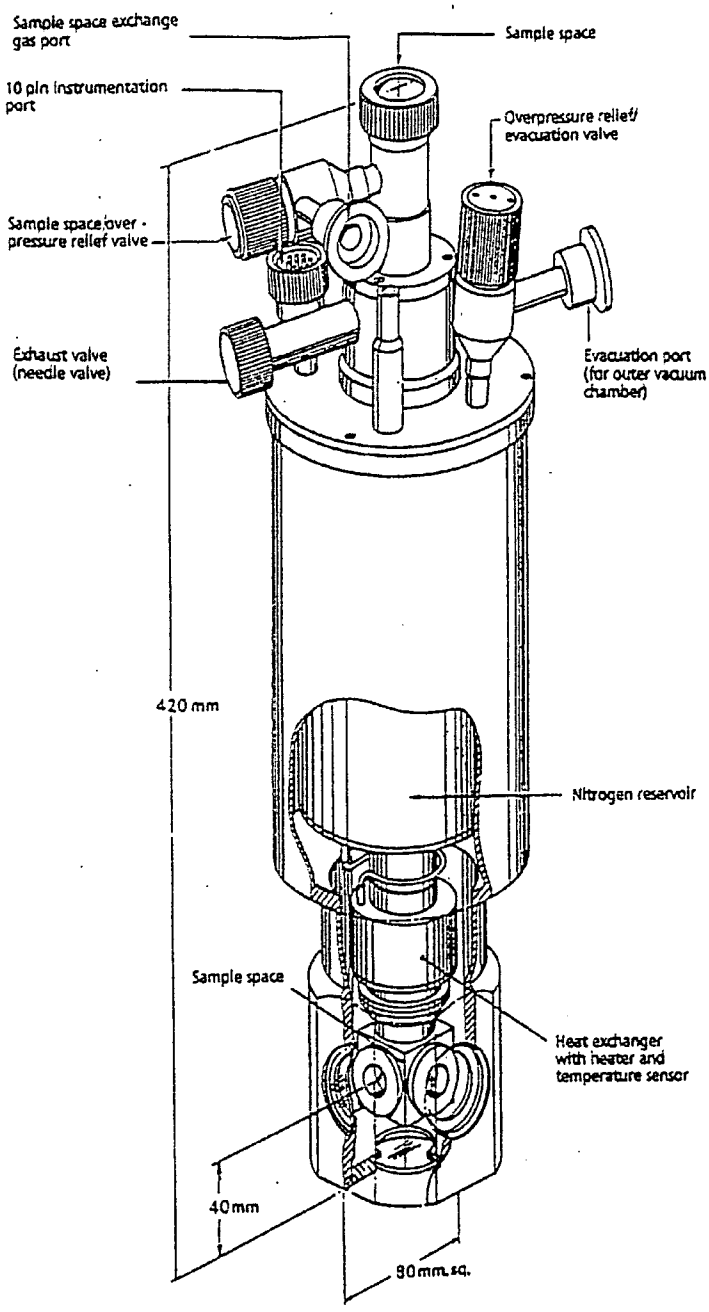

Figure 3. Schematic diagram of the DN1704 cryostat.

2.2 EXPERIMENTAL PROCEDURES

Lanthanides

Four different combinations of Ln with ligands and/or sensitisers in aqueous micellar systems were studied (Table 1).

System	Lanthanide	Ligand	Sensitiser	Aqueous Micellar Solutions
1	$Eu(NO_3)_3$ $5H_2O$. 25	DTPA-K_3. 25	Phenanthrene	CTAB. 29
2	$Eu(NO_3)_3$ $5H_2O$. 0.6 & 1.2	pdc. 1.8 & 3.7	Phenanthrene. 0.875	CTAB. 29
3	$Eu(fod)_3$. 0.045	MK. 0.005		Triton X – 100. 0.5
4	$Eu(fod)_3$. 0.025	MK. 0.025	1,10-Phenanthroline. 0.025	Triton X – 100. 2.5

Table 1. A list of the Ln complexes with and without sensitisers in aqueous micellar systems studied. Actual concentrations are given in mM units.

Stock concentrations of the individual lanthanides, ligands and sensitisers were made up in water or in the aqueous micellar solutions prior to being combined and having their absorption, phosphorescence and lifetimes measured in 1 cm quartz cuvettes. MK and $Eu(fod)_3$ are insoluble in water. They were first dissolved in a small volume of dichloromethane (DCM) and then diluted with the aqueous micellar solution. $Eu(fod)_3$ in DCM formed a white emulsion with TritonX-100. The solution was stirred uncovered in a large beaker for about 30 minutes to allow the DCM to evaporate. The resulting transparent colourless solution was used in the comparative study. In system 3 and 4 the photoluminescence of the Ln-ligand and Ln-sensitiser combinations were studied in DCM for comparative purposes. The photoluminescence of the Ln-ligand combination in system 3 was also studied in toluene.

Phenanthrene and 1,10-phenanthroline were first dissolved in approximately 0.3 ml of DCM then diluted with water. The DCM was then driven off with nitrogen gas before the phenanthrene and 1,10-phenanthroline solutions were combined with the aqueous micellar solutions.

Polyarylethynylenes

1,4-bis(phenylethynyl)benzene (1).

Extinction Coefficient.

The extinction coefficient (ε) of this molecule was determined at the 320 nm peak in cyclohexane using a quartz cell with an optical path length of 1 cm. ε was determined from a Beer-Lambert plot (absorption vs. concentration) using 7 dilutions over the concentration range 100 to 1 μM. $\varepsilon = A/c\,l$, where A is absorbance, c is the concentration of the absorbing species in moles per litre and l is the optical path length in cm. For highly absorbing solutions, short path length cells, $l = 0.1, 0.2$ cm, were used whilst for more dilute samples path lengths of up to 10 cm were used to give a measurable absorbance.

Fluorescence Quantum Yield.

The fluorescence quantum yield is the ratio of the number of emitted photons to the number of photons absorbed by the compound. The meaning of the quantum yield is illustrated in the simplified Jabłoński diagram in figure 4.

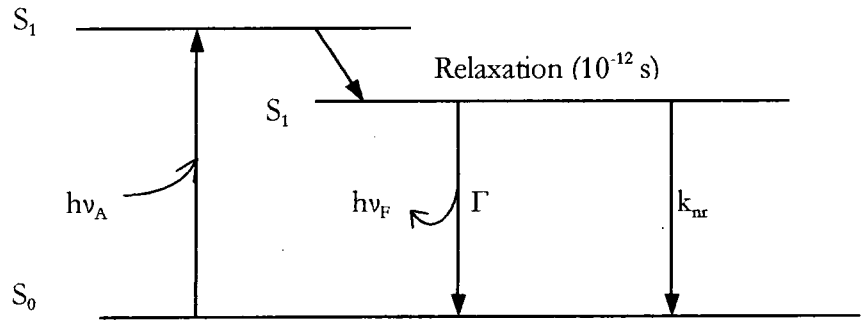

Figure 4. A simplified Jabłoński diagram illustrating the relaxation processes leading to the relaxed S_1 state. $h\nu_A$ and $h\nu_F$ represent absorbance and fluorescence energies respectively. Γ and k_{nr} are the emissive rate of the fluorophore and the rate of nonradiative decay to S_0.

Here the emissive rate of the fluorophore (Γ) and the rate of nonradiative decay (k_{nr}) are responsible for the return to the ground state. The fraction of fluorophores, which decay through emission, and hence the quantum yield, is given by

$$Q = \frac{\Gamma}{\Gamma + k_{nr}} \quad [4]$$

The energy yield of fluorescence is always less than unity because of Stokes' losses.

The quantum yield of **1** was estimated by comparing it with standards of known quantum yields. The quantum yields of the standards used are largely independent of excitation wavelength, which enables them to be used wherever they display a useful absorption. The determination of the quantum yield is accomplished by comparison of the wavelength-integrated intensity of the unknown to that of the standard. The absorbance of the sample is kept below 0.15 to avoid inner filter effects.

The fluorescence quantum yield (Φ_f) was determined for **1** in cyclohexane for 342 nm excitation using quinine sulfate (QS) in 0.1 M H_2SO_4 ($\Phi_f = 0.55$)[4] and β-carboline (BC) in 1 M H_2SO_4 ($\Phi_f = 0.6$)[4] as standards. All solutions ranged from 0.02 to 0.12 in absorption intensity. Excitation and emission slits were set at 1.5 nm. Quantum yields were calculated from the expression

$$\Phi_{unk} = \Phi_{std}\left(grd_{unk}/grd_{std}\right)\left(\eta_{unk}/\eta_{std}\right)^2$$

Where Φ_{unk} and Φ_{std} are the quantum yields of the unknown fluorophore (unk) and the known standard (std) respectively, *qrd* is the gradient and η_{unk} is the refractive index of the cyclohexane and η_{std} is that of water. Here the gradients of the unknown fluorophore (**1**) and the standards are determined from plots of the absorbance versus the wavelength-integrated emission intensities for five increasing concentrations of the fluorophore and each of the standards.

REFERENCES

1. *Jobin Yvon-Spex Fluorolog Tau-3 Lifetime System Hardware Operation Manual.* 1999.
2. *Oxford Research Instruments Variable Temperature Liquid Nitrogen Cryostat Operator's Handbook.* 1993.
3. Lakowicz J. R., ed. *Frequency-domain fluorescence spectroscopy.* Topics in Fluorescence Spectroscopy, ed. Lakowicz J. R. Vol. 1. 1991, Plenum Press: New York. 293-335.
4. Lakowicz J. R., *Principles of Fluorescence Spectroscopy.* 2 ed. 1999, New York: Kluwer Academic/Plenum. 698.

CHAPTER 3

Lanthanide systems results and discussion

Europium nitrate and the lanthanide β-diketonate, $Eu(fod)_3$, were chelated and combined with the ligands and in the micellar solutions listed in the system tables below. Various molecules were also added to act as sensitisers. The luminescence spectra of these systems were recorded in order to determine if the complexes formed stayed intact and if the Ln emission was sensitised in the aqueous micellar environment. The lifetime of the europium emission was also recorded to determine the effect of different ligands and aqueous environments on the rate of decay.

System 1.

Sample	Composition. Concentration in mM.			
	Ln^{3+} ion	**Ligand**	**Sensitiser**	**Aqueous Micellar Solutions**
1			Phenanthrene.	CTAB. 29
2	$Eu(NO_3)_3$ $5H_2O$. 25	DTPA-K_3. 25	Phenanthrene.	CTAB. 29
3	$Eu(NO_3)_3$ $5H_2O$. 25	DTPA-K_3. 25		CTAB. 29

System 1. The compositions of the three samples investigated are given in the table above in 10^{-3} molar concentrations. All solutions were made up in cetyltrimethylammonium bromide (CTAB). The luminescence spectra of europium (III) nitrate with diethylenetriaminepentaacetic acid tripotassium (I) dihydrogen salt (DTPA-K_3) as the ligand were recorded with and without phenanthrene.

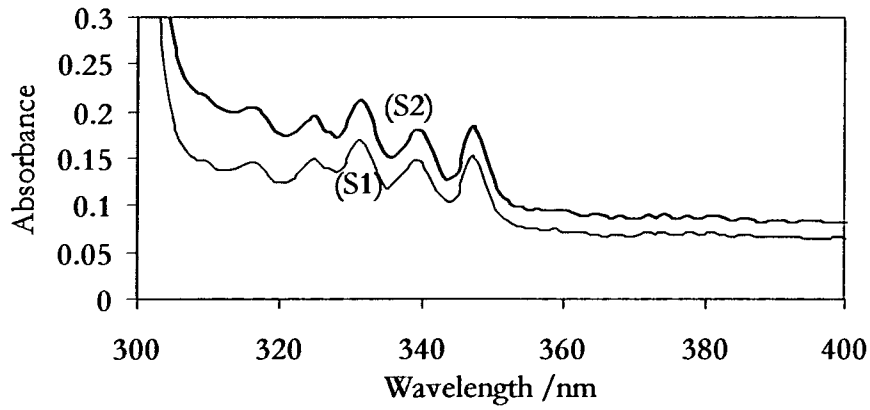

Figure 1. The absorption spectra of the Eu-DPTA complex with phenanthrene in CTAB (S2) and that of phenanthrene only in CTAB (S1).

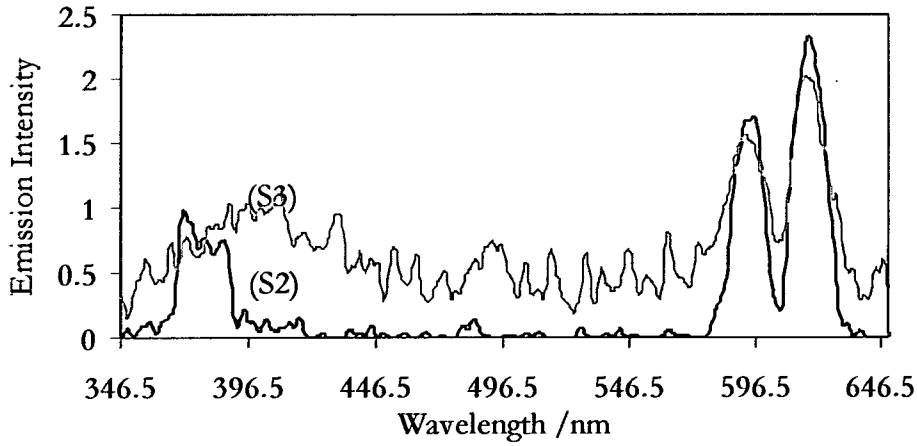

Figure 2. The phosphorescence emission spectra of Eu-DPTA with phenanthrene in CTAB (S2) and Eu-DPTA in CTAB (S3) for a 330 nm excitation wavelength.

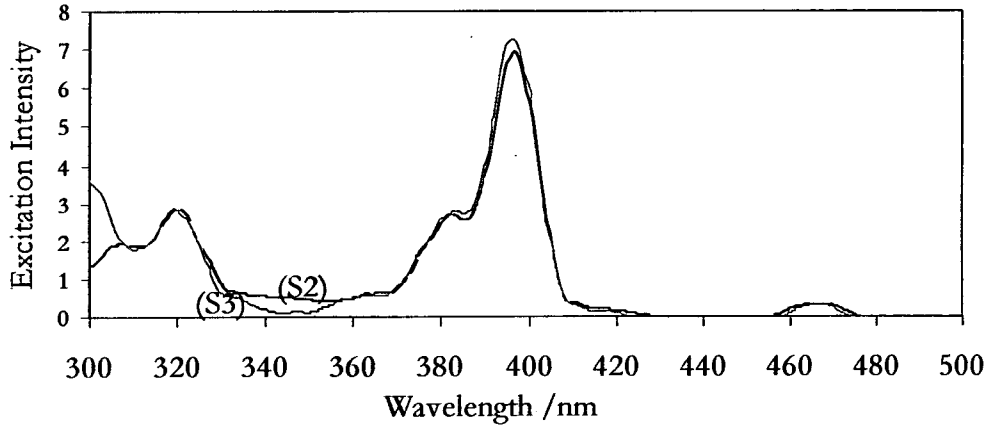

Figure 3. The phosphorescence excitation spectra of Eu-DTPA with phenanthrene in CTAB (S2) and Eu-DPTA in CTAB (S3) for 617 nm emission wavelength.

The absorbance spectra in figure 1 show the absorption bands of phenanthrene incorporated inside the micelles in the two solutions with peaks at 316 nm, 325 nm, 331 nm 339 nm and 347 nm. The weak absorption bands of europium, which should

appear between 350 nm and 420 nm, are not observed. This is due to the phenanthrene absorption overshadowing these peaks. The emission spectra for the Eu-DTPA complex with phenanthrene (S2) in the micellar solution had well defined peaks at 596 nm and 617 nm when excited at 330 nm (figure 2). These emission peaks are characteristic of europium (III). The peak at 371 nm is a phenanthrene emission. When phenanthrene is absent the emission spectrum shows broad bands at 408 nm, 593 nm and 617 nm and an overall less resolved profile. Eu-DTPA is associated with the surface of the micelle and its emission is thus susceptible to quenching by water molecules despite the presence of the rather bulky DTPA ligand. Both spectra are of very low intensity and subject to background noise.

Excitation of the Ln-phenanthrene system with a 330 nm wavelength would result in the excitation of the phenanthrene T_1 triplet state at 21,740 cm^{-1}. The phenanthrene molecules within the micelles are within 3.4 nm of the Eu ion on the outer surface. Intermolecular energy transfer is then possible between phenanthrene and the Eu $^5D_2$ state at 21,600 cm^{-1}. The phosphorescence emission would then occur from the Eu $^5D_1$ and $^5D_0$ states after non-radiative relaxation as illustrated in the energy level diagram in figure 4.

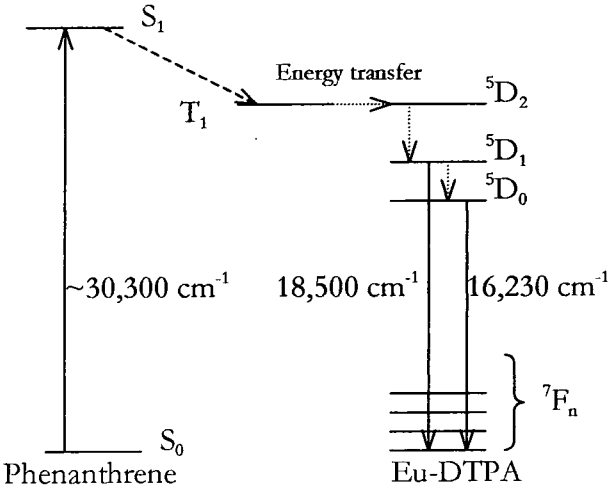

Figure 4. A summary of the processes involved in the possible intermolecular energy transfer from phenanthrene to Eu-DTPA.

The excitation spectra (figure 3) for the 617 nm hypersensitive emission band shows a minor contribution to its intensity is due to absorption over the range 327 nm to 356 nm when phenanthrene is in the system. The major peak with its maximum at 396 nm is due to direct absorption by europium. The absorption profiles of phenanthrene and

europium overlap considerably; thus both are excited at 330 nm but only europium shows phosphorescence emission over the range 540 nm to 650 nm. There is no real evidence of a major contribution to the europium phosphorescence because of energy transfer from the phenanthrene.

System 2.

Sample	Composition. Concentration in mM.			
	Ln^{3+} ion	**Ligand PDC**	**Sensitiser**	**Aqueous Micellar Solutions**
1	$Eu(NO_3)_3$ $5H_2O$. 0.6	1.8	Phenanthrene. 0.33	CTAB. 29
2	$Eu(NO_3)_3$ $5H_2O$. 0.6	1.8		CTAB. 29
3	$Eu(NO_3)_3$ $5H_2O$. 1.2	3.7		CTAB. 29
4	$Eu(NO_3)_3$ $5H_2O$. 1.2	3.7	Phenanthrene. 0.66	CTAB. 29

System 2. Europium nitrate pentahydrate was chelated with pyridine dicarboxylic acid (pdc) in a 1:3.1 ratio in CTAB. Phenanthrene was again the proposed sensitiser encapsulated within the micelles.

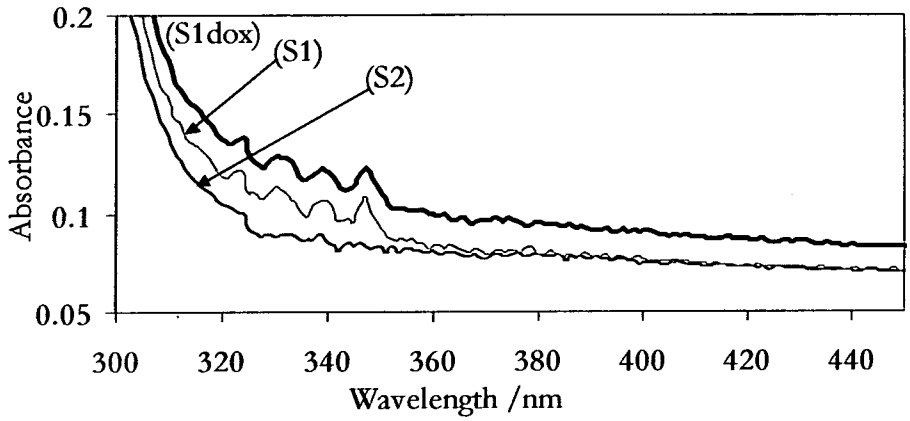

Figure 5. The absorption of oxygenated Eupdc in CTAB (S2), oxygenated Eupdc with phenanthrene in CTAB (S1) and deoxygenated Eupdc with phenanthrene in CTAB (S1dox).

Sample 1 and 2 (S1 and S2) contain Eu ions in low concentrations. The absorption of sample 1 (S1) is enhanced when the sample is deoxygenated (figure 5). This indicates that the presence of dissolved oxygen interferes with the absorption of the system. Its removal via the freeze – pump – thaw method may have altered the properties of the

micellar system resulting in an increase in the absorbance. Again the weak absorption bands of europium are not observed in solution. The major absorption bands of phenanthrene are observed between 319 nm and 355 nm.

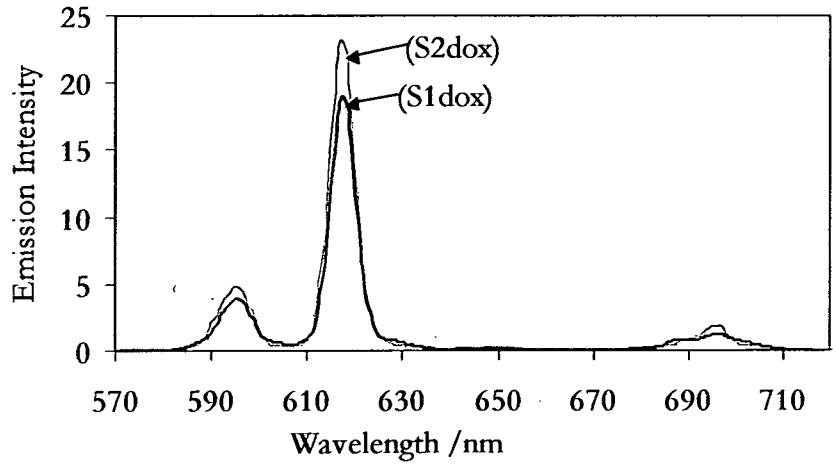

Figure 6. Phosphorescence emission spectra for the 397 nm excitation of deoxygenated Eupdc in CTAB (S2dox) and Eupdc with phenanthrene in CTAB (S1dox).

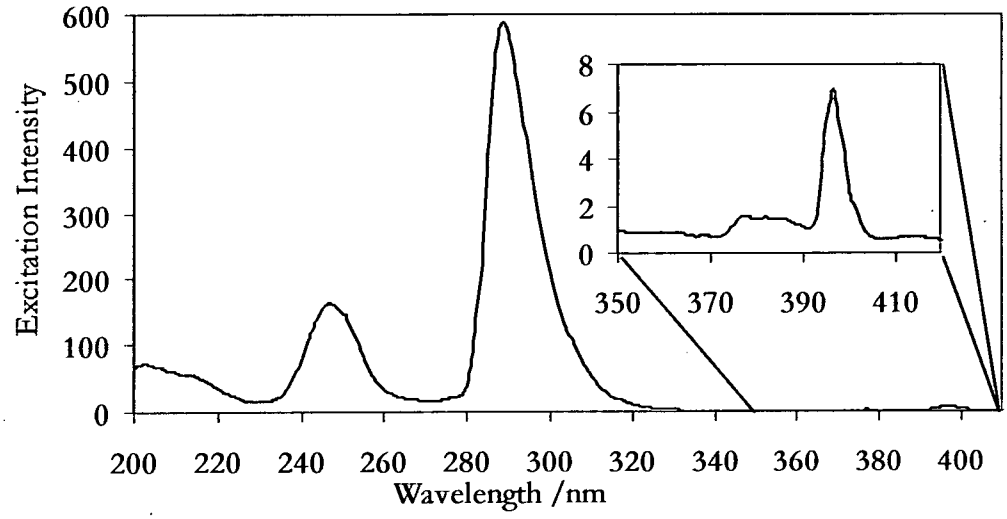

Figure 7. The phosphorescence excitation spectra of deoxygenated Eupdc in CTAB (S2dox) for 616 nm emission. The inset shows the weak excitation spectra of Eu (III) over the 350 to 430 nm region.

The lanthanide and phenanthrene were excited in the two solutions at 397 nm (figure 6). The emission spectrum of the deoxygenated system with phenanthrene (S1dox) is slightly less intense in comparison to the deoxygenated system without it (S2dox). The emission peaks at 595 nm, 617 nm and 695 nm (figure 6) are that of Eu(III). This variation in intensity is slight and maybe due to slight variations in the concentrations of the two solutions. The phosphorescence excitation spectra for the hypersensitive

emission (figure 7) shows most of the energy contributing to this emission came from the near UV region with major excitation bands at 247 nm and 289 nm. This corresponds to direct absorption by europium.

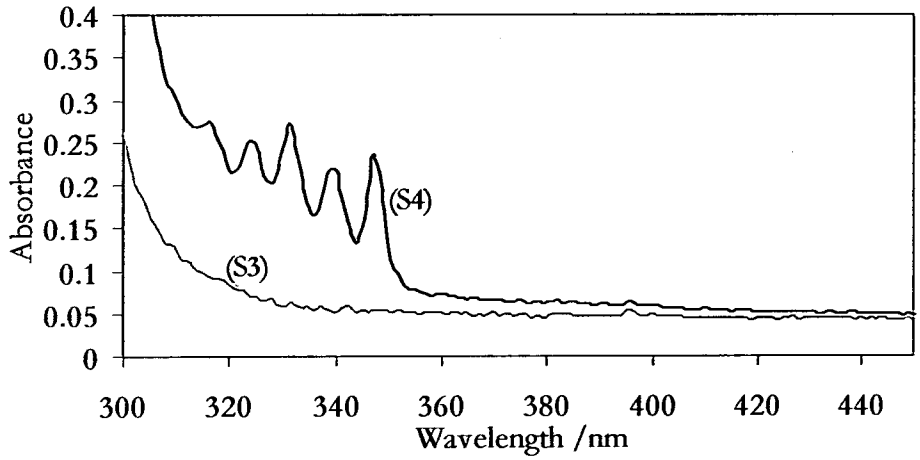

Figure 8. The absorption of Eupdc in CTAB (S3) and Eupdc with phenanthrene in CTAB (S4).

Figure 8 shows the absorption profiles of 1.2 mM Eupdc with 0.66 mM phenanthrene (S4) and 1.2 mM Eupdc only (S3) in CTAB. These two solutions are at twice the concentration of S1 and S2. The phenanthrene profile is well defined.

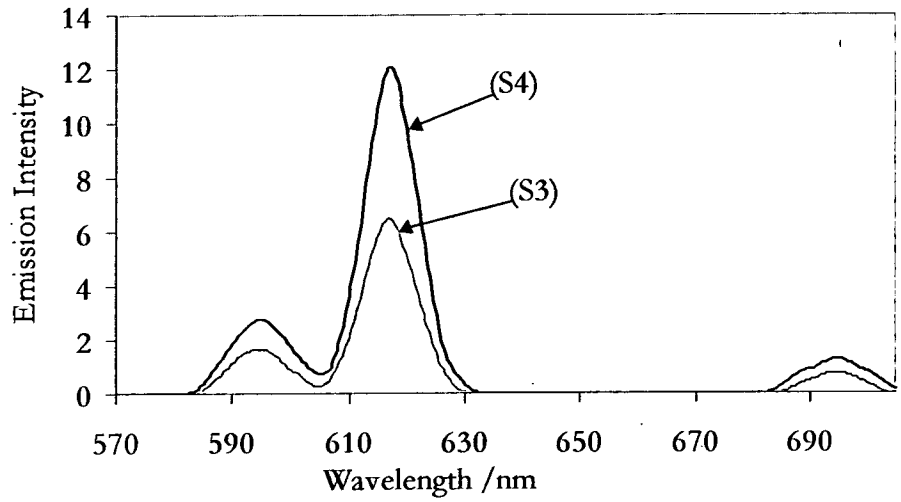

Figure 9. The phosphorescence emission spectra of Eupdc with phenanthrene (S4) and Eupdc (S3) only in CTAB for a 355 nm excitation wavelength.

The oxygenated phosphorescence emission from samples 3 and 4 are shown in figure 9 for excitation at 355 nm. There is a distinct enhancement in the emission when phenanthrene is present in the system. The presence of dissolved oxygen has reduced the overall intensity.

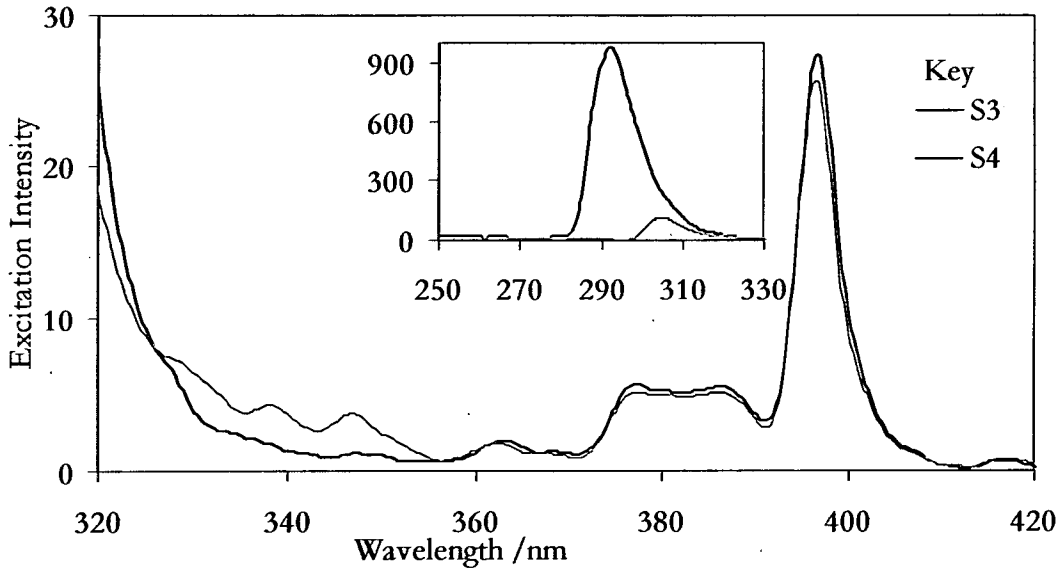

Figure 10. The phosphorescence excitation spectra for Eupdc with phenanthrene (S4) and Eupdc only (S3) in CTAB for a 617 nm emission wavelength. The inset shows the same excitation spectra of S3 and S4 over the 250 to 330 nm region.

The phosphorescence excitation spectra of the S4 and S3 are shown in figure 10. There is evidence of some sensitisation of the Eu emission at 617 nm. The phenanthrene excitation is evident over the 320 to 360 nm wavelength range in the S4 profile. The inset shows the excitation spectra of the solutions in the near UV region. There is a distinct decrease in the energy contribution from this region when phenanthrene is included in the system. These results show evidence of energy transfer from the sensitiser to the Eu occurring via the mechanism illustrated in the energy level diagram in figure 4.

The lifetimes of S3 and S4 were determined at a 355 nm excitation wavelength. The $^5D_0 \rightarrow {}^7F_2$ emission was monitored at a 617 nm wavelength. The emission decay from Eupdc in CTAB (S3) is shown in figure 11. The lifetime for Eupdc in CTAB only was measured as 1.7 ms and that of Eupdc with phenanthrene was determined to be 2.1 ms, which is slightly longer than Eu in water. The results indicate a slight prolonging of the lifetime of the Eu emission in this micellar environment. The variation of the Eu ion environment is expected to affect its emission lifetime. The dependence of the radiative lifetime of Eu(III) on the environment in which it's embedded has been reported[1]. The lifetime decreases as the number of ligands chelated to the ion increases.

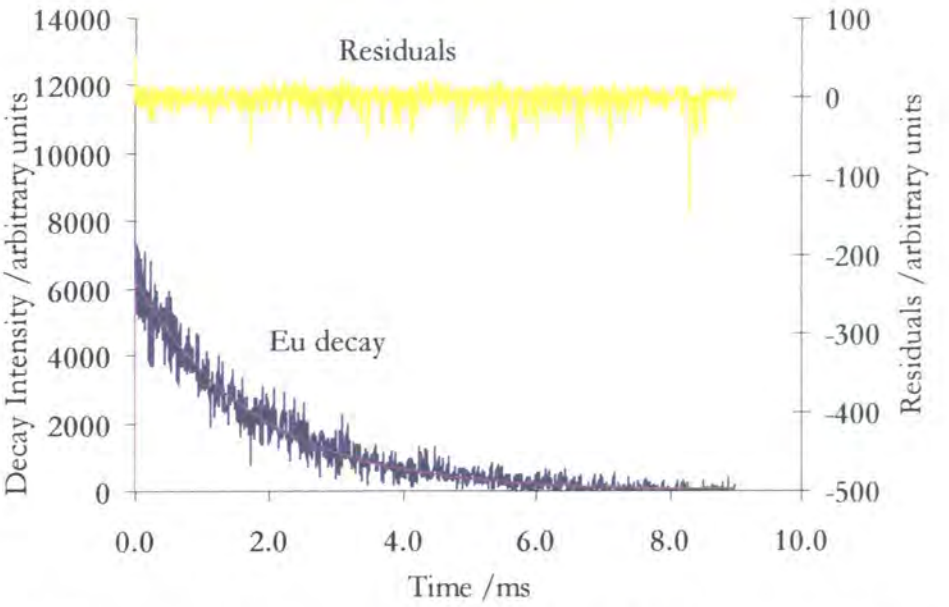

Figure 11. The time resolved emission from Eu in CTAB (S3), monitoring the $^5D_0 \rightarrow ^7F_2$ emission at 617 nm. The Eu decay has a lifetime of 1.7 ms. The randomness of the residuals about zero indicates a good data fit.

The evidence of some energy transfer between phenanthrene and Eu is in keeping with the results reported by Darwent *et al* [2, 3]. They determined that energy transfer between phenanthrene and Ln ions in aqueous micellar solution depended on the relative energies of the aromatic triplet states and the lanthanide excited states. Triplet mediated energy transfer has also been reported as the most likely energy transfer pathway in the sensitised luminescence of Ln complexed with phenanthridine[4] and benzophenone-containing ligands[5], amongst many others.

System 3. (Table caption on next page.)

	Composition. Concentration in mM.		
Sample	**Ln^{3+}complex ion**	**Ligand**	**Solutions**
1	$Eu(fod)_3$. 0.045	MK. 0.005	TritonX-100. 0.5
2	$Eu(fod)_3$ 0.045		TritonX-100. 0.5
3		MK. 0.005	TritonX-100. 0.5
4	$Eu(fod)_3$. 0.045		Pure water
5	$Eu(fod)_3$. 0.025	MK. 0.025	DCM
6	$Eu(fod)_3$. 0.006	MK. 0.006	Toluene

System 3. Europium tris(6,6,7,7,8,8,8 – heptafluoro - 2,2 – dimethyl - 3,5 - octanedionate) $(Eufod)_3$ was chelated with Michler's ketone (MK) in a Triton X-100 (TX-100) micellar solution. In this case MK was acting as the sensitiser and it was desirable to determine if the $Eu(fod)_3$ – MK complex stayed intact in the micellar solution. Sample 5 and 6 were made up in dichloromethane (DCM) and toluene for comparison.

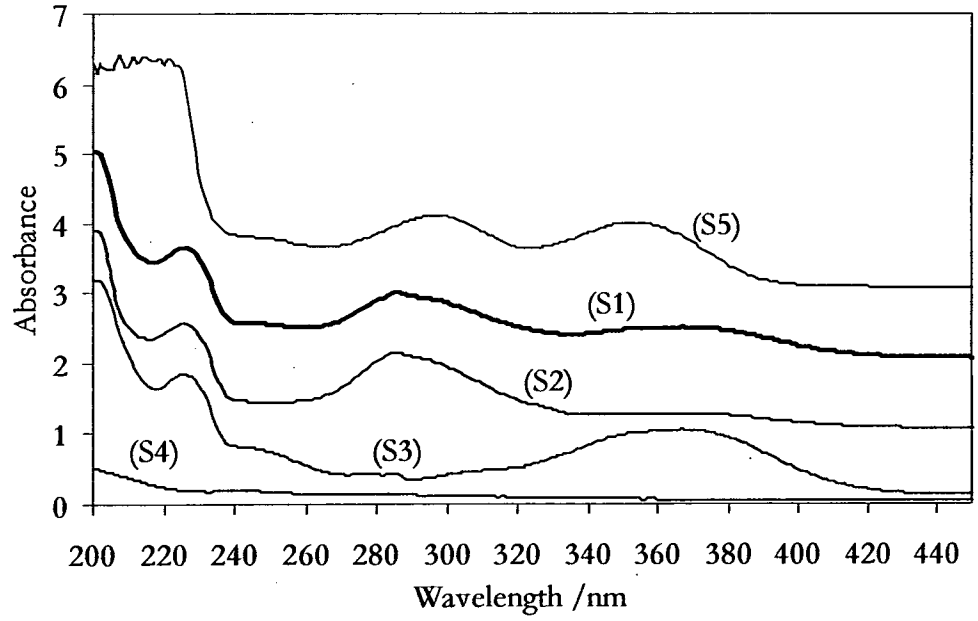

Figure 12. The absorption spectra of $Eu(fod)_3$ with MK in TX-100 (S1) off set by 2 units, $Eu(fod)_3$ in TX-100 (S2) off set by 2 units, MK in TX-100 (S3), $Eu(fod)_3$ in water (S4) and $Eu(fod)_3$ with MK in DCM (S5) off set by 3 units.

In comparing the absorptions of $Eu(fod)_3$ in water (S4) and in TX-100 (S2), in figure 12, it is observed that the micellar solution greatly enhanced the absorption of the europium complex in the near UV to the visible region of the luminescence spectrum. The predominant broad band between 260 nm and 340 nm with a maximum absorbance at 286 nm illustrates this. The characteristic fine structure of europium (III) between 350 nm and 500 nm is not observed. It is expected to be too weak to be apparent in water and in the TX-100 solution there is a minor broad absorbance band observed over the range 340 to 400 nm i.e. where the fine structure should be. The peaks at 223 nm are due to absorption by TX-100 in samples S1, S2 and S3. The broad absorption between 200 nm and 250 nm is that of DCM (S5). The absorbance maximum at 296 nm of $Eu(fod)_3$ with MK in DCM (S5) is blue shifted to 285 nm in TX-100 (S1). The broad peak over the range 320 nm to 425 nm observed in (S1), (S3) and (S5) is the absorption of MK and this appears to be slightly red shifted in the presence of TX-100

when compared to its absorbance in DCM. The shifts in the MK absorption maximum from 355 nm in DCM (S5) to 367 nm in TX-100 (S3) could be the result of the encapsulation of the MK in TX-100.

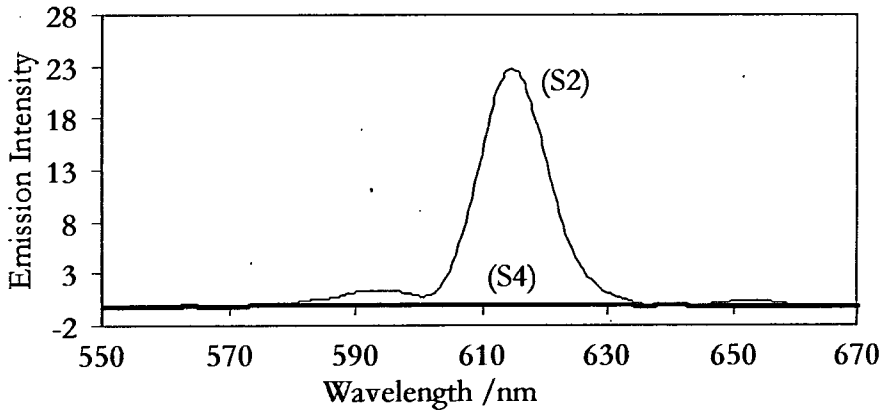

Figure 13. The phosphorescence emission spectra of Eu(fod)3 in TX-100 (S2) and in water (S4) for 397 nm excitation.

The phosphorescence emission of $Eu(fod)_3$ is not detectable in pure water but significantly enhanced when in the micellar environment (figure 13). The hypersensitive band is most affected by this change of environment. This indicates that the micellar solution is reducing the non-radiative decay mechanisms, which results in improved emission from the Ln in the aqueous environment. The presence of MK seems to reduce the europium phosphorescence emission for 365 nm wavelength excitation (figure 14). This excitation wavelength is within the absorption band of MK; MK is absorbing some of the excitation energy and emitting it via non-radiative pathways. This inner filter effect would explain the corresponding decrease in phosphorescence intensity with increasing MK concentration.

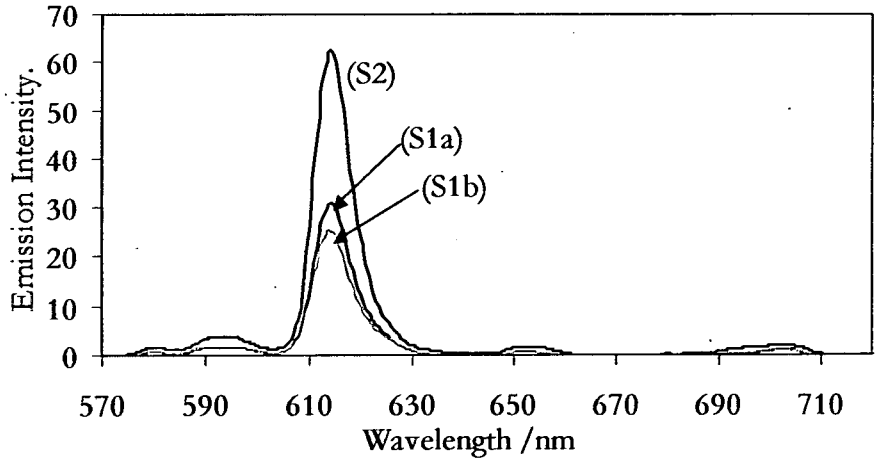

Figure 14. The phosphorescence emission spectra of $Eu(fod)_3$ in TX-100 (S2), $Eu(fod)_3$ in TX-100 with 0.005 mM MK (S1a) and 0.01 mM MK (S1b) for 365 nm wavelength excitation.

The absorption and excitation spectra, for solutions of $Eu(fod)_3$ and MK in TX-100, DCM and toluene are compared in figures 15 to 17. All excitation spectra were recorded for emission at 614 nm. The absorbance bands with maxima at 374 nm in TX-100, 356 nm in DCM and 407 nm in toluene indicate the coordination of MK to $Eu(fod)_3$ in toluene only. The lack of a spectral band in the 320 nm to 480 nm region in the overlaid excitation spectra in figures 15 and 16 indicate that MK does not contribute to the emission at 614 nm from $Eu(fod)_3$ in TX-100 and the chlorinated solvent. In toluene however MK contributes to this emission as illustrated in figure 17 by the presence of the excitation band over the range 380 nm to 450 nm. These results indicate the lack of energy transfer between MK and $Eu(fod)_3$ in micellar and chlorinated solutions while there is clear energy transfer occurring in the organic solvent.

The excitation spectral profile of MK and $Eu(fod)_3$ in toluene is similar to that obtained for the same system in benzene by Werts *et al*[6]. They observed a strong red shift with a maximum at 414 nm in the excitation spectrum upon the coordination of MK with $Eu(fod)_3$. They speculated that the new absorption band was due to a bathochromic shift of the first singlet-singlet transition of MK occurring upon complexation. They found that coordination of MK to lanthanide β-diketonates only occurs in non-coordinating solvents. The emission spectra of Eu(III) β-diketonates are characterised by very intense $^5D_0 \rightarrow {}^7F_2$ bands[7] as observed in figure 14 (S2). A possible reason for the lack of MK-$Eu(fod)_3$ complexation in TX-100 would be the coordinated water

molecules inhibiting the MK and $Eu(fod)_3$ interaction as the MK concentration is quite low (0.005 mM) Also the lanthanide and the ketone may not have been successfully brought together within the micelles to allow Eu sensitisation.

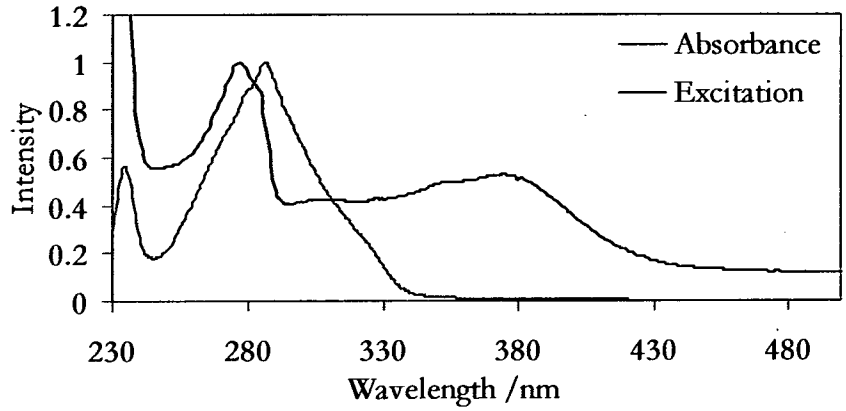

Figure 15. The normalised absorbance spectrum and phosphorescence excitation spectrum for 614 nm wavelength emission from a solution of $Eu(fod)_3$ and MK in TX-100.

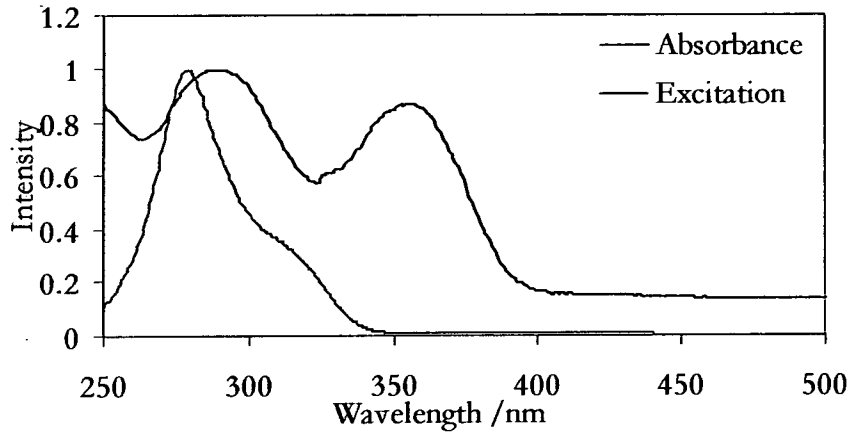

Figure 16. The normalised absorbance spectrum and phosphorescence excitation spectrum for a 614 nm wavelength emission from a solution of $Eu(fod)_3$ and MK in DCM.

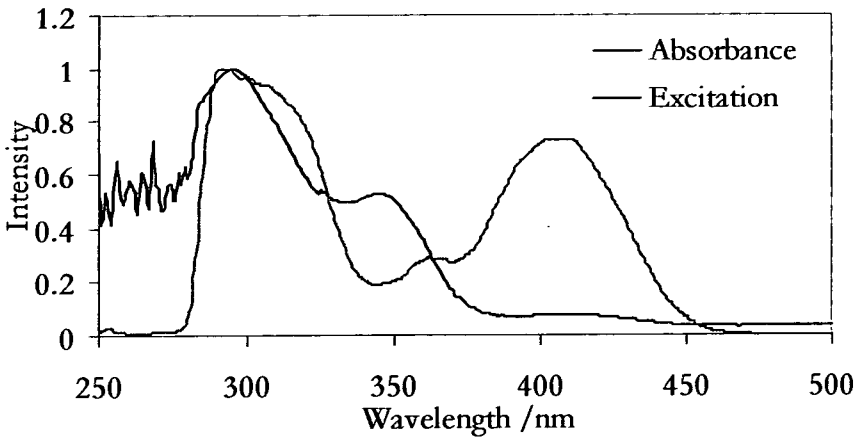

Figure 17. The normalised absorbance spectrum and phosphorescence excitation spectrum for 614 nm wavelength emission from a solution of $Eu(fod)_3$ and MK in toluene.

System 4

	Composition. Concentration in mM.			
Sample	**Ln^{3+} ion**	**Ligand**	**Sensitiser**	**Solutions**
1		MK. 0.025		TritonX-100. 5
2	$Eu(fod)_3$ 0.025			TritonX-100. 2.5
3			1,10-P. 0.025	TritonX-100. 5
4	$Eu(fod)_3$. 0.025		1,10-P. 0.025	TritonX-100. 2.5
5	$Eu(fod)_3$. 0.025	MK. 0.025		TritonX-100. 2.5
6		MK. 0.025		DCM
7	$Eu(fod)_3$. 0.025			DCM
8			1,10-P. 0.025	DCM
9	$Eu(fod)_3$. 0.025	MK. 0.025		DCM
10	$Eu(fod)_3$. 0.025		1,10-P. 0.025	DCM
11	$Eu(fod)_3$. 0.025			Pure Water
12			1,10-P. 0.025	Pure Water
13	$Eu(fod)_3$. 0.025		1,10-P. 0.025	Pure Water

System 4. The absorption and emission spectra of $Eu(fod)_3$ in complexes with Michler's ketone (MK) and 1,10-phenanthroline (1,10-P), in higher concentrations than system 3, were recorded in a micellar solution of TritonX-100 (TX-100). The spectra of the

individual components and the mixtures were also determined in dichloromethane (DCM) and pure water for comparison.

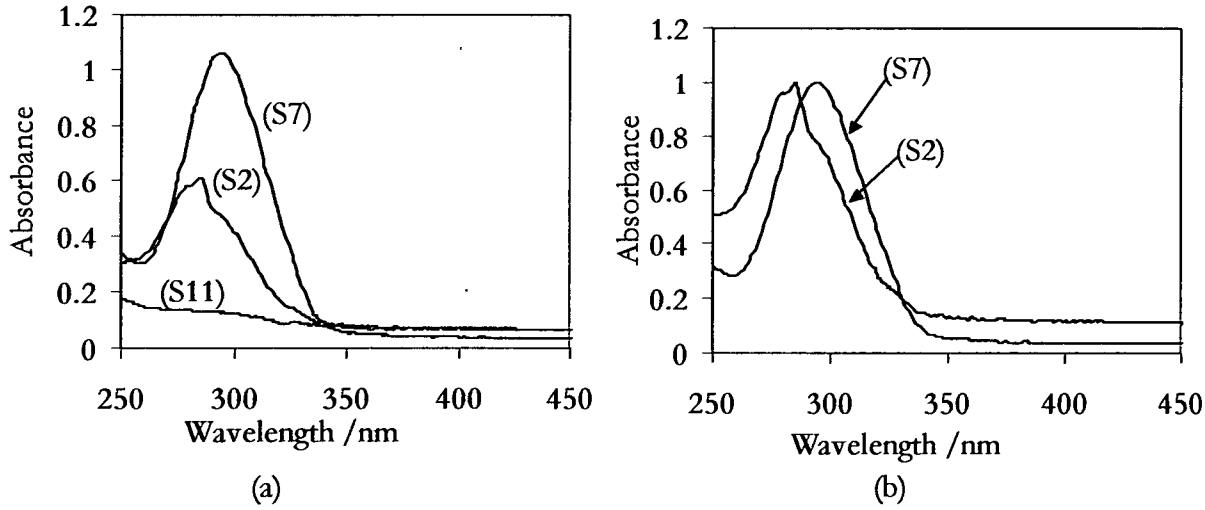

Figure 18. (a). The absorption spectra of $Eu(fod)_3$ in water (S11), TX-100 (S2) and DCM (S7). (b). The normalized absorption of spectra of $Eu(fod)_3$ in TX-100 (S2) and DCM (S7).

Figure 18 (a) shows the absorption spectra of $Eu(fod)_3$ in three different solutions. In water (S11) the absorption profile is almost flat with no distinctive peaks. In TX-100 (S2) and DCM (S7) a broad peak is seen between 250 nm and 340 nm. All three solutions had an approximately 0.025 mM concentration of $Eu(fod)_3$. $Eu(fod)_3$ showed its strongest absorption DCM. The normalised absorption spectra of $Eu(fod)_3$ in DCM and TX-100 in figure 18 (b) shows a 8 nm hypsochromic shift (blue shift) of the absorption maximum of $Eu(fod)_3$ from 293 nm in DCM to 285 nm in TX-100. This is due to the polarity of the TX-100 micellar solution being greater than that of DCM. The weak characteristic line like absorption structure of europium between 350 nm and 450 nm is not observed in any of the solutions. It is observed that TX-100 significantly increases the UV absorption intensity of the lanthanide in water. This is an indication that the lanthanide is associated with TX-100 micelle surface and is thus less likely to be coordinated with the surrounding water molecules.

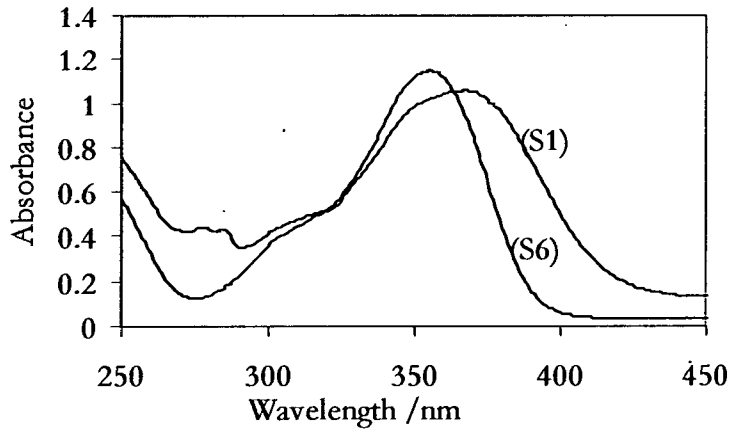

Figure 19. The absorption spectra of MK in DCM (S6) and TX-100 (S1).

MK has a broad absorption band over the range 270 nm to 400 nm in DCM (figure 19). The absorption maximum is red shifted (bathochromic shift) by 12 nm from 355 nm in DCM to 367 nm in TX-100 and the absorption band range extends up to 440 nm.

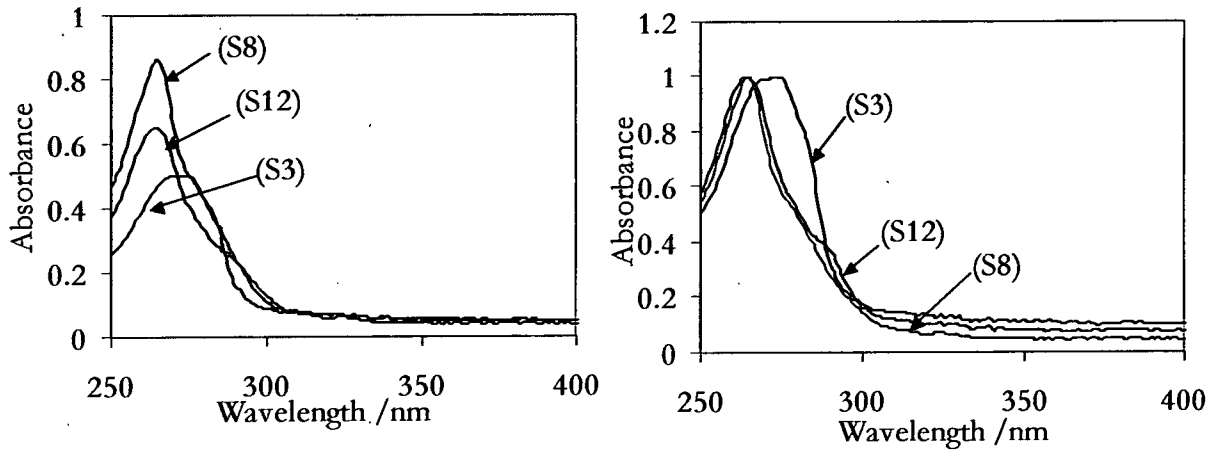

(a) (b)

Figure 20. (a). The absorption of 1,10-phenanthroline in TX-100 (S3), in DCM (S8) and water (S12). (b). The normalized absorption spectra of (a).

Figure 20 (a) shows 1,10-phenanthroline absorbs over the range 250 nm to 300 nm in all three solutions. Its absorption maximum is red shifted by 10 nm from 264 nm in DCM to 274 nm in TX-100 (figure 20 (b)). This shift could be the result of the 1,10-phenanthroline being encapsulated by the TX-100 micelles. The overall absorption band range is unaffected by the solution environment.

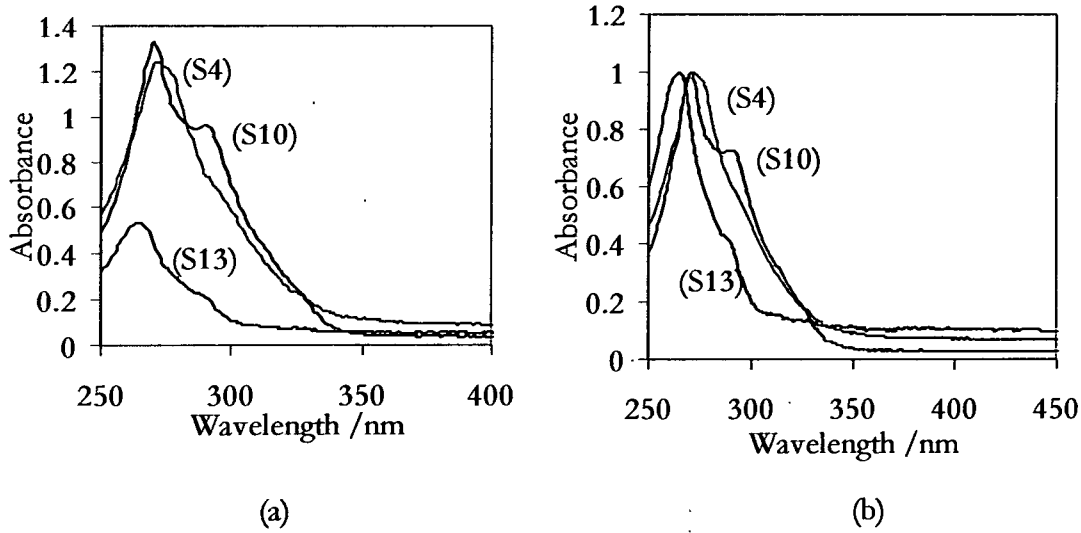

(a) (b)

Figure 21. (a). The absorption spectra of a mixture of $Eu(fod)_3$ and 1,10-phenanthroline in TX-100 (S4), DCM (S10) and water (S13). (b). The normalised absorption spectra of (a).

In figure 21 (a) the mixture of $Eu(fod)_3$ and 1,10-phenanthroline has a broad absorption band over the range 250 nm to 340 nm in DCM and TX-100. The mixture's absorption maxima at 270 nm in DCM and 272 nm in TX-100 are red shifted in comparison to its absorption maximum at 264 nm in water. The $Eu(fod)_3$ and 1,10-phenanthroline mixture in water has a broad absorption band over the range 250 nm to 300 nm and the intensity of the absorption maximum is approximately half that of the absorption intensities of the same lanthanide and sensitiser mixture in DCM and TX-100. The shape and the range of the absorption band for the mixture in water indicate that the 1,10-phenanthroline is the dominant absorption species. In DCM there is a shoulder at around 291 nm on the main absorption peak, which corresponds to the absorption maximum of europium alone in DCM. In the normalised absorption spectra (figure 21 (b)) it is observed that the broad band over the range 250 nm to 350 nm represents the absorption of both europium and 1,10-phenanthroline in TX-100 and DCM.

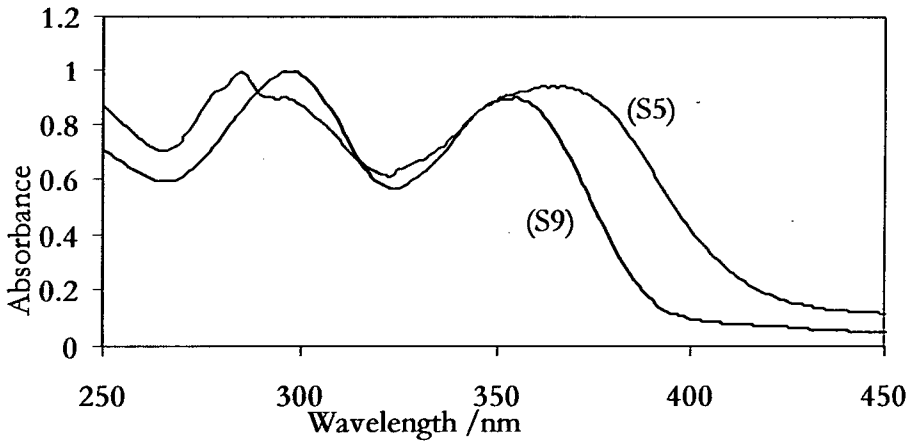

Figure 22. The normalised absorption spectra of a mixture of $Eu(fod)_3$ and MK in TX-100 (S5) and DCM (S9).

Figure 22 shows the absorption spectra of $Eu(fod)_3$ with MK in TX-100 and DCM. It is observed that the peaks at 296 nm and 355 nm in DCM represent the absorption of europium and MK respectively. In the micellar TX-100 solution europium absorption is blue shifted by 11 nm to 285 nm and the MK absorption maximum is red shifted to 362 nm.

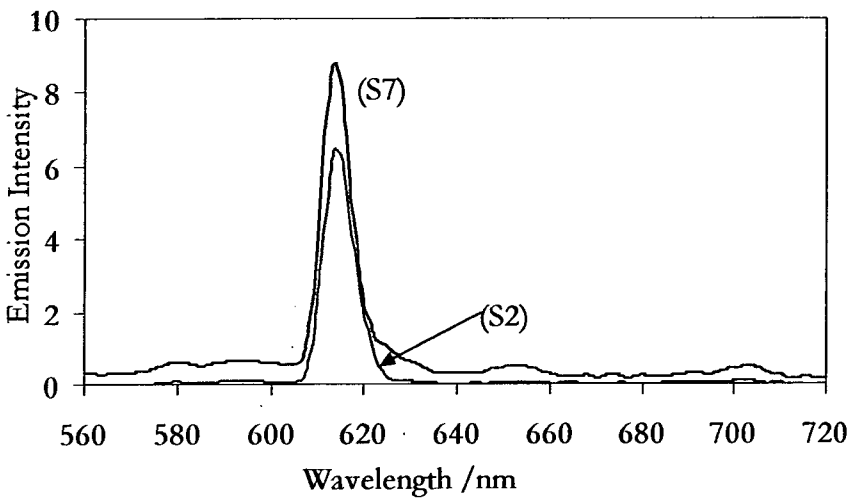

Figure 23. The phosphorescence emission spectra of $Eu(fod)_3$ in TX-100 (S2) and in DCM (S7) for 366 nm excitation.

Figure 23 shows the phosphorescence emission of a 0.025 mM concentration of $Eu(fod)_3$ in TX-100 and DCM. There was no phosphorescence emission from the same concentration of $Eu(fod)_3$ in water under the same conditions. The hypersensitive emission peak at 614 nm is most intense when europium is in DCM. However its emission is greatly enhanced in an aqueous micellar solution. The TX-100 micelles

association with the lanthanide has significantly reduced quenching of the europium emission.

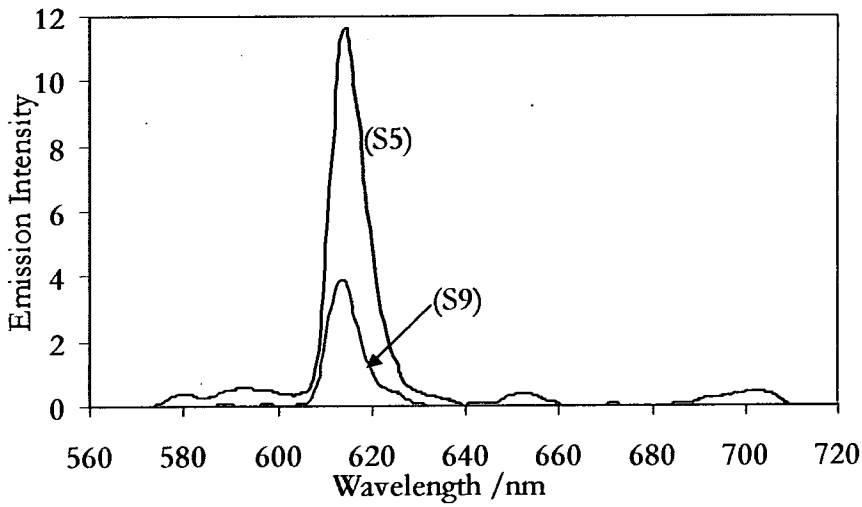

Figure 24. The phosphorescence emission spectra of $Eu(fod)_3$ chelated with MK in TX-100 (S5) and in DCM (S9) for 366 nm excitation.

The phosphorescence emission from europium chelated with MK is significantly enhanced in the aqueous micellar solution of TX-100 (figure 24) in comparison to its emission in DCM for a 366 nm excitation wavelength. In TX-100 there is an approximately 44% increases in the intensity of the hypersensitive ($^5D_0 \rightarrow {}^7F_2$) europium band when $Eu(fod)_3$ is chelated with MK (figure 24 S5) as opposed to when it is not (figure 23 S2). MK shows no significant phosphorescence when excited at 366nm. The observations could be an indication of MK effectively sensitising the europium (III) emission. The possible sensitisation pathway would be the following. MK shows strong absorption at the 366 nm excitation wavelength compared to europium. The excitation of the coordinated MK into its singlet state and subsequent intersystem crossing to its triplet state results in an energy transfer from the ligand triplet state to the europium ion. The singlet triplet energy gap in the coordinated MK must be quite small in order for efficient energy transfer to take place. An electron transfer mechanism may also be involved.

TX-100 has made the complex soluble and stable in aqueous media. The data suggests that at higher concentrations the lanthanide-ligand complex forms and is associated with the micelles, which protect the lanthanide emission from being quenched. The low emission of the complex in DCM is possibly due to the complex falling apart or the

widening of the energy gap between the singlet and triplet states of the MK leading to less efficient energy transfer mechanisms.

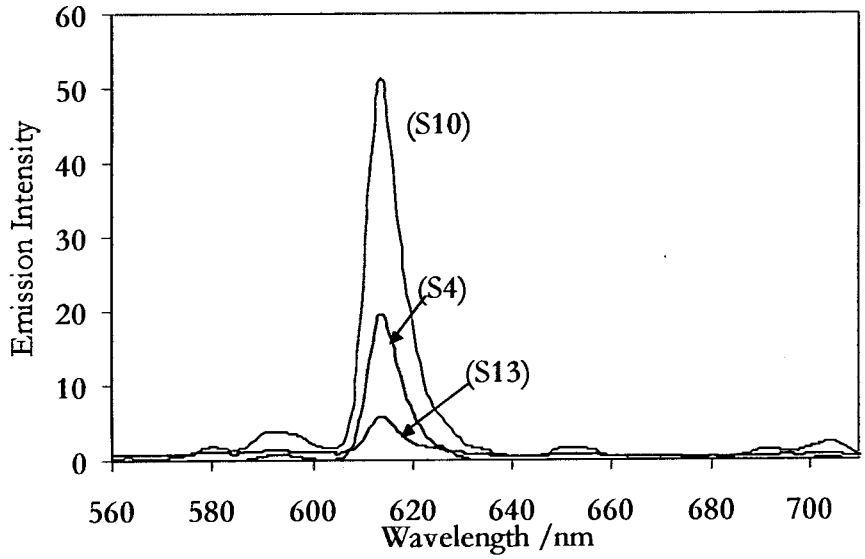

Figure 25. The phosphorescence emission spectra of $Eu(fod)_3$ in the presence of 1,10-phenanthroline in TX-100 (S4), DCM (S10) and water (S13) for 366 nm excitation.

Figure 25 shows the phosphorescence emission of $Eu(fod)_3$ with 1,10-phenanthroline as the proposed sensitiser in different solvent environments. The emission intensity of the europium hypersensitive band at 614 nm in TX-100 is approximately 67% greater with 1,10-phenanthroline (figure 25 S4) than without (figure 13 S2). Compared to the europium-MK complex in TX-100 (figure 24 S5) this europium hypersensitive band in 1,10-phenanthroline and TX-100 increased in intensity by approximately 40%. The observations indicate that the micelles have encapsulated the 1,10-phenanthroline and it is brought into close proximity to the Eu ions allowing for sensitisation of the Ln emission.

In water it is clear that 1,10-phenanthroline has enhanced the europium emission with a 100% increase in the intensity of emission at 614 nm (figure 25 S13). In DCM the europium hypersensitive emission band is 83% more intense when 1,10-phenanthroline is used as a possible sensitiser (figure 25 S10) as opposed to when its not (figure 23 S7). The intensity of the europium hypersensitive band is greatest in DCM (figure 20 S10) because there are no water molecules to compete with 1,10-phenanthroline for binding sites on the lanthanide ion. These observations indicate that 1,10-phenanthroline is bonding with the Ln ion instead of water molecules thus reducing the quenching of the emission. Also the phosphorescence emission data recorded in DCM could be deemed

the result of an energy transfer from the 1,10-phenanthroline to the Eu^{3+}. Thus the increase in intensity of the europium emission is due to a reduction in the quenching mechanisms and sensitisation by 1,10-phenanthroline. Eu(III) complexes with a 1,10-phenanthroline subunit have been synthesised and reported to be highly luminescent in water as a result of the chromophore excluding water from first coordinating sphere of the metal[8].

Lifetime measurements of europium with the free radical TEMPO.

The lifetime of a $Eu(fod)_3$ (0.025mM) 614.5 nm emission after 317 nm excitation with and with out the 2,2,6,6,-tetramethyl-1-piperidinyloxy free radical (TEMPO) (0.025mM) in micellar solutions of TritonX-100 was measured. Measurements were taken with a 400 nm cut off filter to remove scattered light. The lifetime of $Eu(fod)_3$ in TritonX-100 was determined to be ~630 μs. In the presence of TEMPO it decreased to ~540 μs. The life time of $Eu(fod)_3$ was determined to be ~109 μs in pure water and ~370 μs in DCM. The micellar solution clearly enhances the longevity of the europium emission from the $^5D_0$ luminescent state in aqueous medium. In TritonX-100 micellar solutions the free radical does not significantly affect the lifetime of the lanthanide emission which is surprising, given the propensity of TEMPO to quench excited states. This general lack of effect of the free radical on the lifetime of the Ln could be due to the Eu(III) not coming in close enough contact to allow for any energy transfer to occur. It is reported that the binding constants of nitroxyl radicals to micelles are higher to charged micelles than to neutral ones[9].

Conclusion and further work

The results of the photoluminescence and lifetime studies generally show that the luminescent properties of a europium complex, $Eu(fod)_3$, are enhanced in micellar aqueous solution. TX-100 proved to be the better of the two micellar solutions studied. There is evidence that the association of Eu complexes with the micelle surface reduces the quenching of the emission by O-H interactions. The Eu (III) complexes and sensitisers, which are normally poorly soluble in water, dissolve quite readily in micellar aqueous solutions. The ligands and sensitisers studied all absorb in the same near UV to visible region as europium. However 1,10-phenanthroline and phenanthrene shows evidence of having sensitised europium phosphorescence emission via energy transfer from their triplet T_1 state to the Eu $^5D_2$ state. It is known that intramolecular energy

transfer from the triplet state of organic ligands to coordinated Ln is very efficient[10]. The comparison of the excitation spectra of low concentrations of $Eu(fod)_3$ and MK in solutions of TX-100, DCM and toluene proves no energy transfer occurs between the two in aqueous micellar solutions or in chlorinated solvents. At higher lanthanide and sensitiser concentrations there is evidence of complex formation and sensitisation of the Eu emission in the aqueous micellar environment. The variations in the phosphorescence emission spectra are due to sensitivity of the electric dipole transitions to the chemical environment[1].

There is also evidence of the lifetime of the europium phosphorescence being prolonged due to its association with the micellar surface.

Further work needs to be done to conclusively identify the optimum wavelengths in the visible region of the spectrum and the most effective combination of ligands and sensitisers for the enhancement of the phosphorescence emission of europium.

S. Mallik and co-workers have synthesised several fluorescent, polymerisable, metal-chelating lipids[11]. They have made several lipid–terbium complexes which have been incorporated into liposomes and polymerised. This group proposed to use the conjugated dialkyne moiety of the lipids, before polymerisation, or the conjugated alkenes, after polymerisation, as sensitisers for the lanthanide emission.

REFERENCES

1. Werts M. H. V., R. T. F. Jukes, and J. W. Verhoeven. *Phys. Chem. Chem. Phys.*, 2002. **4**: p. 1542-1548.
2. Darwent J. R., C. D. Flint, and N. W. Sharpe. *J. Chem. Soc., Chem. Commun*, 1988: p. 747-748.
3. Darwent J. R., W. Dong, C. D. Flint, and N. W. Sharpe. *J. Chem. Soc. Faraday Trans.*, 1993. **89**: p. 873-880.
4. Beeby A., S. Faulkner, D. Parker, and J. A. G. Williams. *Perkin Transaction 2*, 2001: p. 1268-1273.
5. Beeby A., L. M. Bushby, D. Maffeo, and J. A. G. Williams. *Perkin Transaction 2*, 2000: p. 1281-1283.
6. Werts M. H. V., M. A. Duin, J. W. Hofstraat, and J. W. Verhoeven. *Chem. Commun.*, 1999: p. 799-800.
7. Melby L. R., N. J. Rose, E. Abramson, and J. C. Caris. *J. Am. Chem. soc.*, 1964(86): p. 5117.
8. Quici S., G. Marzanni, M. Cavazzini, P. L. Anelli, M. Botta, E. Gianolio, G. Accorsi, N. Armaroli, and F. Barigelletti. *Inoganic Chemistry*, 2002. **41**(10): p. 277-2784.
9. Almeida L. E., I. E. Borissevitch, V. E. Yushmanov, and M. Tabak. *Journal of Colloid and Interface Science*, 1998. **203**: p. 456-463.
10. Filipescu N. and G. Mushrush. *J. Phys. Chem*, 1968. **72**: p. 3516.
11. Roy B. C., R. Peterson, S. Mallik, and A. D. Campiglia. *J. Org. Chem.*, 2000. **65**: p. 3644-3651.

Discussion. Polyarylethynylenes.

1,4-bis(phenylethynyl)benzene (1).

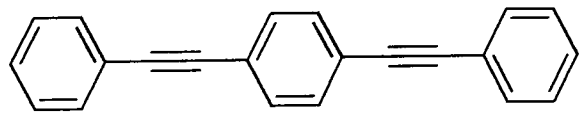

1

The absorption, emission and excitation spectra were recorded in cyclohexane to determine if concentration affected its spectral profile. These spectral data measurements were also recorded in EPA glasses at 77K. The lifetime was recorded in cyclohexane and compared to published results.

The absorption spectra of **1** in cyclohexane featured a series of partially resolved bands between 250 nm and 350 nm including a sharp band edge at the red end of the absorption profile (Figure 1). This profile is consistent over the concentration range 10^{-6} - 10^{-4} mol dm^{-3}. The absorption varies linearly with concentration over this range, suggesting no significant aggregation phenomena takes place in this solvent. This is consistent with that published by Biswas *et al*[1]. Similar spectra were observed by others in toluene, acetonitrile and dioxane solutions[1, 2] The maximum extinction coefficient was determined to be 58,000 ± 1000 mol^{-1} dm^3 cm^{-1} at the 320 nm peak.

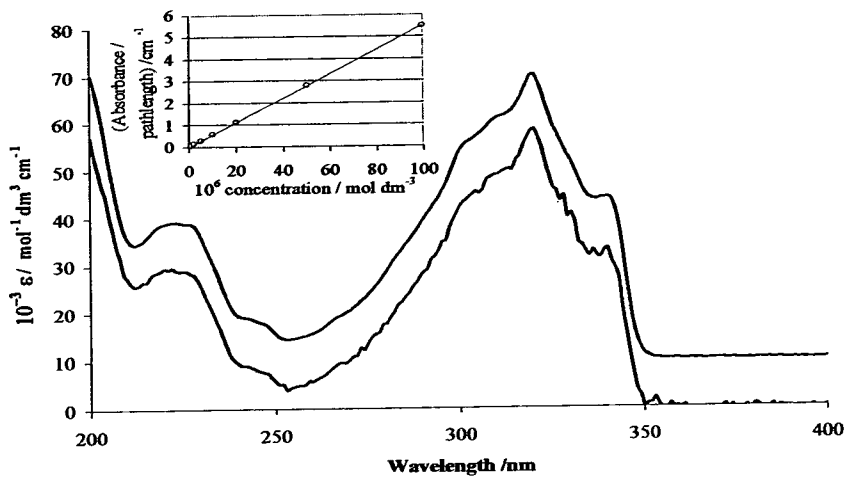

Figure 1. UV Absorption spectrum of 1 x 10^{-6} (lower trace) and 250 x 10^{-6} mol dm^{-3} (upper trace) solutions of **1** in cyclohexane at 293K. The upper trace has been offset by 10,000 $mol^{-1}dm^3cm^{-1}$ for clarity. The inset shows the absorbance at the peak, 320 nm, as a function of concentration[3].

The emission spectra at room temperature were collected using excitation wavelengths from 230 nm to 400 nm (Figure 2). The emission band profiles across this range of excitaion wavelngths are constant with some vibrational fine structure observed at 346 nm, 362 nm and 375nm. The excitation spectra are independent of the chosen emission wavlength and resemble the UV-vis absorption spectrum.

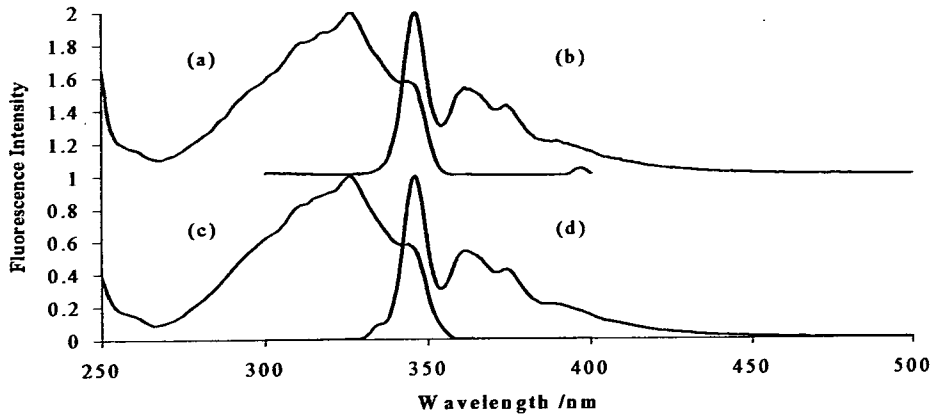

Figure 2. Normalized fluorescence excitation and emission spectra obtained from a 10^{-6} mol dm^{-3} solution of **1** in cyclohexane. The excitation spectra (a) and (c) were obtained using emission wavelengths of 450 nm and 350 nm respectively, and the emission spectra (b) and (d) were obtained using excitation wavelengths of 270 nm and 340 nm respectively. The small peak at 397 nm in spectrum (a) is due to Raman scatter from the solvent. Both the excitation and emission monochromators were set to a band pass of 2.5 nm FWHM[3]. Spectra (a) and (b) have been off set for clarity.

In order to confirm the homogeneity of the fluorescence spectrum at 298 K, the excitation-emission matrix (EEM) of dilute solution of **1** was recorded in cyclohexane (Figure 3). 69 emission spectra over the range 300 nm to 500 nm were recorded. This is achieved by stepping the excitation wavelength from 230 nm to 400 nm in 2.5 nm increments. The resulting emission spectra and corresponding excitation spectra are recorded as a three-dimensional plot against intensity as illustrated in figure 3. The excitation and emission spectra are found to be independent of the emission and excitation wavelengths respectively. The 3-dimensional plot of this data is indicative of the homogeneity of the excitation and emission spectra.

The lifetime was found to be 0.53 ± 0.05 ns and was independent of excitation wavelengths over the range 230 nm to 400 nm and emission wavelengths ever the range 300 nm to 500 nm. This was consistent with earlier measurements made by Biswas *et al*[1] who determined the lifetime to be 0.57 ns in hexane. A typical fit is shown in figure 4.

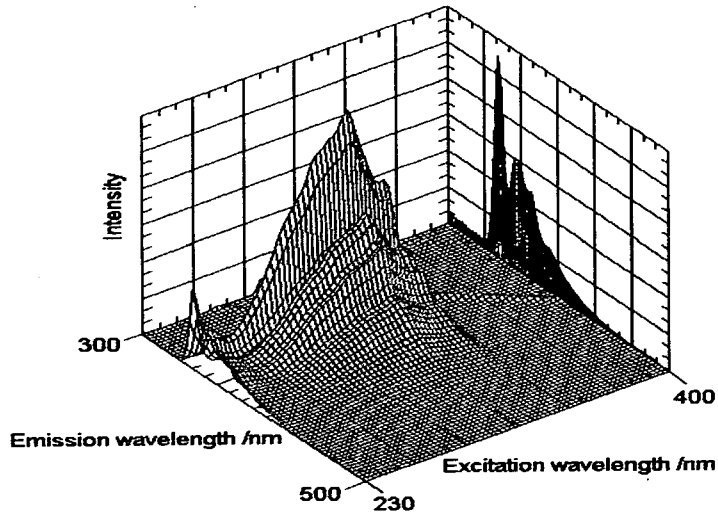

Figure 3. Fluorescence excitation and emission matrix obtained from a 10^{-6} mol dm^{-3} solution of **1** in cyclohexane. The emission spectra have been projected onto the right-hand side panel. The ridge of small peaks that appear at excitation wavelengths longer than 350 nm are the result of Rayleigh scatter by the sample[3]

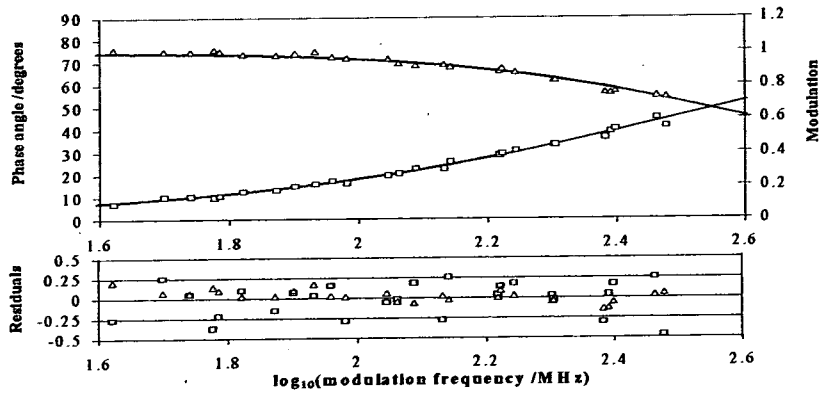

Figure 4. Data obtained by phase-modulation technique for the determination of the fluorescence lifetime of **1** in aerated cyclohexane using excitation at 320 nm and emission at 360 nm. The curves show the fit of the phase (squares) and modulation (triangles) for a single exponential decay with a lifetime of 0.53 ns. The normalized residuals are shown below. $\chi^2 = 0.80$[3].

The variations of the absorption spectra of **1** with changing temperature were recorded for 298 K, 199 K, 100 K and 77.3 K. The absorption spectra were recorded for a solution of **1** in ether pentane alcohol (EPA in the ratio 5:5:2). The absorption spectra of **1** at 77.3 K showed changes in the absorption profile with a significant increase in absorption at the red edge and a slight decrease at the blue edge (Figure 5). Low temperatures results in considerable narrowing of the vibrational features of the spectra. Distinct absorption peaks are observed at 322, 328, 333 and 344 nm at 77.3 K. The red

shift could be due to an increase in the index of refraction, and hence the polarisability, of the solvent in going from liquid to the solid phase. This redistribution of the absorption spectral intensity to the lower energy vibronic features and the spectral narrowing at low temperature may be attributed to a reduction in the thermal population of higher energy vibronic states.

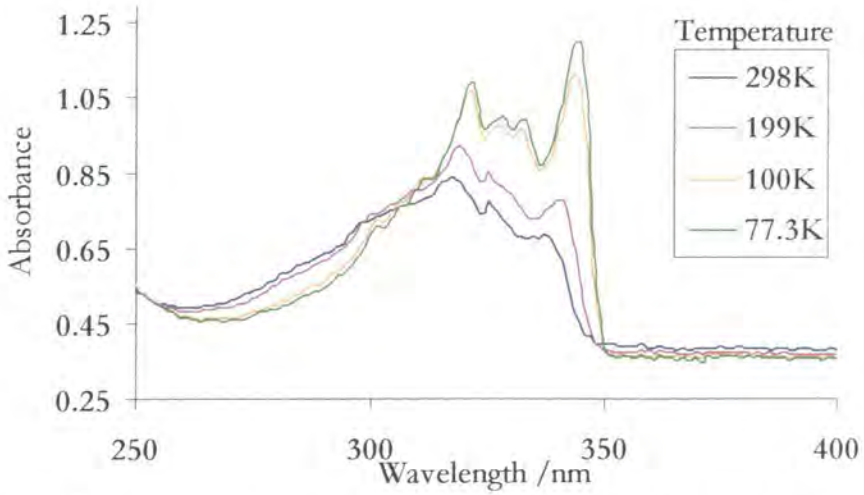

Figure 5. Absorption spectrum of **1** in EPA at 298 K, 199 K, 100 K and 77.3 K.

Figure 6 and 7 illustrates the change in the emission and excitation spectra of **1** with changes in temperature. The emission and excitation spectra were recorded for a solution of **1** in methylcyclohexane/2-methylbutane (MCH/IP in the ratio 4:1). The emission and excitation spectra were determined using excitation at 335 nm and emission at 350 nm respectively. As expected the vibronic features are better resolved at low temperatures and there is an overall increase in peak intensity. The excitation spectra are more affected by the change in temperature than the emission spectra. There is a more dramatic change in the profile at 100 K and 77 K as the vibronic structure becomes much more pronounced and red shifted.

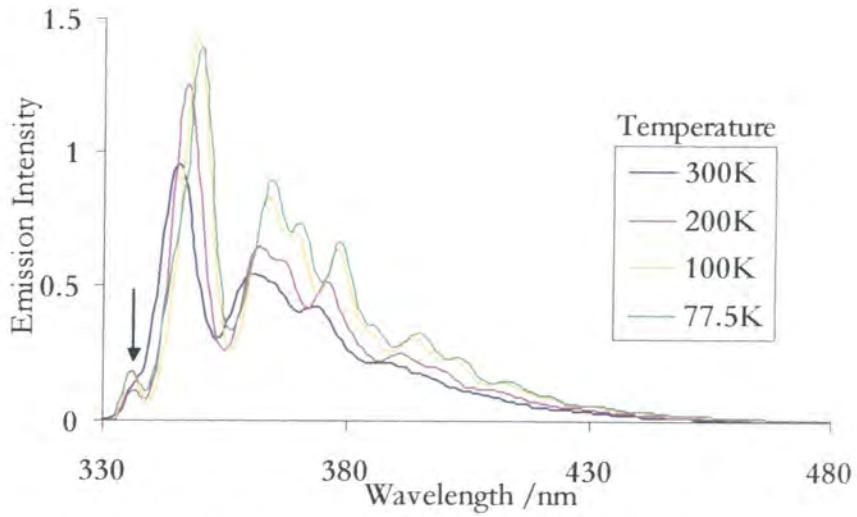

Figure 6. Emission spectra of **1** in MCH/IP for 335 nm excitation at 300 K, 200 K, 100 K and 77.5 K The arrow indicates a peak due to scattered light at 335 nm.

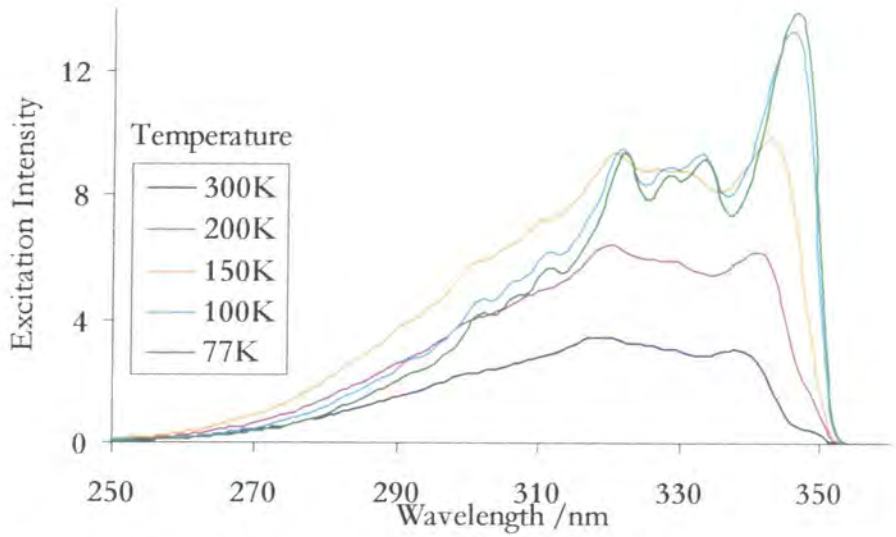

Figure 6. The excitation spectra of **1** in MCH/IP for 350 nm emission at 300 K, 200 K, 150 K, 100 K and 77 K.

The excitation spectra are similar to the absorption spectra at 77K and more like the mirror image of the emission spectrum with a strong (0,0) band and a small Stokes shift (Figure 8).

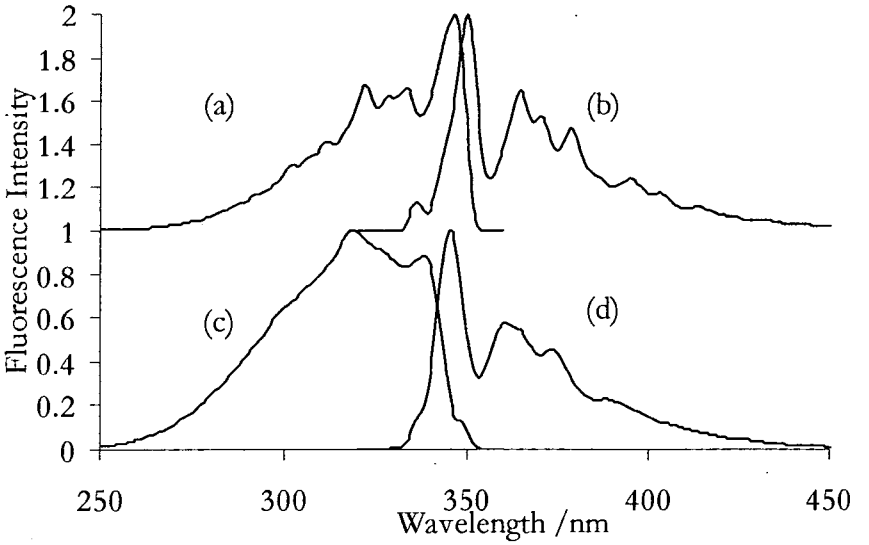

Figure 8. Normalised fluorescence excitation and emission spectra for **1** in MCH/IP at 77 K, (a) and (b), and 300 K, (c) and (d) determined using emission at 350 nm and excitation at 335 nm.

When the normalised fluorescence excitation and emission matrix of **1** at 298 K and 77 K are compared (Figure 9 and 10) evidence of changes in the emission spectrum with excitation wavelength is observed at low temperature. This suggests more complex behaviour in the low temperature glass. This can be attributed to the fact that in low temperature glasses there is a continuum of conformers each having its own absorption and emission spectrum and the rate of rotation of the phenyl rings with respect to one another is now comparable to the fluorescence lifetime. It is possible that the range of conformations is more limited in the low temperature glass with a greater bias towards the planar form. Since the rotational barrier is calculated to be low (about 3.6 kJ/mol) cooling to 77K does not sufficiently reduce kT to limit the material to only the planar form.

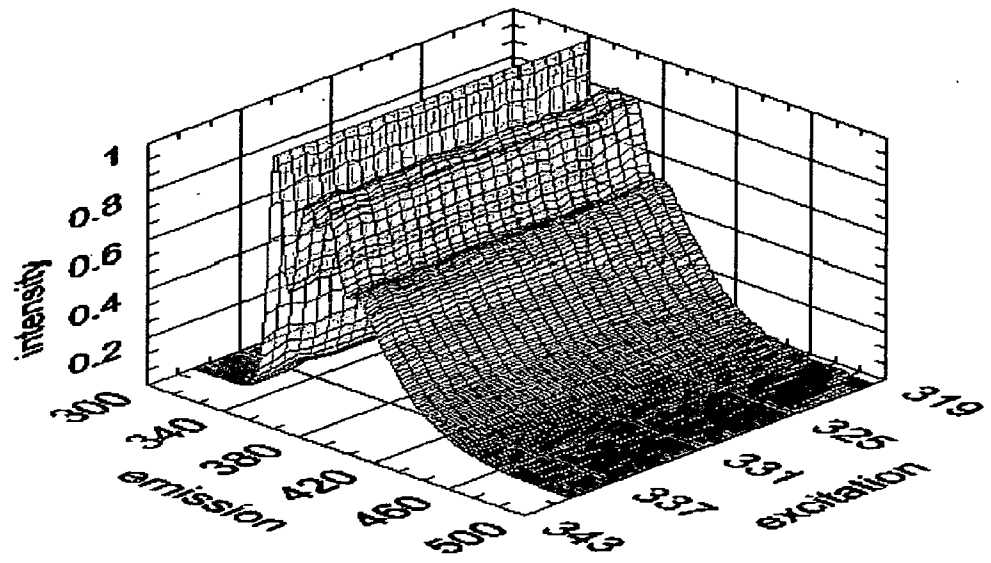

Figure 9. Fluorescence excitation and emission matrix obtained from a solution of **1** in EPA at 298 K normalised at 344 nm.

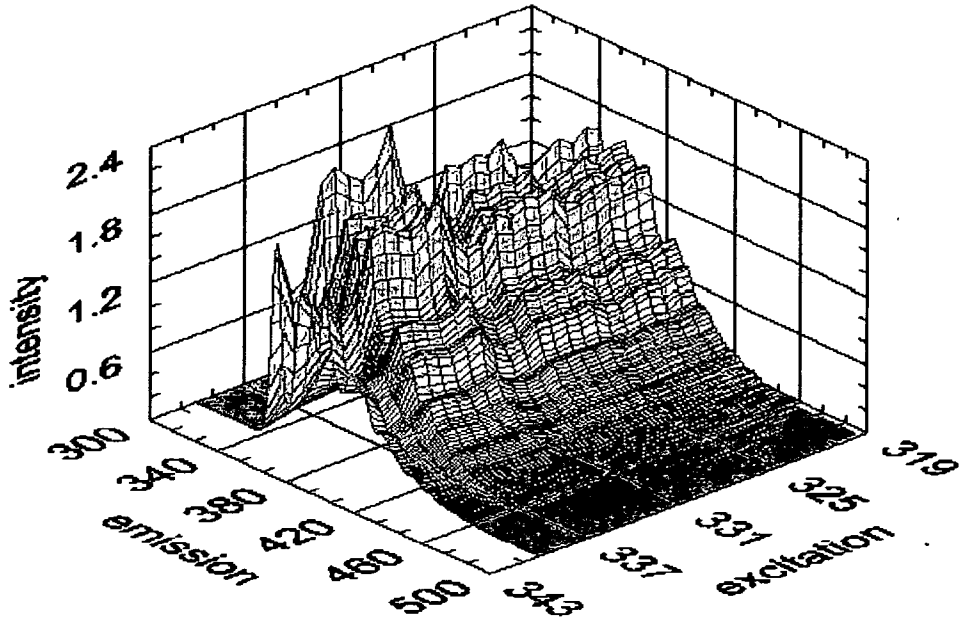

Figure 10. Fluorescence excitation and emission matrix obtained from a solution of **1** in EPA at 77 K normalised at 344 nm.

Several models have been proposed to account for the dynamic behaviour of **1** and structurally related systems on the basis of photophysical studies. A two state model was proposed by Cherkasov *et al* in which the aromatic rings adopt co-planar or orthogonal conformations to account for the low temperature fluorescence behaviour

of 9,10-bis(phenylethynyl)anthracene[4]. A similar description was proposed by Levitus *et al.* to account for their observations of **1**[5].

However, in contrast to these hypotheses, we suggest that there is a continuum of rotational conformers of **1** in solution and that the distribution of these conformers in the ground electronic state changes with temperature[3].

Our observations and interpretations are in agreement with the conclusions of Sluch *et al*, who investigated the dynamics of the fluorescence of a substituted oligophenyleneethynylene, (2) [6].

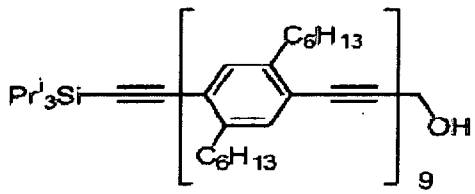

2

Their work indicated that rotational relaxation occurred very rapidly in the excited state, with a recorded time constant of 60 ps, and they interpreted their data in terms of a quadratic coupling model. Using fast time-resolved emission spectroscopy, they demonstrated that the blue edge of the emission shifted in a subtle fashion at early times after excitation, evidence for the rapid planarisation of the excited state. In their model, Sluch *et al.* suggest that the system behaves as though the potential well is very small in the ground electronic state but that in the first excited state the planar form is considerably more stable than the non-planar conformers. These interpretations are further supported by subsequent work on anthrylethynylenes reported by Garcia-Garibay's group.[7, 8].

The fluorescence quantum yield (Φ_f) was determined for **1** in cyclohexane for 342 nm excitation using quinine sulfate (QS) in 0.1 M H_2SO_4 ($\Phi_f = 0.55$) and β-carboline (BC) in 1 M H_2SO_4 ($\Phi_f = 0.6$). The average quantum yield for **1** was found to be 0.85 ± 0.02.

Nakatsuji *et al*[9] found the quantum yield of **1** in $CHCl_3$ to be 0.56 for excitation at 322 nm, using quinine sulphate in 0.1 M H_2SO_4 as their standard and a 90^0 instrument geometry. The reasons for this discrepancy are not yet fully understood. It is possible however that in $CHCl_3$ other processes may have quenched some of the emission. Chlorinated solvents are not ideal for photophysical measurements since they can form radical species.

Ongoing work includes the determination of the lifetime in viscous solvents, anisotropy measurements and time resolved emission spectral measurements.

9,10-bis(phenylethynyl)anthracene (3)

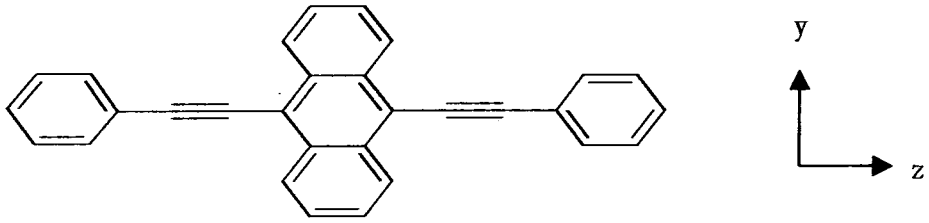

3

The photoluminescence of **3** was studied over the temperature range 298 K to 77 K in non-viscous solutions. Figure 11 shows the variable temperature absorption spectra of **3** in EPA. At 298 K the absorption profile over the visible region is broad and the vibronic structure is not well defined. The characteristic red shift and increased vibronic fine structure as temperature decreases is observed. The broad major peaks in the visible region at 433 nm and 456 nm at 298 K are red shifted to 445 nm and 474 nm respectively. Along with a more highly defined vibronic structure an additional peak is seen at 419 nm at 77 K.

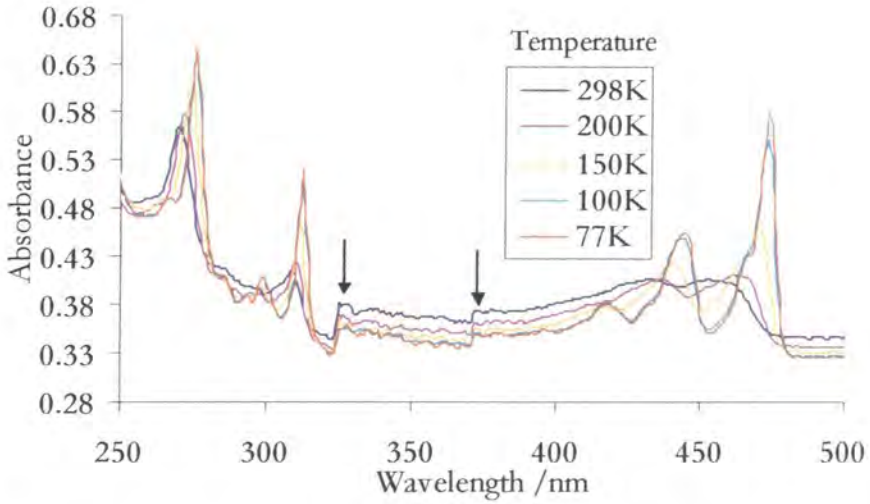

Figure 11. Absorption of **3** in EPA 298 K, 200 K, 150 K, 100 K and 77 K. The arrows indicate diviations due to the spectrometer filter changes and lamp changes.

The emission and excitation spectra of **3** are also temperature dependent as observed in figure 12 and 13. The two main emission peaks when **3** is in solution are 469 nm and 500 nm. At 77 K these peaks are red shifted to 476 nm and 506 nm respectively. A minor peak also appears at 532 nm. The decrease in intensity is probably due to re-absorption of some of the emission as the concentration of molecules with the same lower energy conformation, increases.

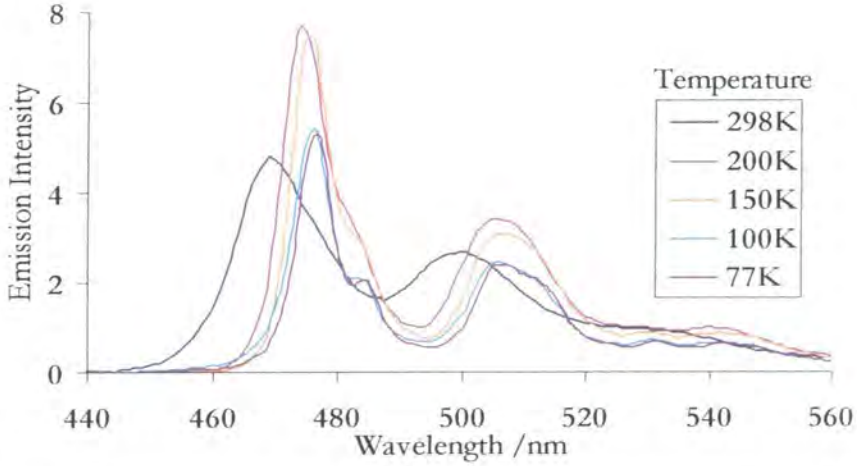

Figure 12. Emission spectra of **3** in EPA for 410 nm excitation at 298 K, 200 K, 150 K, 100 K and 77 K.

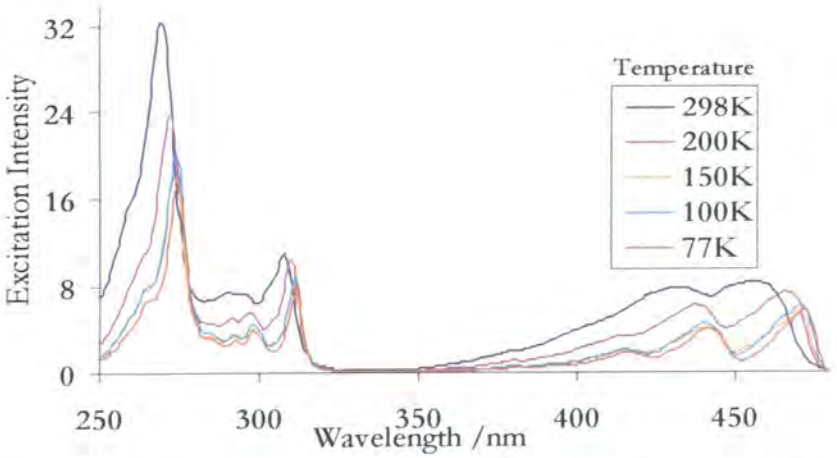

Figure 13. Excitation spectra of **3** in EPA for 498 nm emission at 298 K, 200 K, 150 K, 100 K and 77 K.

At 298 K, in figure 14 (c) and (d), the excitation and emission profiles of **3** are not mirror images of each other. The two profiles (a) and (b) are more like mirror images of each other at 77 K. This indicates the vibrational level spacings are almost the same in both the ground and excited states under these conditions. This could be attributed to the same phenomenon that is observed in **1** at low temperature i.e. there is a limited range of conformers with a bias towards the low energy planar form in low temperature glasses. However at room temperature there is a range of conformers in the ground state (Figure 11) but the planar conformation is predominant in the excited state (Figure 12).

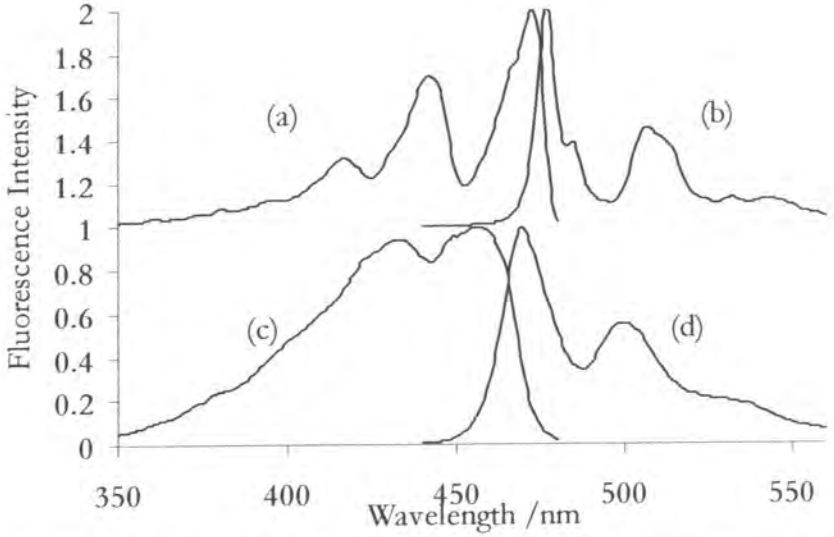

Figure 14. Normalised fluorescence excitation and emission spectra for **3** in EPA at 77 K (upper profiles) and 298 K (lower profiles). The excitation spectra (a) and (c) were determined using a 498 nm emission wavelength and the emission spectra (b) and (d) were obtained using a 410 nm excitation.

Table 1 compiles the possible peak assignments for the energy transitions occurring at 77 K. Here $v'' \rightarrow v'$ indicates absorption from the lowest vibrational level in the ground state to one of the vibrational levels in the excited states. The $v' \rightarrow v''$ annotation represents emission from the lowest excited vibrational level to one of the ground state vibrational levels. There is a small Stokes Shift and very strong (0,0) bands.

Table 1

Absorption Transitions $v'' \rightarrow v'$	λ_{max} /nm	Transition Energies hv_e^{max} / cm^{-1}		Emissive Transitions $v' \rightarrow v''$	λ_{max} /nm	Transition Energies hv_e^{max} / cm^{-1}
$0 \rightarrow 0$	474	21,100		$0 \rightarrow 0$	476	21,000
$0 \rightarrow 1$	445	22,500		$0 \rightarrow 1$	506	19,800
$0 \rightarrow 2$	419	23,900		$0 \rightarrow 2$	532	18,800

A tabulation of the absorption and emissive wavelengths and proposed vibrational energy transitions occurring in **3** at 77 K.

1,4-bis(9-ethynylanthracenyl)benzene (4).

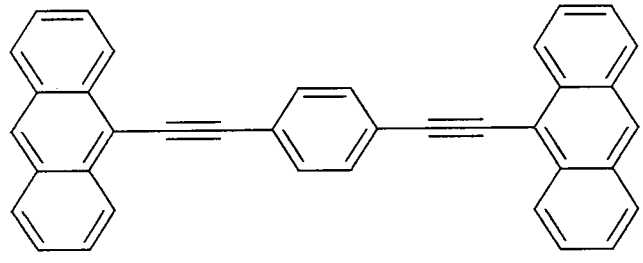

4

The effect of solution viscosity and low temperature on the photoluminescence properties of **4** was studied at 298 K and 195K in viscous solutions. The absorption spectra of **4**, in figure 15, has a broad band between 350 nm and 470 nm with a maximum at about 430 nm. Like **3**, the excitation and emission profiles are not mirror images of each other at room temperature (Figure 16). The emission spectra of **4** is quite well defined in solution at room temperature with major peaks at 456 nm, 485 nm and 506 nm.

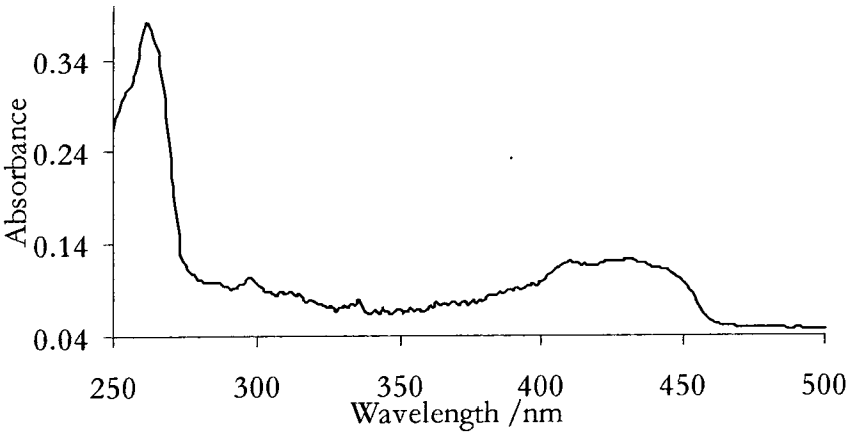

Figure 15. The absorption spectra of **4** in cyclohexane at room temperature.

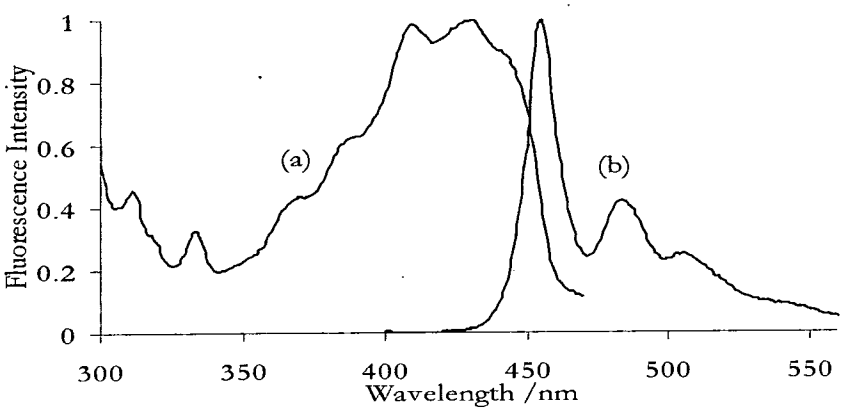

Figure 16. The normalised excitation (a) and emission (b) spectra of a solution of **4** in cyclohexane. The excitation spectrum was obtained using a 500 nm emission wavelength and the emission spectrum was obtained using a 355 nm excitation wavelength.

The excitation spectra showed slight variation across the 540 nm to 480 nm emission range when the temperature of a solution of **4** in paraffin was decreased from 298 K (Figure 17) to 195 K (Figure 18). The excitation spectra were recorded for the emission wavelengths 480 nm, 500 nm, 520 nm and 540 nm. At 298 K the excitation profile is quite consistent across the previously mentioned emission range. They resemble the absorption profile with major bands at about 412 nm, 429 nm and 445 nm. At low temperature, the peak at the red edge is sharper, more dominant, and varies in position with emission wavelength. At shorter emission wavelengths the excitation spectra is significantly blue shifted. For 480 nm emission the excitation peak at 445 nm at 298 K shifts to 447 nm at 195 K. More significantly, for a 500 nm wavelength emission, the maximum at the red edge of the excitation spectra moves from 446 nm at 298 K to

457 nm at 198 K. The excitation spectra for 520 nm and 540 nm emission both have a major peak at 446 nm at 298 K. Both peaks are red shifted to 455 nm at 195 K.

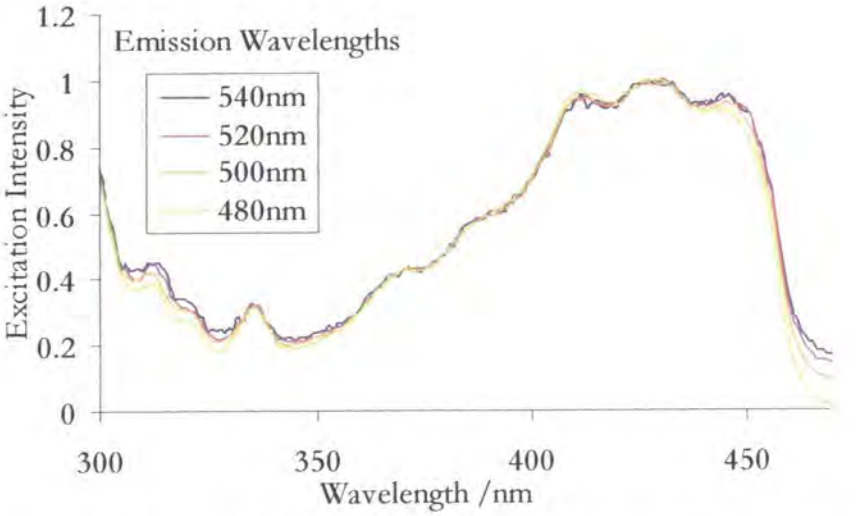

Figure 17. The normalised excitation spectra of **4** in paraffin at approximately 289 K for the emission wavelengths 540 nm, 520 nm, 500 nm and 480 nm.

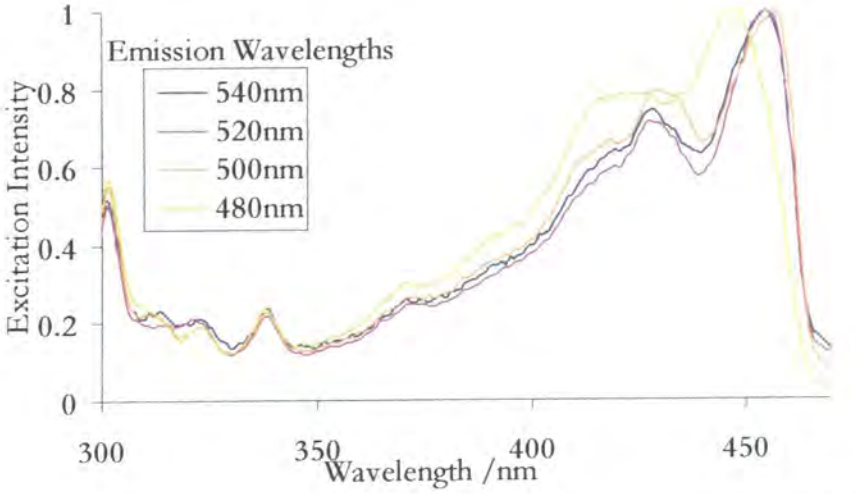

Figure 18. The normalised excitation spectra of **4** in paraffin at 195 K for the emission wavelengths 540 nm, 520 nm, 500 nm and 480 nm.

In a viscous solution of glycerol at room temperature the emission spectra was much broader with less well defined peaks at 463 nm and 489 nm. The profile is slightly blue shifted when compared to the emission of **4** in EPA. The emission profiles were consistent across a range of excitation wavelengths as proven from the data acquired for excitation at 261 nm, 312 nm, 355 nm and 430 nm.

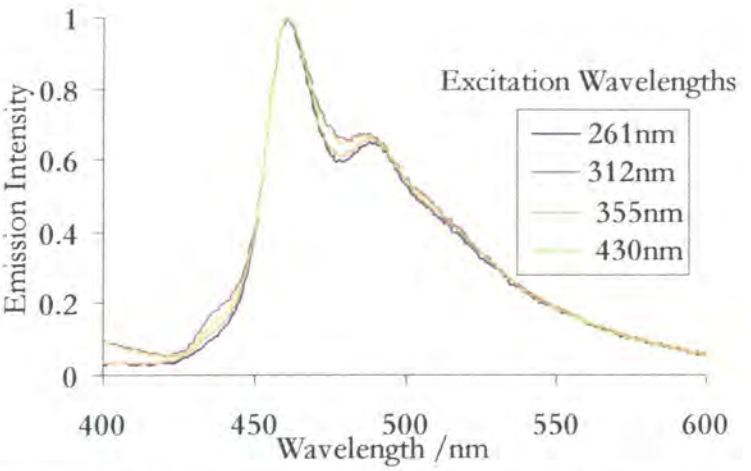

Figure 19. The normalised emission spectra of **4** in glycerol at room temperature for the excitation wavelengths 261 nm, 312 nm, 355 nm and 430 nm.

The lifetime of **4** was recorded in paraffin and was found to be 1.5 ns. A secondary lifetime of 0.5 ns was seen which cannot yet be accounted for. Raman scattered light emission around 447 nm coming from the paraffin was also observed.

The results suggest that these molecules exist in a range of conformers in dilute solution. On excitation in non-viscous solution they twist into a low energy planar configuration before emission, hence the sharp emission spectral profiles. Viscous solutions slow down the rotation and the somewhat broader emission may be a result of the molecules not been able to twist into the preferred low energy configuration quickly enough before emission occurs. Thus the spectrum could be a mixture of relaxed and un-relaxed emission.

The results for **3** and **4** are in keeping with the findings of Levitus and Garcia-Garibay *et al*[7, 10] and Cherkasov *et al*[4]. Levitus *et al* carried out polarization experiments on 9,10-bis(phenylethynyl)anthracene (**3**) in solution and thin films and concluded from their results that there is mixed polarization through out the absorbance band in the visible region of the spectrum. Their results obtained from fluorescence anisotropy measurements showed that the bands at 312 nm and 270 nm are purely polarized along the z-axis and y-axis respectively and suggest the emission is exclusively from the S_1 state. The decrease in vibrational resolution when these molecules are in solution has also been proposed to be due to the existence of a variety of conformations. The calculated UV-vis spectra were in good agreement with their experimental data. According to their calculations the overlap between the z-polarised and y-polarized

transitions in the visible region is smaller in the totally planar conformation, which explains why the visible region of the UV-vis spectrum in the polymer shows better vibrational resolution. This reasoning can be applied to the resulting absorbance and emission spectra of **3** at 77 K. In the low temperature glass the range of conformations will be limited and would tend towards the lowest energy planar form. The result being red shifted higher resolution vibrational transitions in the glass compared to the room temperature solution. The calculated energy difference between the perpendicular and planar conformations of **3** increases from 1.43 kJ/mol[7] in the ground state to 26.46 kJ/mol[7] in the excited state, suggesting the emission occurs mainly from the planar configuration in solution. This increased barrier to rotation is consistent with the experimental results for **3** at room and low temperature. The emission profile is better resolved at low temperature and at room temperature than the excitation spectra (Figure 19).

The results also agree with findings of Cherkasov *et al*[4]. They studied the role of conformational isomers in the formation of stationary electronic spectra of **3** and its derivatives at room and low temperature. They also came to the conclusion that **3** has two types of conformational isomers in solution. They proposed that in the coplanar conformation all the molecular fragments participate in the conjugation and would result in a long wavelength spectrum. In the perpendicular conformation the conjugation chain is shorter and would correspond to a shorter wavelength spectrum. A relative stability was postulated for the perpendicular conformation on the basis of the strong π electron interaction between one of the phenyl rings and the π bond of the anthracene ring. They represented the relative arrangement of the energy levels of the planar and perpendicular isomers in the form of the following scheme

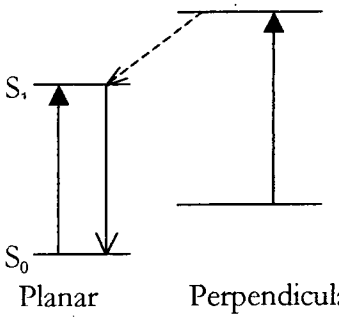

Here both conformers absorb excitation energy but the higher energy isomer is rapidly converted to the planar conformation before emission occurs. This depicts the

predominance of the planar isomer at low temperature and the increase in the fraction of twisted isomers to a certain limiting value as the temperature raises.

The photophysical properties of coplanar and twisted 1,4-bis(9-ethynylanthracenyl)benzene (**4**) have been studied by Schmieder *et al*[10]. The previously described observations are in agreement with their results. They used semiempirical methods to calculate the conformational dependence of the lower electronic energy transitions of compound **4**. The energy difference between the coplanar minimum and twisted maximum (the two anthryl groups being at 90^0 with respect to the central phenyl ring) was calculated to be 1.26 kJ/mol. In the excited state the estimated energy difference between the coplanar and twisted maximum was calculated to be 29.4 kJ/mol. The calculated high barrier to rotation in the excited state explains why the emission spectra are independent of the excitation wavelength and suggests that emission occurs primarily from the S_1 state. The increase in intensity in the lower energy portion of the excitation spectra as the temperature is lowered is accounted for by their calculations. The calculations support the theory that at low temperature there is a redistribution of the conformational population and the lower energy coplanar conformation is dominant. It is observed that planarization causes major changes in the excitation spectrum of **4** (Figures 17 and 18) but minor changes in the emission. Since the emission spectrum reflects the dynamics of the excited state Schimieder *et al* concluded that the lower energy species, the excited planar rotamer, must be the emitting species in all cases[10].

The slowing down of the conformational dynamics in the excited state should in theory create wavelength dependence in the excitation and emission measurements. This should result in compound **4** not being able to attain equilibration within its lifetime. The lifetime of **4** in mineral oil as determined by Schmieder *et al* is 1.8 ns[10] which is 0.3 ns longer than our determination in liquid paraffin. Our observations of strong wavelength dependence when **4** is cooled to 195 K (Figure 18) are in agreement with their findings. These results are interpreted as being indicative of the excited state rotational equilibrium being incomplete in the viscous solution. This means more than one emitting species are now present. At shorter emission wavelengths one observes the increase in contribution form the twisted, higher energy rotamers. This results in the blue shift observed in the excitation spectra.

Further work would include the determination of their quantum yield, behaviour in viscous solutions at low temperature and in polar solvents and anisotropy measurements.

Photoluminescence study of substituted Polyarylethynylenes

The absorption, emission and excitation spectra of the following molecules were recorded at various temperatures. Here their spectra at 298K and 77K are given for comparison. Their molecular structures are given in table 2.

Molecules studied:

1-(3,3-dimethyl-but-1-ynyl)-4-phenylethynyl-benzene (**5**)

1,4-diphenylbut-1,3-diyne (**6**)

1,4-bis(phenylethynyl)-2,5-bis(trimethylsilylethynyl)benzene (**7**)

1,4-dibromo-2,5-bis(phenylethynyl)benzene (**8**)

1,2,4,5-tetra(phenylethynyl)benzene (**9**)

1,1,2,2-tetra(phenylethynyl)ethene (**10**)

Table 2

Molecules Studied	Molecular structures
1-(3,3-dimethyl-but-1-ynyl)-4-phenylethynyl-benzene (**5**)	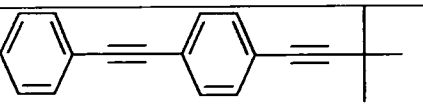
1,4-diphenylbut-1,3-diyne (**6**)	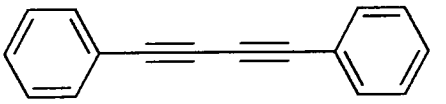
1,4-bis(phenylethynyl)-2,5-bis(trimethylsilylethynyl)benzene (**7**)	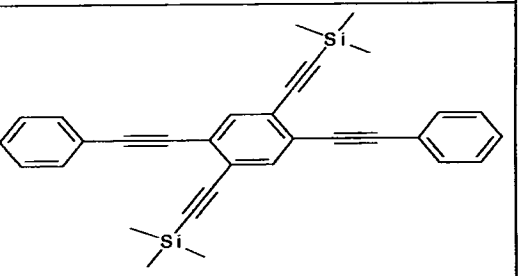
1,4-dibromo-2,5-bis(phenylethynyl)benzene (**8**)	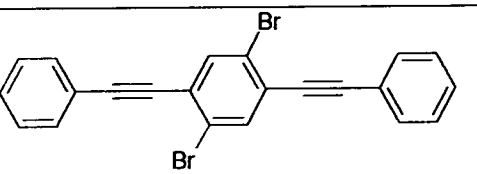
1,2,4,5-tetra(phenylethynyl)benzene (**9**)	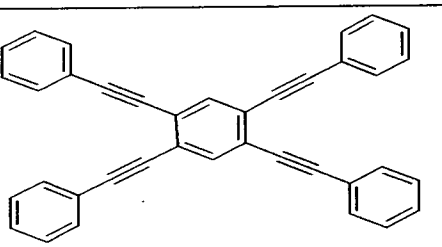
1,1,2,2-tetra(phenylethynyl)ethene (**10**)	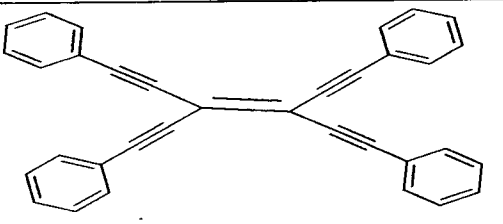

1-(3,3-Dimethyl-but-1-ynyl)-4-phenylethynyl-benzene (5)

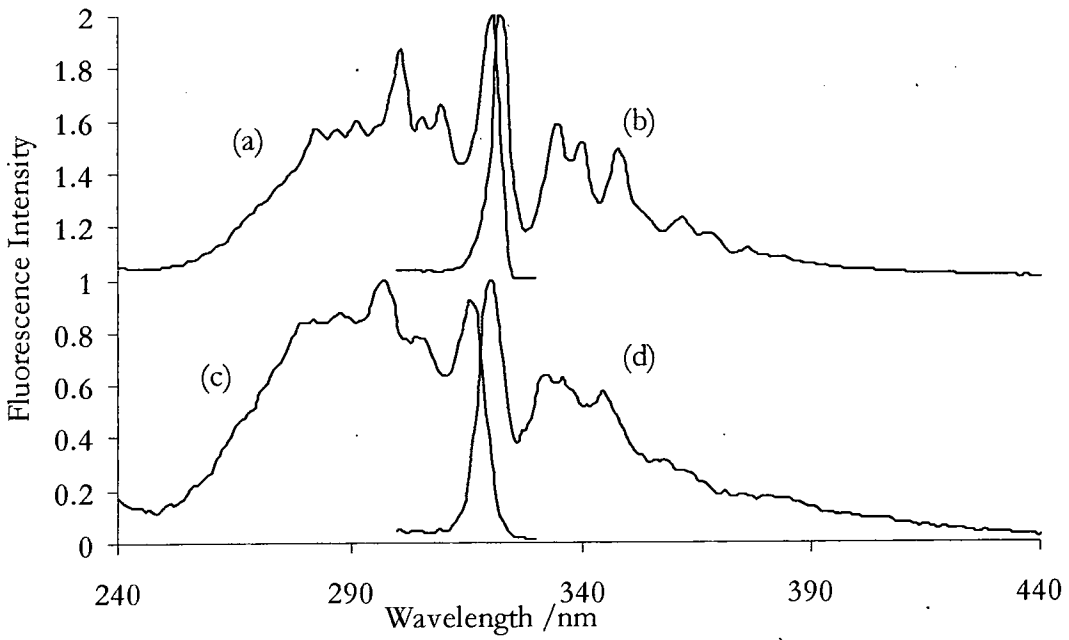

Figure 20. Normalised fluorescence excitation and emission spectra for **5** in EPA at 77 K (upper profiles) and 298 K (lower profiles). The excitation spectra (a) and (c) were determined using a 336 nm emission wavelength and the emission spectra (b) and (d) were obtained using a 288 nm excitation wavelength.

1,4-diphenylbut-1,3-diyne (6)

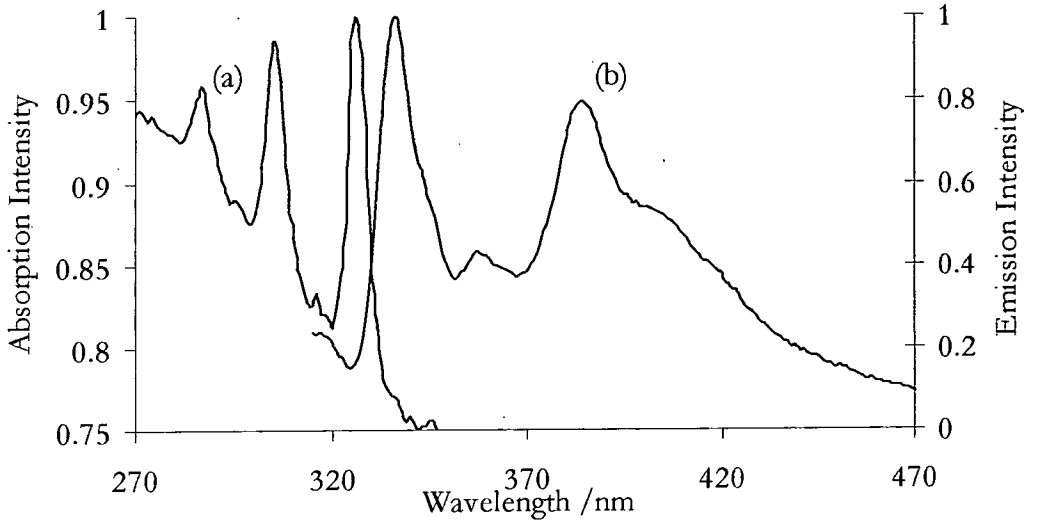

Figure 21 (a). The normalised absorption (a) and emission spectra (b) of **6** in EPA at 298 K. The emission spectrum was determined using a 305 nm excitation wavelength.

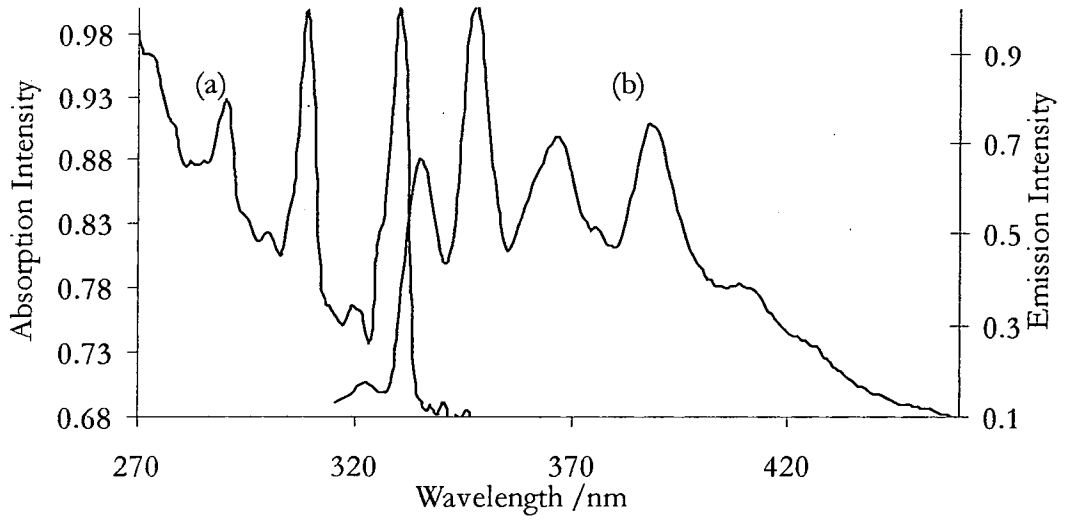

Figure 22 (b). The normalised absorption (a) and emission spectra (b) of **6** in EPA at 77 K. The emission spectrum was determined using a 305 nm excitation wavelength.

1,4-bis(phenylethynyl)-2,5-bis(trimethylsilylethynyl)benzene (7)

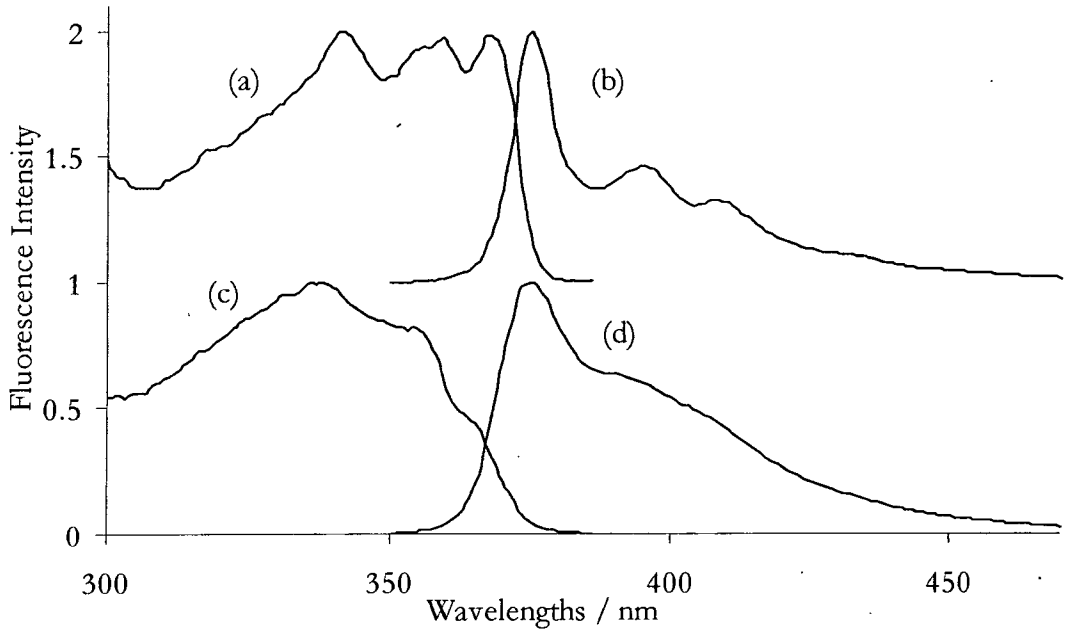

Figure 23. Normalised fluorescence excitation and emission spectra for **7** in EPA at 77 K (upper profiles) and 298 K (lower profiles). The excitation spectra (a) and (c) were determined using a 391 nm emission wavelength and the emission spectra (b) and (d) were obtained using a 341 nm excitation wavelength.

1,4-dibromo-2,5-bis(phenylethynyl)benzene (8)

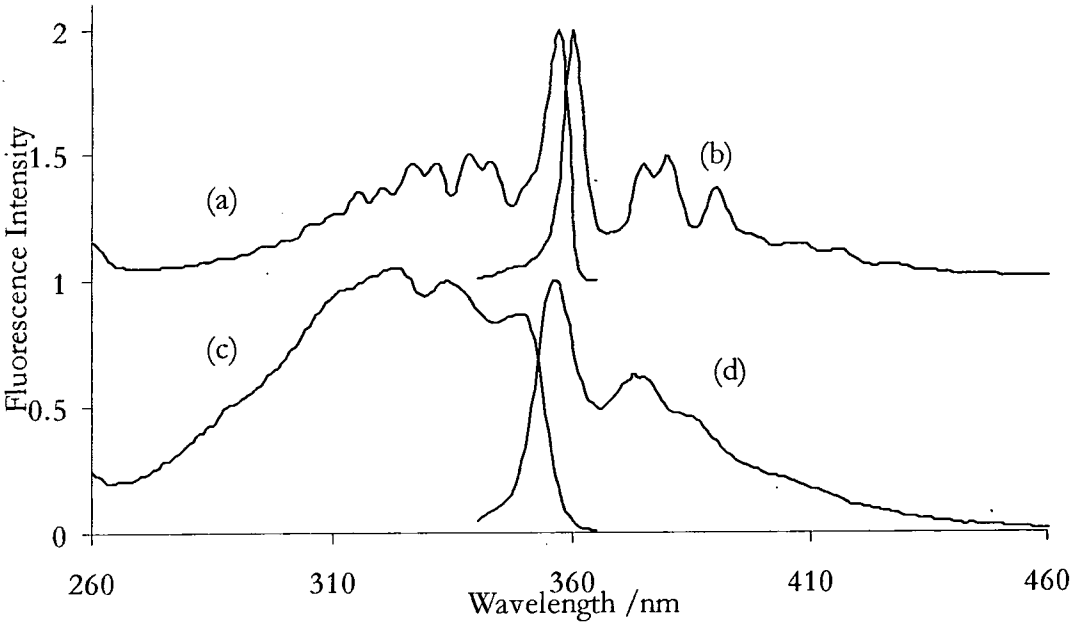

Figure 24. Normalised fluorescence excitation and emission spectra for **8** in EPA at 77 K (upper profiles) and 298 K (lower profiles). The excitation spectra (a) and (c) were determined using a 375 nm emission wavelength and the emission spectra (b) and (d) were obtained using a 330 nm excitation wavelength.

1,2,4,5-tetra(phenylethynyl)benzene (9)

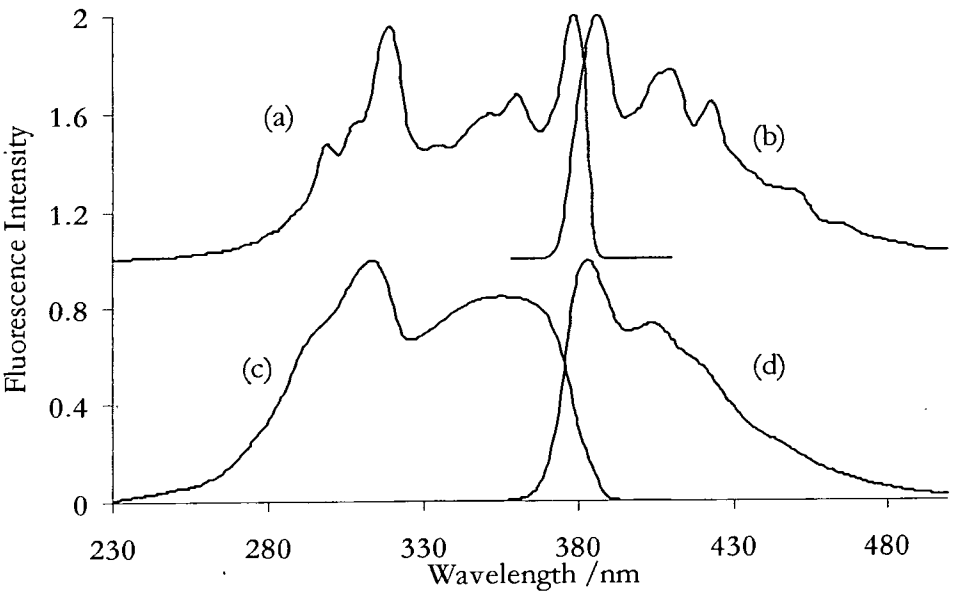

Figure 25. Normalised fluorescence excitation and emission spectra for **9** in EPA at 77 K (upper profiles) and 298 K (lower profiles). The excitation spectra (a) and (c) were determined using a 385 nm emission wavelength and the emission spectra (b) and (d) were obtained using a 313 nm excitation wavelength.

1,1,2,2-tetra(phenylethynyl)ethene (10)

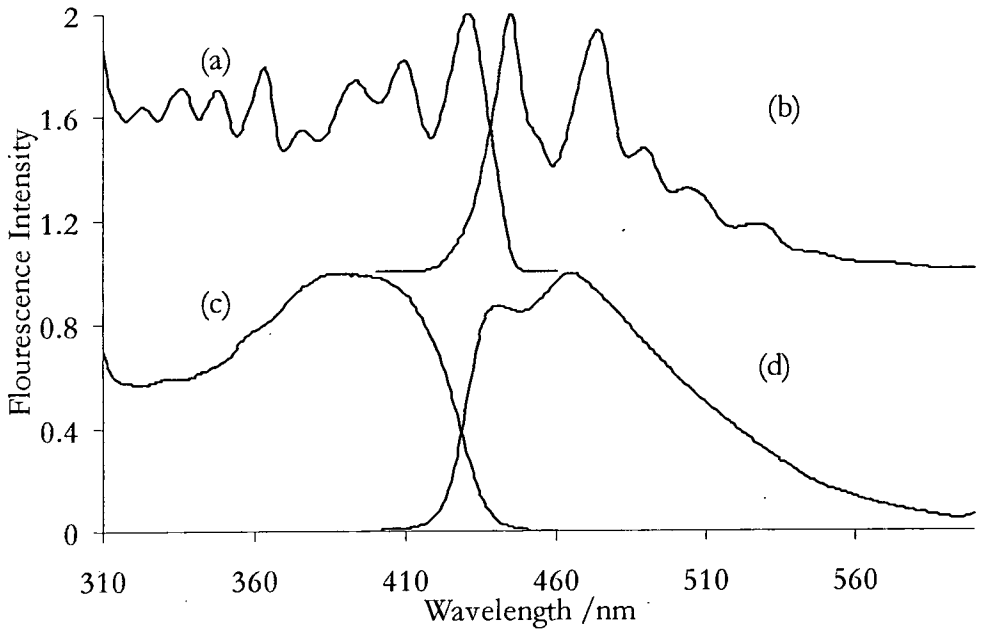

Figure 26. Normalised fluorescence excitation and emission spectra for **10** in EPA at 77 K (upper profiles) and 298 K (lower profiles). The excitation spectra (a) and (c) were determined using a 466 nm emission wavelength and the emission spectra (b) and (d) were obtained using a 301 nm excitation wavelength.

Table 3 is a compilation of the main observations from the spectral data on molecules **5** to **10**. The main excitation and emission peaks from the spectral profiles of each molecule are compared at room and low temperature. The molecules studied all absorbed strongly in the UV region but absorption range of **10** extends into the near UV-visible region. Their absorption and excitation spectra are all red shifted at low temperature. All their spectra have a very small Stokes shift and a strong (0,0) band at 77 K. **5**, **8** and **10** show the best resolved profiles at low temperature with their excitation and emission profiles being almost mirror images of each other.

Table 3

		298K		77K	
		Major Peaks (nm)		Major peaks (nm)	
Molecule	Absorption range nm	Excitation	Emission	Excitation	Emission
5	260-325	288, 297, 316,	320, 333, 345	291, 301, 321	322, 335, 348, 362
6	260-340	288, 306, 327*	337, 360, 385	290, 309, 330*	335, 348, 368, 389
7	300-370	338-broad	376, 392-shouder	341, 359, 369	375, 395, 408
8	260-360	323, 334, 349-broad	356, 375	328, 338, 357	360, 380, 390
9	260-380	313, 355-broad	383, 404	320, 361, 378	386, 410, 423
10	260-450	392-broad	442, 467-broad	336, 348, 363, 393, 409, 430	445, 474, 489, 504, 527

*The major peaks from the absorption profile of **6** at 298 K and 77K.

A tabulation of the absorption ranges and the main excitation and emission peaks in the spectra of molecules **5** to **10**. Their fluorescence is compared at 298 K and 77 K.

All the compounds exhibit a λ_{max} absorbance between 310 nm and 400 nm, which indicates the contribution of the phenylethynyl group to the π-conjugation system.

Table 4, 5 and 6 compiles the possible peak assignments for the energy transitions occurring at 77 K. for molecules 5, 8 and 10.

Table 4

Absorption Transitions $v'' \rightarrow v'$	λ_{max} /nm	Transition Energies hv_e^{max} / cm^{-1}		Emissive Transitions $v' \rightarrow v''$	λ_{max} /nm	Transition Energies hv_e^{max} / cm^{-1}
$0 \rightarrow 0$	321	31,200		$0 \rightarrow 0$	322	31,000
$0 \rightarrow 1$	301	33,200		$0 \rightarrow 1$	335	29,800
$0 \rightarrow 2$	291	34,400		$0 \rightarrow 2$	348	28,700

A tabulation of the absorption and emissive wavelengths and proposed vibrational energy transitions occurring in **5** at 77 K.

Table 5

Absorption Transitions $v'' \rightarrow v'$	λ_{max} /nm	Transition Energies hv_e^{max} / cm^{-1}		Emissive Transitions $v' \rightarrow v''$	λ_{max} /nm	Transition Energies hv_e^{max} / cm^{-1}
$0 \rightarrow 0$	357	28,000		$0 \rightarrow 0$	360	27,800
$0 \rightarrow 1$	338	29,600		$0 \rightarrow 1$	380	26,300
$0 \rightarrow 2$	328	30,500		$0 \rightarrow 2$	390	25,600

A tabulation of the absorption and emissive wavelengths and proposed vibrational energy transitions occurring in **8** at 77 K.

Table 6

Absorption Transitions $v'' \rightarrow v'$	λ_{max} /nm	Transition Energies hv_e^{max} / cm^{-1}		Emissive Transitions $v' \rightarrow v''$	λ_{max} /nm	Transition Energies hv_e^{max} / cm^{-1}
$0 \rightarrow 0$	430	23,300		$0 \rightarrow 0$	445	22,500
$0 \rightarrow 1$	409	24,400		$0 \rightarrow 1$	474	21,100
$0 \rightarrow 2$	393	25,400		$0 \rightarrow 2$	489	20,400

A tabulation of the absorption and emissive wavelengths and proposed vibrational energy transitions occurring in **10** at 77 K.

Compounds **7** and **8**, which are similar in structure to **1**, but with different substituents, exhibit similar photoluminescence properties to **1**. In the case of compound **7** it is observed that steric hindrance affects the low temperature excitation and emission spectra since the vibrational transitions are far less resolved when compared to the photoluminescence spectra of **1** and **8** at 77 K. **7** is unable to relax fully to the lower energy planar form before emission because of the presence of the bulky trimethylsilyl groups. The bromine substituents in compound **8**, however, present little hindrance to the rotation of the phenyl rings. At low temperature the distinct bathochromic shift in the excitation spectra and high resolution of the vibrational features is indicative of the increased π conjugation in compound **8** in its coplanar conformation.

Compound **5** is better resolved than compound **1** at room temperature. This could be the result of the existence of fewer conformations in the solution with a bias towards the low energy planar form. The spectral profiles are not completely symmetrical at 77 K, which could be an indication of the presence of a small range of conformational isomers acting as the absorbing species. The absorption spectrum of compound **6** is well resolved at 298 K and 77 K. This could be the result of a very low barrier to rotation and the possible conformations possessing similar energy potentials.

The spectra of compound **9** show evidence of steric interactions. At room and low temperature there is a distinct high energy peak at 313 nm. This indicates that there is high concentration of stable non-planar conformers that persists even at 77 K. Compound **10** is of lower energy than **9** and its better resolved at 77 K. The excitation and emission profiles of **10** are not completely symmetrical which suggests the persistence of more than one type of conformation being excited at 77K. The broad spectra at room temperature suggest a range of conformers is present in solution.

Further studies are required to determine if, like **1**, compounds **5** to **10** have wavelength dependent excitation and emission spectra and fluorescence lifetime measurements. This would confirm whether or not in low temperature-glasses the relaxation rate of the rotamers of the excited state is slowed down in comparison to the rate of fluorescence.

Conclusions

It has been illustrated that 1,4-bis(phenylethynyl)benzene (**1**) emits from the lowest vibrational energy level of its first excited singlet state and behaves in a conventional manner at room temperature as reported by other groups. At low temperature 3-dimensional matrix scans of **1** shows inhomogeneous fluorescence behaviour and the excitation and emission spectra are wavelength dependent. The results of the photoluminescence study of 9,10-Bis(phenylethynyl)anthracene (**3**), and 1,4-bis(9-ethynylanthracenyl)benzene (**4**) also agreed with previous photoluminescence studies carried out on these compounds. The results indicate the presence of a continuum of conformers in the room temperature solution and the low temperature glass of these three compounds. It also indicates a slow rate of relaxation of rotamers of the excited states compared to the fluorescence. The excitation profile **4** at 195 K shows emission wavelength dependence in viscous solution. The emission spectra were not wavelength

dependent. This implies the rotamers relax to the lowest excited state before emission occurs.

1-(3,3-Dimethyl-but-1-ynyl)-4-phenylethynyl-benzene (**5**), 1,4-bis(phenylethynyl)-2,5-bis(trimethylsilylethynyl)benzene (**7**), 1,4-dibromo-2,5-bis(phenylethynyl)benzene (**8**), 1,2,4,5-tetra(phenylethynyl)benzene (**9**) and 1,1,2,2-tetra(phenylethynyl)ethene (**10**) all appear to possess a continuation of conformations at room temperature as their excitation spectra consist of broad vibrational bands. 1,4-Diphenylbut-1,3-diyne (**6**) appears to have conformations with similar vibrational energies as its absorption spectra is highly resolved at room temperature. The distribution of conformations in the ground electronic state changes with temperature. In the case of **7** there is evidence of stric hindrance preventing the molecule from achieving its lowest energy conformation in its excited state before emission occurs. This indicates there are multiple rotational conformers being excited to the higher energy states

The photoluminescence properties of molecules **5** to **10** were found to be similar to that of **1** at room and low temperature. In the case of **7** there is some evidence that these properties are affected by steric hindrance resulting in a smaller range of rotational conformations.

REFERENCES

1. Biswas M., P. Nyugen, T. B. Marder, and L. R. Khundkar. *J. Phys. Chem.*, 1997. **101**: p. 1689-95.
2. Birckner E., U.-W. Grummt, A. H. Goller, T. Pautszch, D. A. M. Egbe, M. Al-Higari, and E. Klemm. *J. Phys. Chem. A*, 2001. **105**: p. 10307.
3. Beeby A., K. Findlay, P. Low, and T. Marder. *J. Am. Chem. Soc.*, 2002. **124**(28): p. 8280-8284.
4. Cherkasov A. S., T. V. Veselova, B. M. Krasovitskil, and V. M. Shershukov. *Opt. Spectrosc. (USSR)*, 1985. **59**: p. 59-63.
5. Levitus M., K. Schmieder, H. Ricks, K. D. Shimizu, U. H. F. Bunz, and M. A. Garcia-Gariby. *J. Am. Chem. Soc.*, 2001. **123**: p. 4259-4265.
6. Sluch M. I., G. Godt, U. H. F. Bunz, and M. A. Berg. *J. Am. Chem. Soc.*, 2001. **123**: p. 6447.
7. Levitus M. and M. A. Garcia-Gariby. *J. Phys. Chem. A*, 2000. **104**: p. 8632-8637.
8. Schmieder K., M. Levitus, H. Dang, and M. A. Garcia-Gariby. *J. Phys. Chem. A.*, 2002. **106**: p. 1551-1556.
9. Nakatsuji S. i., K. Matsuda, Y. Uesugi, and K. Nakashima. *J. Chem. Soc. Perkin Trans. 1*, 1992: p. 755-758.
10. Schmieder K., M. Levitus, H. Dang, and M. A. Garcia-Gariby. *J. Phys. Chem. A*, 2002. **106**: p. 1551-1556.

APPENDIX

Publication

A. Beeby, K. Findlay, P. Low and T. Marder, A re-evaluation of the photophysical properties of 1,4-bis(phenylethynyl)benzene: A model for poly(phenyleneethynylene, *J. Am. Chem. Soc.*,2002. **124** (28): p. 8280-8284.

Seminars attended

2001-2002

October 24	Prof Bob Denning, University of Oxford Photonic Crystals
October 31	Dr Colin Raston, School of Chemistry, Univ of Leeds Towards benign supramolecular chemistry: synthesis - self organization
November 14	Professor John Goodby, Department of Chemistry, University of Hull Supermolecular liquid crystals - multipodes and dendrimers
January 22	Dr Ian Fallis, University of Cardiff Size is Everything
January 30	Dr Peter Hore, PCL, University of Oxford Chemistry in a spin: effects of magnetic fields on chemical reactions
February 13	Dr Helen Aspinall, Department of Chemistry, University of Liverpool Defining effective chiral binding sites at lanthanides - enantioselective reagents and catalysts
March 12	Professor David Williams, Cardiff Beer and Health: 7000 years of history
May 8	Professor Paul Madden, PCL, University of Oxford Covalent Effects in "Ionic" Systems